



**Politecnico
di Torino**



Politecnico di Torino
in collaboration with
CERN

Corso di Laurea Magistrale in Ingegneria Chimica e
dei Processi Sostenibili
A.a 2023/2024
Sessione di Laurea Luglio 2024

**Design of an SF₆ recuperation
system**

Relatori:

Prof. Alessandro Hugo Antonio Monteverde
Prof. Fabio Alessandro Deorsola
Dott. Roberto Guida

Candidato:

Amin Bouzaiene

Declaration

I hereby declare that, the contents and organization of this dissertation constitute my own original work and does not compromise in any way the rights of third parties, including those relating to the security of personal data.

Amin Bouzaiene
2024



Abstract

Numerous families of particle detectors at CERN utilize gas mixtures containing fluorinated gases, which have significant environmental impacts due to their high Global Warming Potential (GWP). To comply with European emissions regulations, it is essential to either reduce the consumption of these gases or significantly limit their emissions through abatement. Specifically, in Resistive Plate Chambers (RPCs), a mixture of R134a (95.2%), iC_4H_{10} (4.5%), and SF_6 (0.3%) is used. Isobutane, being an organic gas, acts as a quencher, absorbing photons produced from recombination processes and limiting the formation of secondary avalanches. SF_6 is an electronegative gas that captures free electrons, reducing free charges in the gas volume and suppressing the onset of streamers.

This thesis focuses on the simulation, design, and development of a recovery system for SF_6 , the fluorinated gas with the highest GWP (23,600), from a mixture of R134a, iC_4H_{10} , and N_2 originating from the exhaust of the R134a recovery system. The goal is to achieve a recovered gas purity between 90% and 99% SF_6 , with a molar recovery rate of at least 60%. Cryogenic distillation has been selected as the primary separation method due to its efficiency in liquefying modest gas flows.

An overview of CERN and the CMS experiment is provided, including the operation of RPCs and the role of individual gases within these detectors.

The detailed examination of the RPC gas system includes the mixer module, humidifier, pump module, and gas purifier, to comprehensively understand the gas path and purification processes involved. Insights into the R134a recovery system are crucial for the subsequent design of the SF_6 recovery system, which will operate in series.

The thesis also includes testing a prototype for SF_6 separation, supported by simulations to validate experimental conditions. This prototype, already present in CMS, consists of a single-stage buffer and it will be used for testing the cryogenic distillation of SF_6 from other components. The aim of the test is to evaluate the solubility of R134a in SF_6 and to see if the separation occurs or not. Theoretical studies using binary diagrams for SF_6 and R134a, utilizing the McCabe-Thiele approach, estimate the theoretical stages required for separation. The introduction of isobutane as a third component and the analysis of the ternary diagram of these components, derived using Aspen Plus, are also covered.

The core of the thesis is the simulation and design of a new SF_6 recovery system. This system comprises two distillation columns arranged in series. The output from the top of the second distillation column is an SF_6/N_2 mixture with a 70/30 composition. This mixture is then processed through a membrane, where it is expected to be concentrated to a composition of 95% SF_6 and 5% N_2 .

An economic analysis evaluates the feasibility of implementing recovery systems to reclaim gases compared to abatement systems. The thesis concludes with a discussion of the results, offering real-world perspectives on the strengths and weaknesses of the recovery system.

Summary (Sommaro)

Introduzione

Il clima del pianeta terra è fortemente influenzato dai gas che compongono l'atmosfera terrestre. Tra questi, hanno un ruolo centrale i gas serra che intrappolano calore e contribuiscono all'innalzamento della temperatura terrestre e al cambiamento climatico. Tra questi gas riscontriamo CO_2 , CH_4 , N_2O , e i gas fluorinati. Al CERN, centro europeo per la ricerca nucleare, fondato nel 1954, con sede a Meyrin, vicino Ginevra, vengono studiate le particelle e il loro comportamento fisico. Quest'ultimo è situato tra Francia e Svizzera, e ospita il "Large Hadron Collider" (LHC), l'acceleratore più grande e potente del mondo, con un diametro di 27 km. Il LHC è costituito da quattro esperimenti, ci soffermeremo su uno in particolare CMS, il compact Muon Solenoid. Esso, è localizzato a Cessy in Francia. CMS a sua volta è costituito da tanti rilevatori di particelle, tra cui 4 rilevatori a gas. Drift Tube (DT), Cathode Strip Chambers (CSC), Resistive Plate Chambers (RPC) Gas Electron Multiplier (GEM). In particolare, gli RPC utilizzano una miscela di gas costituita da R134a, iC_4H_{10} e SF_6 in composizione (95.2%, 4.5% e 0.3% rispettivamente). Le CSC, invece, utilizzano CF_4 (10%), CO_2 (50%) e Ar (40%). Le miscele sopra citate vengono utilizzate per fluire nelle camere dei rilevatori, e sono costituite da gas fluorinati tra cui SF_6 , R134a e CF_4 . L' SF_6 è il più impattante fra tutti con un GWP misurato di 23900, in seguito abbiamo CF_4 (GWP 6500) ed infine R134a con un GWP di 1300. E' quindi necessario, trovare delle soluzioni per limitarne quanto più possibile il consumo e le emissioni dei gas fluorinati.

La prima delle soluzioni che attualmente è in atto a CMS è il ricircolo della miscela gassosa nei sistemi a gas. Sia le CSC che gli RPC operano con un sistema chiuso, in cui il 90% del gas viene ricircolato e il 10% viene iniettato al mixer. In serie al mixer è presente un humidifier, con la funzione di umidificare la miscela, subito dopo è presente il modulo di distribuzione, in cui il gas viene suddiviso in vari canali che vanno a riempire le camere dei rivelatori, successivamente la miscela viene estratta da un sistema di pompe, queste, reimmettono il gas in un modulo purifier, dove il gas viene pulito dalle impurità che si sono create nel rivelatore, infine, il 10% della miscela viene mandata all'exhaust, il restante 90% invece, viene reimpresso nella loop costituita da tutti i moduli sopra elencati.

Compreso il funzionamento dei sistemi a gas, possiamo ora elencare le principali soluzioni per limitare i consumi e le emissioni dei gas fluorinati a parte quelle già citate. Principale problema che si riscontra a oggi sono le perdite al mixer, su 700 l/h iniettati 200 l/h sono di perdite, che corrispondono circa al 30% di gas iniettato. Per risolvere in parte questo problema sono state disattivate alcune camere RPC e tutt'ora sono in atto delle campagne di riparazione per le perdite. Un'ulteriore soluzione consiste nel miglioramento delle efficienze dei sistemi di recupero presenti. Attualmente, nel modulo exhaust delle CSC, è presente un sistema di recupero per il CF_4 che opera con un'efficienza del 70%, mentre in serie al modulo purifier degli RPC è presente un sistema di recupero per l'R134a, che opera con un'efficienza del 80%, attualmente tutto il gas recuperato viene utilizzato per essere re-iniettato nel mixer. Aumentare le efficienze di recupero di questi sistemi vorrebbe dire comprare meno gas e di conseguenza ridurre i consumi e le emissioni, l'obiettivo ideale sarebbe recuperare il 100% per ridurre il più possibile le emissioni. Un'ulteriore attività sulla quale si sta lavorando è il Design di un sistema per il recupero dell' SF_6 dalla miscela RPC. Il sistema verrà posto in serie al sistema di recupero del R134a. Quest'ultimo, sarà l'argomento della tesi in oggetto.

Un'altra via che si sta perseguendo con le attività di R&S è la ricerca di gas alternativi ai gas fluorinati da mandare nei rilevatori.

Infine un'ultima soluzione, la più risolutiva per le emissioni risulta essere l'installazione di un abbattitore per i F-GHG da installare nel modulo di exhaust, in questo modo le emissioni sarebbero fortemente

limitate. Da questa soluzione derivano delle problematiche di tipo economico, in quanto, la gestione dell'acqua di scarico comporterebbe costi non indifferenti. Per questo, a oggi, quest'alternativa non è ancora stata adottata.

Sistema di recupero per l'R134a

Compreso il funzionamento del circuito a gas in CMS, ci soffermeremo sulla descrizione di un sistema di recupero, situato nella gas room di CMS, esso è connesso alla linea dell'exhaust degli RPC, si tratta del recupero del R134a.

Il primo prototipo del recupero del R134a, venne per la prima volta installato nel 2019, esso risulta essere una versione più semplificata dell'attuale sistema. Il prototipo I era costituito da due componenti principali un buffer "freddo" posto in posizione verticale (alla temperatura di -36°C) e in serie ad esso uno "caldo" posto in posizione orizzontale (alla temperatura di 20°C). Più avanti, nella linea, viene posto un compressore per tirare il gas accumulato nel buffer "caldo". Lo scopo di questo sistema è quello di separare crio-genicamente il R134a (95.2%) da iC_4H_{10} (4.5%) e SF_6 (0.3%). Nel primo buffer alla temperatura di -36 gradi viene fatta condensare la miscela, ci si aspetta viste le temperature di condensazione di (-11°C e -26°C) che l'R134a e l'isobutano, condensino mentre l' SF_6 no (temperatura di condensazione -67.6°C). La fase liquida, presente nel buffer, inizia la sua discesa nel tubo che connette il buffer freddo a quello caldo, quando il sensore di livello si attiva. In questo modo, la valvola pneumatica viene aperta automaticamente e la miscela discende verso il buffer caldo per gravità. L' SF_6 , presente in fase vapore uscirà interamente dalla zimmerly valve connessa alla linea dell'exhaust alla pressione settata nella valvola. Il sistema a singolo buffer presenta un problema di gestione, ovvero che se un componente si guasta è necessario fermare la separazione, tutto il recupero viene fermato e all'incirca 900 l/hr vengono dirottati all'aria il che vorrebbe dire :

- fermare il recupero, ovvero iniettare al mixer la frazione che manca dal recupero, di conseguenza aumentare il consumo di gas fresco.
- emettere 900 l/hr di gas fluorinati all'aria il che vorrebbe dire emettere un quantitativo di 1845 tCO₂eq/hr, sicuramente una quantità non trascurabile.

Per evitare ciò, risulta quindi di fondamentale importanza, la costruzione di un sistema più versatile che sia in grado di operare nonostante ci sia della manutenzione da effettuare sul sistema. Per questi motivi, nel 2022, è stato commissionato il design del nuovo recupero dell'R134a. Il nuovo sistema, attualmente installato, al posto del prototipo I si divide in quattro unità: il rack elettrico, il buffer per la distillazione, il compressore e la sezione di stoccaggio.

Il rack elettrico, ospita componenti elettrici ed elettronici essenziali per l'automazione del sistema tramite PLC. È monitorato remotamente tramite WinCC Open Architecture di Siemens. All'interno, componenti cruciali includono il regolatore di flusso di massa per il miscuglio d'ingresso e il trasmettitore di punto di rugiada Vaisala per garantire l'assenza di acqua, con una temperatura massima di -40°C . Una valvola a tre vie permette la deviazione del flusso verso la linea di azoto per favorire la pulizia del sistema, quando necessaria.

L'unità di distillazione è composta da due rack chiusi in ambiente ATEX, ciascuno con due colonne verticali per la separazione della miscela d'ingresso. Ogni colonna ha serbatoi superiori e inferiori per facilitare il processo. Il sistema include due unità di refrigerazione: HUBER UNISTAT 915w per il circuito di raffreddamento del serbatoio superiore e Huber Ministat 125 per il serbatoio inferiore.

I serbatoi variano nelle dimensioni: colonne 1 e 2 hanno serbatoi superiori alti 30 cm e inferiori alti 10 cm, mentre colonne 3 e 4 hanno serbatoi alti 20 cm per entrambe le parti. Tutti i serbatoi hanno diametri interni ed esterni identici (114,3 mm e 139,7 mm).

Il sistema opera con quattro colonne in parallelo. Durante il riempimento, il miscuglio viene liquefatto in uno scambiatore di calore controcorrente prima di entrare nel serbatoio superiore, dove avviene la distillazione a temperature tra $-32,3^{\circ}\text{C}$ e $-26,4^{\circ}\text{C}$. Il liquido scorre verso il serbatoio inferiore tramite gravità, evaporando rapidamente tra 14°C e 23°C . Il vapore sale, si condensa nel serbatoio superiore e i componenti volatili escono attraverso la linea di scarico.

Per lo svuotamento, la valvola pneumatica posta al di sotto del buffer caldo si apre e la miscela recuperata fluisce attraverso valvole di regolazione del flusso. Qui, il compressore viene attivato e tira la miscela di isobutano e R134a verso la bombola del recuperato. Il sistema a oggi 2024, ha un'efficienza dell'80% e una purezza del recuperato compresa tra 95-99%. Di particolare importanza, invece risulta essere la descrizione della linea dell'exhaust del sistema del recupero del freon in quanto a essa andrà poi connesso il sistema del recupero del SF₆. In questa, vi passa un flusso discontinuo di una miscela 79% R134a, 19% iC₄H₁₀ e 1.2% SF₆ e N₂ 0.3% alla temperatura di 20 °C e alla pressione di 1.2 bara. Da questo punto, si connette la linea al sistema di recupero del SF₆.

Prototipo 0 per il recupero del SF₆

Simulazione del prototipo 0

Attualmente all'exhaust del R134a è connesso il prototipo I, (descritto sopra) costituito da due buffer uno freddo e uno caldo. Con questo sistema già installato si vuole testare se scendendo ancora in temperatura sotto i -50 °C si ha una condensazione totale del freon e dell'isobutano che liquefano rispettivamente a -11°C e a -26°C, ben prima, in modo da avere poi in fase gas solo SF₆ e qualche traccia di N₂. Il test, servirà a studiare da un punto di vista sperimentale quanto è possibile concentrare la miscela in SF₆, con un singolo stadio di distillazione. Altro scopo del test è quello di studiare le proprietà chimico-fisiche che caratterizzano il sistema multicomponente, per poter comprendere le interazioni che le molecole dei singoli componenti hanno tra di loro. Per via di varie problematiche inerenti all'installazione del sistema, il test sperimentale non è stato tutt'ora effettuato, e infatti i risultati sperimentali di questo test non verranno presentati nella tesi.

E' stato comunque effettuato un lavoro di simulazione con il software Aspen Plus, al fine di verificare quando i risultati della simulazione siano mimici delle condizioni reali. Per la simulazione, sono stati selezionati i componenti della miscela ed è stato scelto il metodo termodinamico di tipo REFPROP. La scelta di questo modello termodinamico è stata effettuata in quanto, nella miscela in esame vi è presente per la maggior parte R134a (79%) un gas refrigerante. Aspen, consiglia la scelta di questo modello ove siano presenti gas refrigeranti. Per la simulazione è stato selezionato un singolo flash, la temperatura e la pressione in ingresso, sono quelle reali 95 l/hr alla pressione di 1,2 bara. Dalle analisi di sensitività si è voluto valutare quale variabili influenzano di più la purezza del SF₆ ed è stato visto che:

- La portata e la pressione della miscela in ingresso, non influenza in alcun modo la purezza dell'SF₆
- al variare della pressione del Buffer si nota invece che il più alto valore di molar fraction in SF₆ viene raggiunto a una pressione di 0.8 bara
- al variare della temperatura del Buffer, la purezza in SF₆ aumenta.

Nella tabella 5.2, vengono mostrate le condizioni ottimali da impostare in Aspen, per avere la più alta purezza possibile in SF₆. Settando quindi, queste condizioni, si ottiene una purezza del 11.4% del SF₆ da un 1.3% iniziale, in testa al buffer, più precisamente, nella corrente del vapore.

Infine, sono stati valutati recupero, rapporto di distillato rispetto all'alimentazione, temperatura del vapore e il calore scambiato al buffer. Nella tabella 5.4, i principali risultati vengono riassunti e si evidenzia che il D/F è molto basso, e il recupero molare è intorno al 44%. Di conseguenza, visti i risultati per un singolo stadio si è voluto fare un'analisi di sensitività con due flash posti in serie. Si è quindi riscontrato che alimentando al secondo buffer, la corrente di testa del primo buffer, una portata costante di 4 l/h alla temperatura di -40 gradi viene alimentata al secondo buffer. Quest'ultimo è tenuto a una temperatura di -66 gradi alla pressione di 0.4 bara. Con questa configurazione la composizione dell'SF₆ in testa al secondo buffer passa da 11.4% a 28.7% nella tabella 5.7, vengono specificate le composizioni degli altri componenti della miscela.

Anche per quest'ultimo buffer vengono calcolati rapporto di distillato rispetto all'alimentazione, recupero molare del SF₆ e Calore scambiato al buffer, i risultati sono riassunti nella tabella 5.8. In questo caso, il D/F è pari al 33% e il recupero molare pari al 84%, il calore scambiato al buffer invece, risulta essere nettamente più basso, questo è normale in quanto le portate risultano essere sensibilmente ridotte. Infine,

è stata inoltre valutata la produttività e il recupero molare totale dei due buffer i valori di questi ultimi, sono rispettivamente 1.6% e 37%.

Prototipo 0

Il prototipo 0 è un sistema di recupero che verrà sperimentato per testare la separazione del SF₆ dalla miscela di R134a, iC₄H₁₀ e N₂. Questo sistema, è stato inizialmente costruito e implementato per il recupero del R134a. Il sistema di recupero è composto da tre componenti principali (Figura 5.6): uno scambiatore di calore, un buffer freddo verticale e un buffer caldo orizzontale. Il sistema riceve una miscela di R134a (79%), iC₄H₁₀ (19%) e SF₆ (1,3%) a 20°C dalla linea dell'esausto del recupero dell'R134a. Dopo aver attraversato il primo scambiatore di calore, la miscela liquefatta riempie il Buffer 2, dove il livello del liquido è controllato da un sensore di livello. A causa della differenza di punti di ebollizione tra SF₆ (-67,6°C a 1 bar) e gli altri due componenti, R134a (-26°C a 1 bar) e iC₄H₁₀ (-11°C a 1 bar), la temperatura del Buffer 1 è impostata a -45°C. Ci si aspetta che tutti i componenti tranne l'SF₆ condensino, quindi SF₆ uscirà dal sistema attraverso la valvola Zimmerli, PCV-002 (vedi Appendice G.1 per riferimenti). Inoltre, una frazione di isobutano e R134a esce dal sistema come miscela azeotropica, rappresentando il componente più volatile a causa del suo punto di ebollizione inferiore rispetto a quello del R134a puro (-32,3°C e -26,4°C, rispettivamente, a 1 bar).

Il monitoraggio della composizione è essenziale, è quindi necessario mandare tutto il gas esausto dalla Zimmerly valve all'analisi del GC.

La miscela liquefatta poi scende fino al fondo del buffer, dove la temperatura supera i 0°C, causando l'evaporazione. Infine, l'unità del compressore pompa il gas separato nella linea di scarico. Tutti i vari componenti/sensori sono elencati nel dettaglio nella tabella 5.10.

Proprietà termodinamiche della miscela gassosa

Al fine di comprendere meglio le caratteristiche chimico fisiche della miscela in esame, uno studio termodinamico è stato effettuato. Per poter far ciò, si è voluto analizzare i diagrammi binari delle varie coppie di componenti. Questo, naturalmente risulta essere una semplificazione rispetto alla situazione reale. Ma è comunque stata effettuata in quanto in letteratura non sono presenti informazioni rispetto alla miscela ternaria in esame.

Ne sono quindi stati innanzitutto studiati i coefficienti di attività delle coppie SF₆/R134a, R134a/iC₄H₁₀ e SF₆/iC₄H₁₀ dai grafici presentati in 6.2, si vede che sia la coppia SF₆/R134a, che la coppia SF₆/iC₄H₁₀ hanno coefficiente di attività unitario, quindi presentano un comportamento ideale, la stessa cosa non può essere detta per la miscela R134a/iC₄H₁₀, (coefficiente di attività = 3), i quali formando un azeotropo di minima, non presentano quindi un comportamento ideale. In seguito, è stata effettuata un'analisi dei diagrammi binari per i due componenti chiave SF₆/R134a a pressione costante (T_{xy}) 6.5.

L'analisi inizia con il diagramma binario dei componenti chiave da distillare e dell'altro componente presente in maggior quantità, nel nostro caso SF₆ e R134a. Dall'esame della Figura 6.5, è emerso che la temperatura varia da 0 a -70°C alla pressione di 1 bar. Raggiungere queste temperature richiederebbe una grande quantità di raffreddamento, con conseguenti costi operativi elevati. Per mitigare questo problema, è stata selezionata una pressione di lavoro di 3 bar.

Considerando che la composizione della miscela in ingresso è stata menzionata nella sezione precedente (fare riferimento alla Tabella 5.1 per dettagli), per l'analisi binaria sciammo le nuove composizioni considerando la somma delle due composizioni (79% di R134a e 1,3% di SF₆), portandole quindi su una base dell'80,3%. Questo si traduce in 1,6% di SF₆ e 98,4% di R134a. Esaminando il diagramma binario a questa composizione, possiamo vedere che con il 1,6% a una temperatura di -7,5°C, ci troviamo nella regione bifasica con la composizione di equilibrio menzionata di seguito: 6.3: possiamo quindi dividere la frazione liquida e la frazione di vapore a questa temperatura per avere una fase liquida e una fase di vapore a questa composizione di equilibrio. La fase vapore è più ricca in SF₆ rispetto a quella liquida, questo significa che quando viene effettuata la separazione alla temperatura di equilibrio, la fase gassosa sarà quella recuperata perché più concentrata in SF₆.

Approccio di McCabe-Thiele per la determinazione del numero di stadi ideali dalla miscela SF₆/N₂

. Per semplificare il problema, si è voluto effettuare una valutazione del numero degli stadi ideali per la separazione dei due componenti chiave in esame l'SF₆ e l'N₂. È stato quindi utilizzato l'approccio di McCabe-Thiele per la determinazione del numero di stadi ideali. La composizione della miscela in esame è la stessa (R134a (98.4%), e SF₆ (1.6%) a 20°C alla pressione di ingresso di 3 bar). Le specifiche di progetto sono, frazione del distillato $x_d = 0,99$ e un recupero molare del 70%.

Successivamente, assumiamo che la miscela si comporta come un vapore saturo, e quindi si setta la q (retta di alimentazione) uguale a zero. Per determinare il numero di stadi ideali sono state utilizzate le equazioni dalla 6.4 alla 6.8, in maniera iterativa, un codice Matlab è stato quindi scritto per calcolare agevolmente le iterazioni nell'appendice I.1. Per la distillazione, in totale sono stati identificati sette stadi, sei nella zona di rettifica e una nella zona di strippaggio, con alimentazione al sesto stadio. Evidentemente, il risultato ottenuto di sette stadi ideali (considerando un'efficienza di stadio del 100%) ci aiuta a capire quanti stadi ci sarebbero in una colonna di distillazione ipotetica se la separazione fosse ideale e coinvolgesse solo i due componenti chiave. Per un sistema multicomponente come il nostro, l'approssimazione utilizzata da McCabe-Thiele non è esaustiva ma, funge da un buon punto di partenza per lo studio della separazione binaria di questi due componenti.

Diagramma ternario SF₆/R134a/iC₄H₁₀

In questa sezione, verrà spiegato e rappresentato il diagramma ternario per i tre componenti SF₆/R134a/isobutano. La lettura e la comprensione di questo diagramma ternario ci permetteranno di capire i limiti che abbiamo nella nostra distillazione azeotropica. Analizzando la figura 6.7, vediamo che il vertice del diagramma ternario è occupato da R134a, che ha una temperatura di ebollizione situata tra gli altri due componenti. L'isobutano occupa il vertice in basso a sinistra con il punto di ebollizione più alto, mentre SF₆ è situato in basso a destra con un punto di ebollizione intermedio.

Successivamente, segniamo un altro punto significativo sulla linea R134a-isobutano alla composizione dell'azeotropo. Da questo punto, disegniamo una linea retta fino a che non interseca il componente chiave leggero nel vertice in basso a destra del diagramma ternario (vedi Figura 6.4). Si posiziona quindi l'azeotropo omogeneo a basso punto di ebollizione con una composizione 81,6% - 18,4%.

In seguito, identifichiamo i nodi stabili, i punti di sella e i nodi instabili nel diagramma ternario. Nel nostro caso, consideriamo un equilibrio liquido-vapore-liquido (VLL). Qui abbiamo due nodi stabili, un punto di sella e un nodo instabile.

Successivamente, tracciamo le curve residue identificate dal software Aspen Plus. Queste curve illustrano la variazione della composizione del liquido durante il processo di ebollizione della miscela, assumendo una distillazione discontinua (vedi Figura 6.9). Identificare la curva dei residui appropriata ci consente di stabilire la composizione del distillato secondo le specifiche richieste. Ad esempio, per i tre componenti nel nostro sistema, abbiamo una miscela gassosa con una composizione di alimentazione dettagliata nella tabella 6.2.

Si posiziona quindi il punto di alimentazione lungo la curva dei residui appropriata e si imposta la composizione del distillato in uscita, assicurandoci che questi due punti giacciono sulla stessa curva del residuo. Si connettono questi due punti e si estende la linea fino a che non interseca il limite definito dal diagramma. Questo, assicura che anche la composizione del prodotto di fondo sia determinata lungo l'intersezione della linea operativa e della curva dei residui. Dalle curve dei residui possiamo dedurre informazioni importanti: innanzitutto, è evidente che l'alimentazione è molto vicina al ribollitore. Questo posizionamento è logico perché, come menzionato da Henry Z. Kister nel suo libro "Distillation Design", più vicino è l'alimentazione al ribollitore, più difficile è la separazione, e posizionare l'alimentazione più vicino aiuta a ottenere una migliore separazione.

Dalla tabella 6.5, si nota come la composizione dell'alimentazione e del ribollitore siano molto simili tra di loro. Questo, si verifica in quanto l'alimentazione è posizionata nello stadio superiore al ribollitore. Pertanto, questo aspetto deve essere adeguatamente considerato durante le fasi di progettazione e dimensionamento della colonna di distillazione.

Progettazione e simulazione del sistema di recupero del SF₆

In questa sezione, verrà riassunta la metodologia e la strategia utilizzata per simulare e progettare il sistema di recupero del SF₆.

Il sistema è diviso in tre grandi sezioni : sezione di accumulo e di pompaggio, sezione di distillazione e sezione di stoccaggio.

Sezione di accumulo e di pompaggio

Nella sezione di accumulo, il gas dall'esausto del sistema di recupero del R134a viene interamente convogliato in un tank dal volume di 1 m³ attraverso una valvola tre vie, questa può essere direzionata o verso il tank oppure alla linea di spurgo nel caso sia necessario spurgare il sistema con azoto. Prima di entrare nel tank il gas incontra una linea di analisi GC dove, viene controllata la composizione del gas in ingresso.

Il tank ha la funzione di equalizzare la composizione del gas siccome dall'exhaust del R134a arriva una miscela in flusso e composizione non costante. La pressione in quest'ultimo viene monitorata attraverso dei sensori di pressione. Inoltre, in protezione al tank, sono installate delle valvole di sicurezza, queste si aprono nel caso si raggiunga una certa pressione di set point. Discuteremo ora delle due differenti fasi:

- **Fase di Accumulo** : La miscela gassosa proveniente dall'esausto del R134a recupero viene convogliata nel tank, qui un ipotetico problema si potrebbe riscontrare, ovvero per convogliare il gas nel tank sarebbe ottimale avere un compressore che spinga il gas nel tank, ma questo non può essere montato sulla linea dell'esausto, in quanto andrebbe a influenzare notevolmente il recupero dell'R134a. Questo perchè in ogni colonna del recupero del freon vi è una pressione settata alla quale si apre la zimmerly compresa tra 20 e 50, se si posiziona il compressore nella linea dell'esausto del R134a, l'apertura della zimmerly sarebbe alterata, e questo influenzerebbe la qualità del recupero. Il flusso di gas a bassa pressione potrebbe quindi incontrare degli ostacoli per poter entrare nel tank.
- **Fase di Pompaggio** : Dopo la sezione di accumulo, si entra nella sezione di pompaggio, subito dopo il tank il gas viene mandato in un compressore dove la pressione viene aumentata da 1 a 3 bar, dei sensori di pressioni sono posizionati prima e dopo l'apparecchio per monitorarne in continuo la pressione. In seguito, la miscela, viene mandata attraverso un regolatore di flusso, dove viene regolata la portata in ingresso alla colonna a 95 l/hr.

Sezione di distillazione

Successivamente alla sezione di accumulo e pompaggio si entra nella sezione di distillazione, la portata di 95 l/hr viene quindi mandata in ingresso alla colonna, e qui la separazione ha inizio. La colonna uno, opera con una temperatura compresa fra gli 0 e i-6 gradi , qui il primo stadio della separazione ha atto. La linea di testa della colonna 1 viene quindi utilizzata come alimentazione per la seconda colonna, qui il secondo stadio della separazione alla temperatura di -50/-60 °C e alla pressione di 3 bar ha luogo. Il distillato di questa colonna, viene infine mandato nella sezione di stoccaggio.

Sezione di stoccaggio

In seguito alla sezione di distillazione, si entra nella sezione di stoccaggio, in quest'ultima sezione, si immette il distillato in un tank e successivamente in un compressore ad alta pressione, il quale comprime la miscela da 3 a 30 bar, qui la miscela viene immessa in una bombola ad alta pressione. Infine, la miscela stoccata viene poi mandata in una membrana per la separazione di SF₆/N₂.

Simulazione delle due colonne con ASPEN Plus

Al fine di massimizzare purezza e recupero delle sensitivity analysis sono state effettuate per ottimizzare quest'ultime. In particolare, sono state indagate quale fossero le variabili operative che più influenzano la purezza e il recupero molare dell'SF₆. Tra queste:

- Numero di stadi : si è analizzata la variazione della purezza in funzione del numero di stadi, si è quindi visto che dopo 10 stadi la purezza molare del SF₆ non cambia, di conseguenza verrà selezionato un numero di stadi pari a 10.
- Boilup Ratio : il Boil up ratio è definito come il rapporto di liquido evaporato rimandato in colonna rispetto alla portata di liquido estratta dalla colonna, esso varia tra 0 e 1 . Dove un boilup ratio di 0 indica che tutto il liquido viene rimandato al ribollitore e poi al flusso di uscita, viceversa un boilup ratio di 1 vuol dire che tutto il liquido, viene bollito e rimandato in colonna. Dall’analisi di sensitività si nota che all’aumentare del boilup ratio la purezza del SF₆ aumenta, viene quindi selezionato un boilup ratio di 0.8.
- stadio di alimentazione: dalla sensitivity analysis si è visto che più lo stadio di alimentazione si avvicina al ribollitore più la qualità del recuperato viene aumentata. Viene quindi selezionato come stadio di alimentazione il nono quello subito prima del ribollitore
- rapporto di riflusso: è il parametro più influenzante per aumentare la purezza molare del componente di interesse. Per la prima colonna, all’aumentare del rapporto di riflusso, una purezza crescente viene raggiunta, mentre il recupero molare rimane pressoché costante. Viene quindi selezionato un rapporto di riflusso pari a 20. Viceversa, nella seconda colonna, il rapporti di riflusso selezionato è di 13. Questo perché il trend della purezza e del recupero molare non è analogo, e il miglior compromesso tra le due variabili viene raggiunto a questo rapporto di riflusso. Si è inoltre visto che all’aumentare di quest’ultimo, la spesa termica al condensatore e al ribollitore aumenta.

Nelle tabelle 7.2 e 7.3 vengono riassunte tutti i risultati delle variabili sopra elencate, per il raggiungimento delle migliori condizioni in colonna. In particolare, per la prima colonna si evince che il rapporto di distillato rispetto all’alimentazione è solo di 0,09 mentre il recupero molare è del 95% , mentre la purezza molare è del 14%. Invece, per la seconda colonna il distillato to feed ratio è di 0,14 mentre il recupero molare è del 79% e la purezza del SF₆ è del 73%.

Dimensionamento delle colonne di distillazione

Terminata l’analisi di sensitività, si può quindi effettuare il dimensionamento delle colonne di distillazione. Per prima cosa, si definiscono le condizioni della portata in ingresso (riferirsi alla tabella 7.1). Successivamente verrà scelto il tipo di condensatore, verrà determinato il profilo idraulico e di pressione all’interno della colonna.

Si sceglie di operare con un condensatore parziale, in quanto, la scelta di quest’ultimo riduce il carico termico a esso fornito, e ci permette di trattare quest’ultimo come stadio di equilibrio.

In aggiunta, si assume inizialmente una perdita di pressione costante di 50 mbar tra il punto di alimentazione e il condensatore della colonna. Si assume, che la prima colonna operi in condizioni adiabatiche e che quindi i calori scambiati al ribollitore e condensatore siano rispettivamente di 59 W e -131W. Nella prima colonna la condensazione parziale al condensatore avviene alla temperatura di -6,07 bar alla pressione di 3 bar, per raggiungere tali condizioni sarà sufficiente un LAUDA o un HUBER MINISTAT. Raggiunto lo stazionario, le condizioni nella prima colonna si stabilizzano e si registrano nel distillato le composizioni elencate in tabella 7.5.

Il distillato della prima colonna, viene quindi immesso nella seconda colonna, qui il secondo della separazione ha inizio come già spiegato nelle sezioni precedenti. Nella tabella7.6, vengono mostrate le condizioni della miscela in ingresso alla seconda colonna. Le stesse assunzioni fatte per la prima colonna, vengono riproposte per la seconda colonna. Sebbene per la seconda colonna si debba raggiungere una temperatura molto più bassa di -55°C, il calore scambiato al condensatore e al ribollitore della colonna risulta sensibilmente ridotto, (5.1 W e -11 W rispettivamente), in quanto le portate coinvolte sono sensibilmente ridotte. Raggiunto lo stazionario, le composizioni del distillato sono elencate nella tabella 7.7. Con queste considerazioni in mente, si passa quindi al dimensionamento della colonna di distillazione. Si è scelto di utilizzare una colonna impaccata, in quanto, le portate sono molto piccole e i diametri della colonna sono nell’ordine dei centimetri. Il dimensionamento viene diviso in tre parti principali :

- selezione di un diametro appropriato, e nella determinazione di portate di vapore e di liquido appropriate per ogni stadio.
- scelta di un impaccamento e analisi del profilo idraulico e di pressione all’interno della colonna

- dalle perdite di carico, determinare un'efficienza del riempimento e stimare altezza della colonna.

Il diametro della colonna (D_c) è stato fissato a 3 cm, le portate volumetriche della fase liquida V_L , della fase vapore V_v e l'F-factor (fattore caratteristico del riempimento), vengono determinate utilizzando le equazioni da 7.2 a 7.4. Successivamente, viene selezionato un riempimento appropriato. Il riempimento scelto è il modello DX di Sulzer Chemtech AG. Le proprietà del riempimento e le curve caratteristiche sono riportate nella Tabella 7.8 e nelle Figure 7.10b e 7.7. La Figura 7.7 mostra HETP/m in funzione del F-factor, un parametro cruciale per determinare l'altezza del letto di riempimento (Z). Per calcolare Z :

- Scegliere un valore iniziale della perdita di carico.
- Valutare l'F-factor.
- Trovare HETP corrispondente dalla Figura 7.7
- Calcolare l'altezza totale del riempimento con l'Equazione 7.5.

La perdita di pressione totale (ΔP) si calcola moltiplicando le perdite di pressione per metro ($\Delta P/Z$) per l'altezza totale del letto di riempimento (Z) usando l'Equazione 7.7. Si esegue quindi il processo in maniera iterativa, poiché l'F-factor è funzione della velocità e della densità del gas, che a loro volta dipendono dalla pressione operativa della colonna. Per iterare questo processo, viene utilizzato il software Aspen Plus, aggiornando le perdite di carico e calcolando un valore medio del F-factor. Con un F-factor di 0,25, si ottiene un HETP di circa 0,03-0,04 m. La simulazione finale determina un'altezza teorica del riempimento di 0,05 m. Inoltre, per garantire precisione e margine di sicurezza:

- Raddoppiare l'altezza teorica a 1 m.
- Aumentare ulteriormente del 25% per garantire una distribuzione adeguata del liquido e del gas, ottenendo un'altezza di 0,5 m.
- Aggiungere 0,1 m per il distributore di liquido e supporto per il riempimento.
- Calcolare l'altezza relativa all'hold-up di liquido con un tempo di residenza di 5 minuti, ottenendo 0,3 m.
- Aggiungere 0,3 m sopra e sotto il riempimento per uniformità del flusso, raggiungendo un'altezza totale di 1 m.

In sintesi, un'altezza totale dell'impaccamento di 0,3 m è stata calcolata, con un'altezza totale della colonna di 1,5 m. In seguito, un procedimento analogo viene eseguito per dimensionare la seconda colonna, di seguito ne vengono riassunti i risultati. L'altezza teorica per stadio è stata stimata essere di 0,0321 m per stadio. Quindi, l'altezza totale HETP ammonta a 0,4 (m). Tutti i 5 step sopra elencati devono essere ripetuti. In sintesi, per la seconda colonna, si ha un'altezza totale dell'impaccamento di 0,3 m (HETP). L'altezza totale stimata della colonna è di 1,5 m.

Dimensionamento del condensatore e del ribollitore

Condensatore Il condensatore riceve vapore dal secondo stadio, con flussi di distillato e riflusso in uscita. Le condizioni operative sono riportate nella Tabella 7.13 e il sistema è mostrato nella Figura 7.13. Una simulazione "shortcut" utilizza etanolo come refrigerante a -80°C e 1 bar, con una temperatura di "pinch" di 20°C e un coefficiente di scambio termico di $340 \text{ W/m}^2\text{K}$. L'area di scambio termico richiesta è di $0,02 \text{ m}^2$ con una portata di refrigerante di $0,7 \text{ kmol/h}$. Per quanto riguarda il condensatore, è stato assunto un tempo di residenza del liquido nel condensatore di 15 minuti, possiamo quindi stimare il volume di liquido occupato in condizioni standard. Assumendo che il volume di liquido riempie il 30% del volume totale disponibile sotto queste condizioni, si dimensiona il condensatore utilizzando le equazioni 7.7 e 7.8. Il volume del liquido nel serbatoio di riflusso, indicato come V_{reflux} , è determinato dal tempo di residenza (τ_{RD}) e dalle dimensioni del serbatoio di riflusso, in particolare la sua altezza (H_{RD}) e il diametro interno (D_{RD}). Questo calcolo, utilizza il volume totale del serbatoio di riflusso (V_{RD}) come riportato nella Tabella 7.14.

Nel caso in cui il refrigerante liquido fornito allo scambiatore di calore si rivelasse insufficiente, viene fornito un volume aggiuntivo della camicia di raffreddamento per garantire una capacità di raffreddamento ottimale **Ribollitore**. Il ribollitore viene dimensionato per occupare circa il 30% del volume totale disponibile, con un tempo di residenza di 15 minuti. Le dimensioni e la geometria sono illustrate nella tabella 7.14. Per il condensatore è stata quindi calcolato un diametro di 0.17 (m) e un'altezza del serbatoio di 0.3 (m), mentre, per il ribollitore un'altezza di 0.5 (m) è stata selezionata con un diametro di 0.22 (m).

La stessa procedura viene ripetuta per calcolare il condensatore e ribollitore della seconda colonna, i risultati vengono quindi riassunti nella tabella 7.16. Il diametro, l'altezza del condensatore e del ribollitore dimensionati per la seconda colonna sono pressoché identici e valgono rispettivamente 0.1 m e 0.2 m. Completato il dimensionamento delle colonne, i risultati dell'intero processo di distillazione vengono riassunti nella tabella 7.17.

Logica di controllo dell'impianto

La descrizione inizia con l'introduzione della prima colonna di distillazione dell'impianto. La seconda colonna opererà con la stessa metodologia di controllo, quindi non è necessaria un'ulteriore elaborazione.

All'ingresso del sistema, il gas incontra il regolatore di flusso di massa (XMFC-10180), che garantisce una portata di 95 l/h. Prima dell'ingresso in colonna è situata una linea di analisi W2 per controllare la composizione della colonna in ingresso.

Il gas viene alimentato al nono stadio della prima colonna alla temperatura di 20°C e alla pressione di 3 bar. All'interno di essa, la temperatura varia tra -6°C e -0,5°C, questa è monitorata da diverse termocoppie posizionate strategicamente.

La regolazione della pressione nella colonna è facilitata dal sensore di pressione (PI-10276) posizionato all'apice della colonna. In caso di allagamento o intasamento, che potrebbe portare a sovrappressione, vengono attuate misure protettive. Due valvole di sicurezza (PSV-10232 e PSV-10233) sono installate nella parte superiore sinistra della colonna e si aprono automaticamente al raggiungimento della soglia di pressione preimpostata.

Passando alla sezione di rettifica, il gas viene diretto allo scambiatore di calore, dove la miscela di gas viene raffreddata da -3°C a -6°C. La temperatura prima e dopo lo scambiatore di calore è monitorata da due emettitori di temperatura (TE-102810 e TE-102813). Successivamente, il gas viene diretto nel condensatore.

La regolazione del rapporto di riflusso per raggiungere la composizione desiderata prevede due strategie:

- La prima strategia prevede il monitoraggio continuo della composizione del flusso liquido in uscita dal condensatore. Un gascromatografo (GC) monitora la composizione della corrente riflussata in continuo (linea L22). Il monitoraggio continua fino al raggiungimento della composizione desiderata, momento in cui si apre una valvola pneumatica (YV-101236) nella corrente del distillato (vedi Figura 7.21).
- La seconda configurazione, mostrata in Figura 7.20, prevede il controllo del condensatore utilizzando un sensore di livello del liquido (LSH-10281) e una valvola Zimmerly (PCV-10257) nella linea di scarico del condensatore. Il monitoraggio della pressione è facilitato dal trasmettitore di pressione (PT-10278). La logica è impostare la valvola Zimmerly a un valore di pressione presetato, che la fa aprire alla pressione specificata. Questa configurazione mira a ottenere un livello di purezza desiderato, regolando la quantità di liquido reimpresso nella colonna di distillazione. Per questo scopo, è necessario un regolatore di flusso di massa.

Confrontando le due configurazioni, la prima (Figura 7.21) è più efficiente per controllare la composizione desiderata, ma ha un costo più elevato. Invece la seconda, è più economica ma meno efficiente (circa 30kCHF di differenza). Visto il budget disponibile per il costo dell'intero impianto, si opta per la seconda soluzione, sebbene meno accurata.

R&D di una membrana per la separazione della miscela SF₆/N₂

. Nella sezione precedente, è stata condotta un'analisi approfondita sul dimensionamento delle due colonne di distillazione in serie nel nostro impianto, considerando le specifiche del progetto. È stato stabilito che alla fine del secondo stadio della colonna di distillazione si ottiene 1 l/h di gas con la composizione riportata nella Tabella 7.7. Quest'ultima viene poi stoccata in una bombola alla pressione di 30 bar.

Come evidente, al termine del secondo stadio di distillazione si ottiene una miscela di SF₆/N₂ che necessita di ulteriore concentrazione. Questa sezione si concentra sugli sforzi di ricerca e sviluppo intrapresi in laboratorio per determinare la fattibilità della separazione della miscela SF₆/N₂ utilizzando la membrana in poliammide a fibra cava prodotta dalla UBE Corporation. Nella sezione successiva verranno quindi fornite ulteriori spiegazioni sulla procedura sperimentale e sui risultati.

Modellazione della membrana

Prima di entrare nella descrizione della modellazione della membrana, si vuole esaminare la variazione della pressione della membrana, dall'alimentazione al permeato della membrana (vedi Figura 7.23). Una miscela di gas ad alta pressione a p_r viene alimentata, mentre il permeato viene rimosso a una pressione più bassa p_p sul lato a valle. Il profilo di pressione all'interno della membrana è assunto costante e uguale a p_r . La diffusione attraverso la sezione trasversale è trascurata. La permeabilità, la pressione di alimentazione e quella di ritenzione sono considerate costanti su tutta l'area della membrana. Con queste ipotesi in mente, l'equazione di bilancio utilizza è la 7.14. Dove :

- dn_{N_2} è la portata molare differenziale di N₂.
- dn_{SF_6} è la portata molare differenziale di SF₆.
- F_{N_2} è la portata molare di N₂ espressa in $\frac{kmol}{h}$.
- F_{SF_6} è la portata molare di SF₆ espressa in $\frac{kmol}{h}$.
- p_{SF_6} è il coefficiente di permeabilità di SF₆ espresso in $\frac{kmol}{h \times bar \times m^2}$.
- p_{N_2} è il coefficiente di permeabilità di N₂ espresso in $\frac{kmol}{h \times bar \times m^2}$.
- dA è l'area differenziale ed è espressa in (m^2).
- x_f e y_f sono le composizioni molari rispettivamente nella regione di alimentazione e nel permeato.
- x_p e y_p sono le composizioni molari rispettivamente nella regione di alimentazione e nel permeato.

Per risolvere il problema di modellazione, è necessario risolvere il sistema di equazioni differenziali lineari 7.14, e per farlo dobbiamo impostare le nostre condizioni al contorno. Le condizioni al contorno saranno le seguenti:

- per $A = 0$ $n_{SF_6} = 0.00415 \frac{kmol}{h}$.
- per $A = 0$ $n_{N_2} = 0.001247 \frac{kmol}{h}$.

Nella figura 7.24 è fornito uno schema per comprendere come la membrana è discretizzata. Inoltre, per affrontare questo problema, è importante determinare i valori di permeabilità dei due gas attraverso la membrana, denominati p_{SF_6} e p_{N_2} . Questi valori rappresentano le chilo moli totali permeate attraverso la membrana in un'ora per unità di area, sotto una pressione di 1 bar, e sono espressi come $\frac{kmol}{h \times bar \times m^2}$. Inoltre, la pressione di alimentazione p_f e la pressione del permeato p_p , insieme alle composizioni dei gas nei lati di alimentazione e permeato, sono parametri essenziali per risolvere questo problema.

I coefficienti di permeabilità sono ottenuti dalla letteratura [23], mentre tutti gli altri parametri elencati nella tabella sono scelti per mimare da vicino le condizioni sperimentali reali. Un riassunto di queste informazioni è fornito nella Tabella 7.17. Con tutti questi dati di input, l'equazione differenziale del primo ordine a variabili separabili 7.14 può essere risolta numericamente. La soluzione dell'equazione differenziale è riportata nella figura 7.25: I risultati indicano chiaramente che l'efficienza di recupero

del gas SF₆ raggiunge quasi il 65% con una purezza superiore al 92% a un'area equivalente di 8 (m²). E' interessante notare che oltre questo valore di area equivalente, l'efficienza di separazione non migliora.

Considerando questi risultati, è evidente che aumentare l'area non migliora significativamente il processo di separazione. Pertanto, per la nostra applicazione, opteremo per un'area di permeazione equivalente a quella della membrana stessa.

Nella prossima sezione, i test sperimentali condotti con la membrana saranno utili per confrontare i dati simulati con i risultati sperimentali.

R&S di una membrana per la separazione della miscela SF₆, N₂

In questa sezione, descriveremo l'attività di R&S svolta in laboratorio per testare le prestazioni di separazione della membrana.

Per il test, è stata utilizzata una membrana in poliammide a fibre cave nel nostro sistema. L'obiettivo dell'esperimento è verificare se la membrana UBE, ottimizzata per la separazione della CO₂ (vedi Figura 8.1) separa anche una miscela di N₂ SF₆, mantenendo un rapporto costante dei due componenti ma variando la portata di alimentazione e la pressione del ritentato. Si è voluto effettuare il test, in quanto in letteratura, veniva citato che la CO₂ ha un comportamento simile all'SF₆ in membrana.

Per condurre i test, è stato prima assemblato un set up sperimentale, il cui P&ID è fornito per una chiara comprensione nella Figura 8.2.

In questo set-up, i due gas SF₆ e N₂ vengono mandati in due linee separate. La pressione dei gas viene controllata attraverso due regolatori di pressioni separati, nel P&ID saranno denominati con la sigla PCV. Dopo la PCV, un rotometro regola il flusso, e un flussimetro misura la portata.

I gas, sono quindi mescolati in un buffer. Prima dell'ingresso della membrana, è installato un sensore di pressione per monitorare la pressione. All'uscita della membrana, sono posizionati rispettivamente un secondo sensore di pressione e un flussimetro per misurare la pressione e la portata.

Sul lato del ritentato, è implementato un ricircolo per ricircolare il gas. Per creare il necessario differenziale di pressione (ΔP) tra l'ingresso e il lato del ritentato, è necessaria una pressione negativa. Questa, viene generata da una pompa a vuoto situata all'uscita del ritentato. Un buffer di equalizzazione è posto all'uscita della pompa per evitare fluttuazioni che potrebbero essere registrate dal flussimetro posto in serie. Il gas, viene poi ricircolato nel buffer di miscelazione.

Questa configurazione iniziale, purtroppo risulta essere inefficace. Questo perchè il flusso di ricircolo è collegato dalla linea di scarico alla linea di aspirazione per regolare la pressione sul lato del ritentato. Tuttavia, l'aspirazione della pompa è troppo forte, causando l'aspirazione di tutto il flusso nella pompa a vuoto 8.2.

Per la configurazione corretta adottata per il test sperimentale. Nella Figura 8.3, è presentata la configurazione finale utilizzata in laboratorio.

Questa configurazione ha risolto il problema del ricircolo del gas nella linea di aspirazione installando una valvola ad ago molto piccola (4 mm) nel lato del ritentato, denominata HV-10142. Questa valvola è più sensibile alla regolazione della pressione sul lato del ritentato. Il principio di funzionamento rimane quasi lo stesso, con la principale differenza che non c'è ricircolo sul lato del ritentato.

In questa configurazione, il bilancio di massa dei tre flussi è mantenuto. Di seguito è riportata una tabella che fornisce una comprensione delle attrezzature presenti nel P&ID 8.1. Per una comprensione più chiara, si fa riferimento a una figura del setup montato in laboratorio 8.4.

Nella prossima sottosezione, discuteremo i test sperimentali eseguiti con la membrana.

Test sperimentali

In questa sezione, descriveremo in dettaglio i test sperimentali condotti con la membrana.

I test sono stati eseguiti a varie portate e a diverse pressioni del ritentato. Con questo, vogliamo testare quali parametri influenzano maggiormente la separazione della membrana e se ci sono parametri più influenti di altri.

Dato che il processo della membrana è un processo controllato dalla velocità, ci aspettiamo che il ΔP

(gradiente di pressione) tra il lato di ingresso e il ritentato sia il parametro più influente, 8.2.

Procedura sperimentale

In questa sottosezione viene spiegata la procedura sperimentale dei test. Nella Tabella 8.1, sono riportati tutti gli elementi necessari nel P&ID. Di seguito, forniamo una descrizione dettagliata di questi componenti:

- **Regolatore di pressione con indicatore:** Questi regolatori controllano la pressione del gas. Il PICV-10132 è direttamente collegato alla linea di idrogeno da una fornitura di gas, mentre il PICV-10131 è collegato direttamente al cilindro di SF₆.
- **Rotometro-Regolatore di flusso:** Questi dispositivi indicano e regolano manualmente la portata, regolando la valvola. Anche se tutti sono calibrati in aria, per una misurazione più accurata della portata è necessario un flussimetro. Per i test, viene utilizzato un flussimetro OMRON D6F-10A61-000 (vedi Appendice K.1). Questo ha un range di 0/50 l/min calibrato in aria ed è collegato direttamente a uno Yoctopuce, che invia un segnale elettrico a un PC, consentendo il monitoraggio in tempo reale della portata. Tutti i flussimetri sono calibrati in aria, il che significa che per letture accurate con gas diversi è necessaria una calibrazione con un drycal. Un drycal fornisce una misurazione effettiva del volume del gas iniettato indipendentemente dal tipo di gas. Il flussimetro Omron, calibrato in aria, richiede misurazioni multiple a diverse portate per determinare il volume di gas corrispondente alla portata indicata. Questa tendenza è tipicamente lineare, e le linee di calibrazione per SF₆ e N₂ sono fornite in appendice (vedi Figure J.1 e J.2).
- **Buffer:** Il sistema include due buffer con funzioni diverse: il primo buffer miscela i gas, mentre il secondo smorza le vibrazioni causate dalla pompa a vuoto sul lato del ritentato.
- **Trasmettitori di pressione:** Questi dispositivi rilevano la pressione in punti specifici. Quando sono collegati a un dispositivo Yoctopuce (essenzialmente un Raspberry Pi), rilevano le variazioni della portata del gas proporzionali alla corrente inviata a loro. Se necessario, le variazioni di pressione possono essere monitorate e registrate con il software Yocto-Visualization.
- **Analizzatore di gascromatografo:** Quando si conducono esperimenti con due gas, un gascromatografo è essenziale per determinare la composizione reciproca dei gas. In laboratorio, lo strumento utilizzato per rilevare la variazione nella composizione del gas, quando la miscela binaria viene inviata, è un gascromatografo.

Test a portata costante

In questa sezione, riassumeremo tutti i test sperimentali condotti a portata di ingresso costante ma a diverse pressioni del ritentato, per testare le prestazioni della membrana. Nella sottosezione successiva, riportiamo tutti i test eseguiti e i risultati finali ottenuti dai dati raccolti.

Test 0

Nella Tabella 8.2 è riportato il test sperimentale condotto con la membrana UBE per il gas N₂ a 50 l/h.

Come notato dai risultati sperimentali, il bilancio di massa (7.9) non è esattamente rispettato, a causa di errori nella calibrazione del flussimetro e del fatto che più bassa è la portata, maggiori sono gli errori.

Possiamo quindi stimare rapidamente la permeabilità della membrana calcolando la portata media all'ingresso (7.11) e nel lato del permeato (8.3).

- $\dot{V}_{p,i}$ è la portata volumetrica nel lato del permeato espressa in (l/h).
- $\dot{V}_{f,i}$ è la portata volumetrica nel lato di alimentazione espressa in (l/h).
- N è il numero totale di dati sperimentali.

Nella tabella 8.3 sono riassunte le portate medie del lato di alimentazione e del permeato. Dopodiché, il rapporto di queste due portate calcolate è la permeabilità della membrana (7.7.1). La permeabilità della membrana è solo 0.154, il che significa che solo il 15% del N_2 in ingresso permea attraverso la membrana, mentre il resto non permea. Ciò indica che la membrana è molto inefficiente per la permeazione del N_2 .

Test 1

In questa sezione, condivideremo i risultati dei test condotti in laboratorio con SF_6 a una portata costante di 50 l/h, come riportato nella tabella 8.4.

Come osservato dai risultati sperimentali, il bilancio di massa (7.9) non è esattamente rispettato. Questa discrepanza è attribuita agli errori di taratura nel flussimetro, più evidenti a basse portate. Di conseguenza, possiamo stimare rapidamente la permeabilità della membrana calcolando la portata media nel lato di alimentazione (7.11) e nel lato del permeato (8.3).

Successivamente, il rapporto di queste portate medie ci fornisce la permeabilità della membrana (8.3). Il valore della portata media calcolata è ancora inferiore al precedente, pari a 0,147. Ciò indica che, nella configurazione iniziale, la membrana non è in grado di separare efficacemente i due gas.

Per confermare i risultati ottenuti, verrà eseguito un test a 100 l/h per entrambi i gas N_2 e SF_6 .

Test 2

Nella seguente tabella 8.6 sono presentati i risultati del test sperimentale condotto con la membrana UBE per il gas N_2 a 100 l/h. Come osservato dai risultati sperimentali, il bilancio di massa non è mantenuto con precisione e, per stimare la permeabilità della membrana, dobbiamo calcolare le portate medie sul lato di alimentazione (7.11) e sul lato di permeazione (8.3). Nella tabella seguente, sono riassunte le portate medie per i lati di alimentazione e di permeazione. Successivamente, il rapporto di queste portate calcolate fornisce la permeabilità della membrana, che viene calcolata tramite l'equazione (8.3).

La permeabilità della membrana è 0.159, indicando che solo il 15,9% dell' N_2 in ingresso permea attraverso la membrana, mentre la parte rimanente non viene permeata. Questo suggerisce che la membrana è piuttosto inefficiente per la permeazione dell' N_2 .

Test 3

Questa sottosezione presenta i risultati del test di laboratorio condotto con SF_6 a una portata costante di 100 l/h, con una pressione variabile del retentato come mostrato nella tabella 8.8.

Come osservato dai risultati sperimentali, il bilancio di massa (7.9) non è rispettato a causa di errori di taratura nel misuratore di flusso di massa, più significativi a basse portate. Per stimare la permeabilità della membrana, valutiamo quindi la portata media nel lato di alimentazione e nel lato di permeato (7.11) e (8.3).

Successivamente, il rapporto di queste portate medie fornisce la permeabilità della membrana (8.3). Il valore medio della portata calcolata è pari a 0,147, questo è addirittura inferiore al risultato precedente. Ciò indica che, nella configurazione iniziale, la membrana non è efficace nella separazione dei due gas.

In conclusione, con questo secondo risultato abbiamo confermato che la membrana non è in grado di separare questi due gas.

Come evidenziato da Yang Chuah e Lee nella loro recensione [30], la permeazione di N_2 è più rapida rispetto a quella di SF_6 nelle membrane polimeriche, rendendo le prestazioni delle membrane tipicamente valutate in base alla separazione di N_2/SF_6 [26].

Inoltre, è importante considerare che la permeabilità di N_2 in una membrana è generalmente bassa, e SF_6 ha diametro cinetico maggiore, risultando in una bassa diffusività. La permeabilità può anche

essere definita come il prodotto di solubilità (S) e diffusività (D) di un componente dato, come mostrato nell'Equazione 8.4 [30].

N_2 ha bassa solubilità, mentre SF_6 ha bassa diffusività, il che significa che la permeabilità di questi due componenti nella membrana dovrebbe essere comparabile. Questo è stato verificato nei nostri test sperimentali, dove la permeabilità dei due componenti era quasi la stessa (0,157 per N_2 e 0,148 per SF_6). Pertanto, per una miscela 50/50 di N_2 e SF_6 , determinare la permeabilità come rapporto delle due permeabilità restituisce un valore vicino a 1. Questo valore è coerente con i risultati della letteratura, come mostrato nella Figura 8.5.

Nel confronto tra il modello MATLAB eseguito nel capitolo precedente e i test sperimentali, abbiamo riscontrato una discrepanza. Nel modello di membrana (Figura 7.25), è stato mostrato che dopo una superficie specifica modellata di $8 m^2$, l'efficienza di recupero di SF_6 nel lato del permeato era del 65%. Tuttavia, ciò non è stato verificato sperimentalmente, dove abbiamo osservato un recupero di soli il 17% di SF_6 .

Questa discrepanza è spiegata dalla semplicità del nostro modello MATLAB, che ha considerato solo il gradiente di pressione (ΔP) come forza spingente, trascurando il significativo contributo diffusivo.

Questo significa che l'equazione utilizzata per il modello, che non era corretta, avrebbe dovuto tenere conto del termine diffusivo.

In conclusione, i test R&S condotti con la membrana UBE non sono stati efficaci per la separazione di SF_6/N_2 . Il prossimo passo per i nostri scopi di R&S sarà testare i setacci molecolari 5A e 13X, per esplorare la possibilità di ottenere la separazione desiderata.

Analisi economica sui sistemi di recupero

Viste le condizioni in cui la separazioni deve essere effettuata, risulta sicuramente molto complicato portare a concentrare una miscela diluita all'1% , infatti, a prima vista costruire un sistema per concentrare l' SF_6 , risulta essere sconveniente rispetto al suo abbattimento. Per questo motivo, un intero capitolo è stato dedicato per le spiegazioni alla base della costruzione del sistema di recupero. In più, un'analisi economica è stata effettuata al fine di comparare i costi dei sistemi di recupero a CMS rispetto al sistema di abbattimento.

Sistema di recupero per SF_6 , e costo del fresh

Come già sopra menzionato il sistema di recupero dell' SF_6 è pianificato per essere costruito a CMS, in serie al sistema di recupero del R134a, nella figura 9.1, viene mostrata la sua posizione esatta nel modulo dell'exhaust.

In ingresso al sistema dell'R134a viene mandata la miscela gassosa degli RPC in due configurazioni differenti, a flusso alto 500-600 l/h per 26 settimane all'anno e a basso flusso 100-200 l/h per 24 settimane all'anno. Considerando quindi che la miscela gassosa è quella menzionata nella tabella 2.1, e considerando che l' SF_6 non condensa nel sistema di recupero del R134a, oggi giorno questo viene interamente esausto all'aria. Più precisamente vengono esausti 2,4 l/h in high flow e 1 l/h in low flow, nella tabella 9.1 ne viene mostrato il dettaglio.

In totale quindi, vengono esausti $14 m^3$ all'anno di gas 9.3. Considerando quindi che nel 2024 il costo del fresh è di 617 CHF/kg e che annualmente si consumano al mixer all'incirca 84 kg/anno, la spesa totale di SF_6 è di 52 kCHF/anno. Implementando il recupero del SF_6 , che opera con un'efficienza del 60 %, si risparmiano annualmente all'incirca 31 kCHF anno. Di conseguenza l'implementazione del recupero risulta essere un'ottima scelta, in quanto, l'impianto verrebbe quindi ripagato dopo soli 7 anni. In più, la normativa europea sulle emissioni, prevede di ridurre la distribuzione di SF_6 fino a rimuovere quest'ultimo dal mercato europeo nel 2050, la conseguenza di ciò è che i costi del SF_6 tenderanno sempre più ad aumentare. Per tutti questi motivi recuperare SF_6 risulta fondamentale. Per provare a dare una prospettiva più ampia sui sistemi di recupero si è quindi voluto effettuare un'analisi economica. Quest'ultima è stata svolta per comparare il costo dei sistemi di recupero rispetto al costo di un singolo impianto per abbattimento dei gas fluorinati. In primis, si è stimato il gas consumato negli anni compreso tra il 2012 al 2024 e si è fatta una stima di consumi di gas fino al 2035 9.2. In seguito, è stata stimata la spesa media annua per gas, per ogni periodo LS (Long Shutdown) e RUN, i dettagli di questa spesa, vengono mostrati nella tabella 9.6 per lo stesso periodo 2012-2035. Successivamente, si è effettuata un'analisi sui costi degli impianti di recupero. Il costo capitale (CAPEX) che si spende

nel costruire tutti i sistemi di recupero è di 525 kCHF. Per la loro gestione sono necessari un tecnico e un dottorando 60 kCHF/anno mentre per la manutenzione dell'impianto si spende in totale di 35 kCHF/anno. In più si è evinto che recuperando il gas si arriva a break even dopo 20 anni (2012-2031) questo perchè fino al 2022 solo il recupero del CF_4 era implementato. Dal 2023 con il recupero del R134a che opera con un efficienza del 80% i soldi recuperati si alzano notevolmente, fino ad arrivare al 2025 (anno in cui il recupero del SF_6 verrà implementato). Il costo del fresh consumato e recuperato viene mostrato nella tabella 9.8 Per quanto riguarda il sistema di abbattimento, invece, i costi capitali per la sua intera costruzione sono circa 625 kCHF/anno, mentre il costo annuo per un operatore è di 84 kCHF/anno. La manutenzione annuale è stimata essere di 22 kCHF/anno (costo del gas escluso, nella figura 9.12) Dall'analisi economica si è quindi evinto che dal 2012 al 2025 con i sistemi di recupero vengono recuperati 17200 kg di R134a, 96 kg SF_6 e 6505 kg di CF_4 . I soldi risparmiati in gas recuperato sono circa 455 KCHF. I soldi spesi per la costruzione sono di 525 kCHF mentre i costi per la M&O sono di circa 75kCHF/ anno. Le emissioni di 39000 tCO₂eq/anno. Per contro, per i sistemi di abbattimento i costi di CAPEX e OPEX sono più alti. In più, se si considera che tutto il gas immesso non viene recuperato, ma solo consumato, le spese salgono ulteriormente. Unica voce positiva per i sistemi di abbattimento, sono le emissioni che si aggirano intorno alle 2607 tCO₂ all'anno. Nella tabella 9.13, vengono mostrati tutti i risultati menzionati.

In conclusione, sebbene i sistemi di abbattimento emettono meno gas fuorinati, il loro costo di manutenzione e la spesa del gas risulta essere più elevata.

Acknowledgements

Dedico questo spazio per ringraziare tutti coloro che hanno contribuito al mio percorso e che tutt'ora continuano a farlo. Ringrazio innanzitutto il mio supervisore al CERN, il Dott. Roberto Guida, per avermi seguito durante il mio percorso e per avermi dato la fiducia e la possibilità di esprimere e sviluppare al meglio le mie idee e pensieri in modo libero e aperto, i miei relatori il Prof. Alessandro Monteverde e il Prof. Fabio Deorsola, per avermi seguito per lo svolgimento della mia tesi.

Ringrazio la mia famiglia per il sostegno che mi avete sempre dato e per tutti i vostri insegnamenti. A voi, dedico ogni mio successo e traguardo, siete e sarete sempre il mio più grande punto di riferimento.

Ringrazio tutti i miei amici e colleghi al CERN, per tutto quello che mi avete insegnato e per quello che continuate ancora a insegnarmi. Vi ringrazio inoltre, per tutte le attività, i sorrisi e i bei momenti passati insieme.

Ringrazio i miei migliori amici per essermi sempre stato di sostegno, per avermi incoraggiato nelle scelte e per avermi spinto a tirare fuori il meglio di me in tutti i contesti. A tantissime altre esperienze insieme.

Infine, ringrazio, i miei colleghi all'università per avermi accompagnato e per essermi stati di sostegno in questo percorso.

Contents

1	Introduction	2
1.1	Fluorinated greenhouse gases and Global Warmin Potential	2
1.2	Green house gases emissions at CERN	4
1.3	Fluorinated Green house gases use in CMS	5
1.4	CSC and RPC gas system design, and gas consumption and emission in Run 1, Run 2 and Run 3	6
1.4.1	Estimated gas consumption and costs for Run 4	7
1.5	CERN strategies to minimize emissions	8
1.5.1	Solutions to decrease F-GHG gas consumption in CMS	8
2	CERN, The epicenter of Science	10
2.1	Introducing to CERN	10
2.2	CMS-Compact Muon Solenoid	11
2.3	RPC-Resistive Plate Chambers	13
3	RPC gas system	16
3.1	Mixer	16
3.2	Humidifier	17
3.3	Pump Module	18
3.4	Gas Purifier	18
4	R134a recovery system	20
4.1	Prototype II configuration	20
4.2	New R134a recovery system	21
4.2.1	Electric rack	21
4.2.2	Distillation Unit	21
4.2.3	Pumping and storage units	24
4.3	Exhaust line of R134a recovery system	26
5	Recovery of SF₆ with prototype 0	27
5.1	Single stage simulation with Aspen Plus	27
5.1.1	Selection of thermodynamic method	27
5.1.2	Setting on the simulation	27
5.1.3	Sensitivity Analysis	28
5.2	Double stage separation with Aspen Plus	31
5.2.1	Simulation of the second stage	31
5.3	Prototype 0	34
6	Investigation on gas mixture's distillation	37
6.1	VLE equilibria	38
6.1.1	McCabe-Thiele Approach for the determination of Theoretical number of stages for a biphasic separation of SF ₆ and R134a	41
6.2	Azeotropic distillation	43
6.2.1	Homogenous Azeotropic distillation	43
6.2.2	Pressure sensitivity azeotrope	44
6.2.3	Ternary diagram for SF ₆ /R134a/isobutane	44

7	Design and simulation of an SF₆ recovery System	48
7.1	Design of the new plant	49
7.2	Design of the accumulation tank and pumping station	49
7.3	Design of the two Distillation Columns	51
7.3.1	Introduction to the Distillation Process	51
7.3.2	Defining the Specifications and the Goals	52
7.3.3	Simulation and specifications findings with two distillation columns	55
7.3.4	Sizing and Optimization of the Distillation Columns	58
7.3.5	Reboiler and Condenser's Sizing	66
7.4	Accumulation tank and storage in cylinders	69
7.5	Control logic of the plant	69
7.5.1	Control of the two distillation columns	69
7.6	R&D of a membrane for the separation of SF ₆ /N ₂ mixture	72
7.7	Theory of membrane separation	72
7.7.1	overall mass balance of a membrane module	72
7.8	Membrane modelling for gas separation	74
8	Experimental R&D of a separation membrane	77
8.1	Introduction to experimental set-up	77
8.1.1	Final Set-up Configuration	78
8.2	Experimental test	79
8.2.1	Experimental Procedure	79
8.3	Test held at constant flowrate	81
8.3.1	Test 0	81
8.3.2	Test 1	82
8.3.3	Test 2	82
8.3.4	Test 3	83
8.4	Conclusion of the R&D Activity Performed with Membrane	84
9	Reasons behind the SF₆ recovery plant	86
9.1	SF ₆ recovery system, and cost of fresh	86
9.2	Economic Analysis	88
9.2.1	Gas Consumption at CMS	88
9.2.2	Recovery system cost estimation	89
9.2.3	Abatement system- economic Analysis	93
9.2.4	Comparison of abatement system and recovery system- economic and enviromental analysis	95
9.2.5	Discussion of the results of the analysis	98
10	Conclusions	99
A	R134a system P&ID	101
B	WinCC OA software interface	102
C	First and Second Buffer P&ID of R134a recovery system	103
D	Third Buffer P&ID of R134a recovery system	104
E	Fourth Buffer P&ID of R134a recovery system	105
F	Huber Unistat 915w, Technical data sheet	106
G	P&ID for SF₆ recovery system, Prototype 0	107
H	Matlabe code : McCabe-Thiele method for the design of a distillation column Ideal mixture	108
I	P&ID of new SF₆ recovery system	112

J	Calibration lines for SF₆/N₂ with Omron Flowmeter	113
K	OMRON D6F-10A6-000	114

List of Figures

1.1	Carbon dioxide emission in US from 1990 till 2021	2
1.2	Fluorinated gas emission in US from 1990 till 2021	3
1.3	CERN Scope 1 Emissions for 2017–2022 by Category	4
1.4	Flow diagram of the CSC (left) and RPC (right) gas systems of CMS. Indicated flow rates and consumption figures are from the 2018 (Run 2) LHC running	6
2.1	CERN accelerator complex	11
2.2	MUON system on CMS	12
2.3	Cross section of CMS detectors	12
2.4	Resistive Plate Chambers	13
2.5	RPC gas system strycture	15
3.1	: RPC gas mixer with the WinCC OA software layout. Starting from the top to the bottom input lines , the following gas are injected: R134a, isobutane, and SF ₆	17
3.2	Gas Humidifier module with WinCC OA software layout.	17
3.3	Pump module with WinCC OA software layout	18
3.4	Gas Purifier with WinCC OA software layout. [24]	19
4.1	Prototype II of R134a recovery system	20
4.2	Electrick rack P&ID	21
4.3	Column 1 P&ID. All columns have the same structure since they are designed in parallel.	22
4.4	Pumping unit P&ID	24
4.5	Storage unit P&ID	24
4.6	P&ID of the Exhaust line.	26
5.1	Aspen Plus, single stage FLASH separation	28
5.3	First stage, sensitivity Analysis results	29
5.4	Aspen Plus, double stage FLASH separation	31
5.5	Second stage, sensitivity Analysis results	32
5.6	Prototype 0 for SF ₆ separation in the gas room of the CMS experiment.	34
6.1	Activity coefficient for binary mixtures at 3 bar	38
6.2	Txy diagrams for SF ₆ /R134a at different pressures	40
6.3	Equilibrium curve for SF ₆ /R134a at temperature of -20 °C and pressure of 1 bar	41
6.4	Evaluation of theoretical Plate for SF ₆ /R134a using McCabe Thiele method	42
6.5	Minimum and maximum boiling azeotrope	43
6.6	Txy curves of R134a-IC ₄ H ₁₀ at 1 and 10 bar	44
6.7	Ternary diagram and boundary limits for SF ₆ /R134A/IC ₄ H ₁₀	45
6.8	Residue curves and boundary limits for SF ₆ /R134A/iC ₄ H ₁₀	46
6.9	Residue curves and boundary limits for SF ₆ /R134A/IC ₄ H ₁₀	47
7.1	Pumping and accumulation section	50
7.2	Diagram of a basic distillation column	53
7.4	Sensitivity Analysis results respect to Molar Purity	54
7.5	Condenser and Reboiler Duty respect to the Molar Reflux Ratio	54
7.6	Molar Recovery vs Molar Reflux Ratio	55

7.7	Main Flowsheet of the two distillation columns, made by Aspen Plus	56
7.11	Temperature (left-side) and Pressure (right-side) profiles along the first column.	59
7.12	Liquid mole fraction (left-side) and Gas mole fraction (right-side) profiles along the first column.	59
7.13	Temperature (left-side) and Pressure (right-side) profiles along the second column.	60
7.14	Liquid mole fraction (left-side) and Gas mole fraction (right-side) profiles along the second column.	60
7.15	DX TM structured packing as reported by <i>Sulzer Chemtech AG</i>	62
7.16	Normalized Height Equivalent to Theoretical Plate (HETP) as a function of normalized F-factor as reported by <i>Sulzer Chemtech AG</i>	63
7.17	Normalized Pressure drops per meter of column, $\Delta P/Z$, as a function of normalized F-factor as reported by <i>Sulzer Chemtech AG</i>	64
7.18	Heat exchanger and reflux drum at condensre stage for the first column	66
7.19	Accumulation and storage section of the SF ₆ recovery Plant.	69
7.20	First distillation column, with controllers	70
7.21	First distillation column, FIRST configuration with controllers	71
7.22	Membrane module configuration	72
7.23	Pressure and concentration profiles in a gas separation process	74
7.24	Schematic scheme of the discretization for the membrane modelling	75
7.25	Results of ODE, SF ₆ permeate side and N ₂ retentate side.	76
8.1	Mini CO ₂ separator	77
8.2	Membrane module configuration	78
8.3	Membrane module configuration	78
8.4	Laboratory setup description	80
8.5	Polymeric membranes, Permeability and Selectivity	84
9.1	Exhaust module of the RPC detectors	86
9.2	Gas consumption for each period divided in LS (Lung Shutdown) RUN (Run of the beam)	88
9.3	Amount of money spent per each gas in the period (2012 to 2035)	89
9.4	Amount of money spent per recovery systems in the period (2012 to 2035)	90
9.5	Cumulative curve of all the recovery system at CMS(blue curve). Cumulative cost saving from the gas recovered (yellow curve) in the period (2012 to 2035)	91
9.6	Cumulative curve of all the recovery system at CMS, cost of fresh gas at the mixer included (red curve). Cumulative cost saving from the gas recovered (blue curve) in the period (2012 to 2035)	92
9.7	The EBARA G5 and EDWARDS ATLAS waste gas abatment units	93
9.8	Flow diagram of the abatment process	93
9.9	Chemical reactions occurring during the waste-gas abatment process	94
9.10	Wate water pant scheme <i>Envirochemie</i>	95
9.11	Comparison of Costs between Recovery and Abatement Systems	96
9.12	Equivalent amount per year of tCO ₂ emitted in the period (2012-2050). The yellow curve represent the emission per each ear having the recovery systems while the green curve represent the emission from the abatment system	97
9.13	Summary of recovery systems and abatment system in the years 2012 to 2025	98
A.1	R134a recuperation system P&ID	101
B.1	WinCC OA software interface.	102
C.1	Buffer with a 10 cm height, used as bottom buffers for columns 1 and 2.	103
D.1	Buffer with a 20 cm height, used as bottom buffers for columns 3 and 4.	104
E.1	Buffer with a 30 cm height, used as bottom buffers for columns 1 and 2.	105
F.1	Technical data of Huber Unistat 915w	106

G.1	P&ID for SF ₆ recovery system, Prototype 0	107
I.1	Full P&ID of the new SF ₆ recovery system	112
J.1	Calibration line for N ₂	113
J.2	Calibration line for SF ₆	113
K.1	Flowmeter datasheet: Omron D6F-10A6-000	114

List of Tables

1.1	Life time and GWP of fluorinated gases	3
1.2	Fluorinated Gas Emissions (in tons of CO ₂ equivalent)	5
1.3	Lifetime in atmosphere, Global Warming Potential (GWP) and Mass of GHG contained in CMS CSC and RPC detector gas mixtures. Source: [[11]]	5
1.4	F-GHG emissions in CMS at the end of Run 2 (2018) and their CO ₂ equivalent masses.	7
1.5	F-GHG average annual consumption in CMS in Run 1 and Run 2 estimated from supplier procurements. SF ₆ in 2018 profited from previous year carry-over.	7
1.6	F-GHG emissions and consumptions averaged over 2017-2018. One must note that gas storage batteries are usually not completely emptied by the end of a given year of operation	7
1.7	F-GHG emissions and consumptions averaged over July 2022 till June 2024.	7
1.8	F-gas volumes and cost predictions for 5 years running at the LHC during Run 4. Volumes are calculated assuming a gas flow of 13 m ³ /h (RPC), averaged over 5 years, and 6 m ³ /h (CSC). Cost figures are based on 2024 gas prices.	8
2.1	Components of the gas mixture in CMS RPCs (with respective volumetric percentages and boiling temperatures).	14
4.1	Component and Index of Distillation unit	23
4.2	Component and Index of Pumping and storage unit	25
5.1	Components of the gas mixture in the exhaust line of R134a recovery system at CMS. (with respective volumetric percentages and feeding conditions).	28
5.2	Optimal Feed Flowrate, Pressure and Temperature in Buffer 5.1	29
5.3	Distillate composition of stream VAPOUR(see figure 5.1). Results of the single stage separation with Aspen Plus simulation).	30
5.4	Result of the Distillate-to-feed-ratio, molar recovery outlet Temperature and thermal duty of the Vapour stream 5.1	30
5.5	Inlet conditions of BUFFER2 5.2a	31
5.6	Inlet conditions of BUFFER2 (5.4)	32
5.7	Distillate composition of stream VAP2 (see figure 5.4). Results of the double stage separation with Aspen Plus simulation.	32
5.8	Result of the Distillate-to-feed-ratio, molar recovery, outlet Temperature and thermal duty 5.4	32
5.9	Productivity and molar recovery of entire Separation, results. Conducted by Aspen plus simulator	33
5.10	Component and Index of Prototype 0	36
6.1	Liquid and Vapour phase equilibria at Temperature of -7.5 °C at pressure of 3 bar	40
6.2	Feeding condition for the distillation column	41
6.3	Azeotrop investigation: Classification of nodes	45
6.4	Components of the gas mixture in the exhaust line of R134a recovery system at CMS. (with respective volumetric percentages).	46
6.5	Distillate and Bottom concentration expectation	47
7.1	Input parameters and simulated specifications	55
7.2	Input parameters and simulated specifications for first column	58

7.3	Input parameters and simulated specifications for second column	58
7.4	Feed conditions of the first column	58
7.5	Distillate composition of column 1	59
7.6	Feed conditions of the second column	60
7.7	Distillate composition of column 2	61
7.8	Specifics of the DX TM packing material	62
7.9	Molar liquid fraction and vapor fraction along the first column	63
7.10	Temperature profile ($^{\circ}C$), Pressure profile (<i>bara</i>), Specific liquid flowrate ($m^3/h/m^2$), Specific vapor flowrate ($m^3/h/m^2$), F-factor($((m/s)Pa^{0.5})$), for the first column 7.7	64
7.11	Molar liquid fraction and vapor fraction along the second column in series 7.7	65
7.12	Temperature profile ($^{\circ}C$), Pressure profile (<i>bara</i>), Specific liquid flowrate ($m^3/h/m^2$), Specific vapor flowrate ($m^3/h/m^2$), F-factor($((m/s)Pa^{0.5})$), for the second column in series 7.7	66
7.13	Condenser input and output, stream conditions for first column	67
7.14	First column, Condenser and Reboiler sizing.	67
7.15	Condenser input and output, stream conditions for second column	68
7.16	Second column, Condenser and Reboiler sizing.	68
7.17	Performances of the separation with the distillation column.	68
7.18	Inet parameter for membrane module.	75
8.1	Component and Index of membrane set-up	79
8.2	N ₂ gas in UBE membrane. Test 1 at Constant inlet flowrate : 50 l/h	81
8.3	Average feed and permeate flowrate of N ₂ gas.	82
8.4	SF ₆ gas in UBE membrane. Test 1 at Constant inlet flowrate : 50 l/h	82
8.5	Average feed and permeate flowrate of N ₂ gas.	82
8.6	N ₂ gas in UBE membrane. Test 1 at constant inlet flowrate: 100 l/h	83
8.7	Average feed and permeate flow rates of N ₂ gas.	83
8.8	SF ₆ gas in UBE membrane. Test 1 at constant inlet flow rate: 100 l/h	83
8.9	Average feed and permeate flow rates of SF ₆ gas.	83
9.1	Flowrate of SF ₆ injected at the mixer	87
9.2	Flowrate of SF ₆ injected at the mixer.	87
9.3	Yearly expenditure on fresh SF ₆	87
9.4	Cost savings from SF ₆ recovery per year.	87
9.5	Average Mass flowrate consumption of gas per year kg/year	89
9.6	CAPEX + M&O for each recovery system at CMS	90
9.7	Recovery and Emissions Data	92
9.8	Carachteristics, Efficiencies, and costs of the two abatment systems	94
9.9	CAPEX, M&O, FSU costs for <i>Envirochemie</i> waste water treatment plant	95
9.10	Fresh Gas consumption, costs, and emissions if no recovery system is present	95

Chapter 1

Introduction

1.1 Fluorinated greenhouse gases and Global Warmin Potential

The Earth’s climate is intricately influenced by the delicate balance of gases that compose our atmosphere. Among these, greenhouse gases play a pivotal role in trapping heat and shaping the planet’s climate. Greenhouse gases encompass a spectrum of compounds, each with its unique sources and environmental impact. Carbon dioxide (CO₂), methane (CH₄), nitrous oxide (N₂O), and fluorinated gases collectively contribute to the greenhouse effect, retaining heat within our atmosphere. Human activities, such as the combustion of fossil fuels, industrial processes, and agricultural practices, release these gases into the air, altering the delicate equilibrium that has prevailed for millennia. Carbon dioxide, the primary greenhouse gas stemming from human endeavors, takes center stage. Its sources span from the combustion of fossil fuels to industrial processes and land-use changes. As we investigate the mechanisms behind carbon dioxide emissions, it becomes evident that human activities have disrupted the Earth’s natural carbon cycle, resulting in an unprecedented rise in atmospheric CO₂ levels since the industrial revolution [9]. In the figure (1.1), the emissions of CO₂ in the atmosphere in the U.S.A from 1990 to 2021 are depicted. The graph clearly illustrates a 2% decrease in the amount of emitted CO₂ during this period.

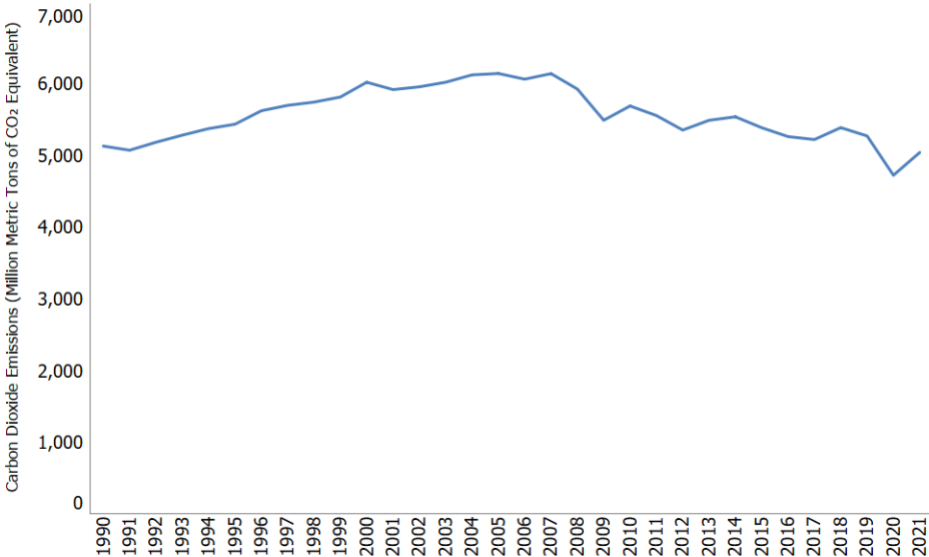


Figure 1.1: Carbon dioxide emission in US from 1990 till 2021

While each greenhouse gas contributes to the warming of the planet, their impact depends on three crucial factors: abundance in the atmosphere, longevity, and the potency of their warming effect. The concept of Global Warming Potential (GWP) emerges as a metric to gauge the relative impact of different gases, offering a standardized measure for comparison. GHGs are classified according to their Global Warming potential (GWP), defined as “the climatic warming potential of a greenhouse gas relative to that of carbon dioxide CO₂, calculated in terms of the 100-year warming potential of one kilogram of a greenhouse gas relative to one kilogram of CO₂” [29]. In this section we are clearly going to discuss about fluorinated gases and which are the focus of the thesis work. Unlike many other greenhouse gases, fluorinated gases have no significant natural sources and come almost entirely from human-related activities [9]. Fluorinated gases are emitted through various substances such as refrigerants or different industrial processes. Many of these gases have very high Global Warming Potential (GWP), meaning that even small concentrations released into the atmosphere can significantly contribute to the increase in temperature. Here, a list of various fluorinated gases is provided along with their GWP and life time in the atmosphere 1.1.

Chemical formulas	Life time in Atmosphere	GWP
HFCs	up to 270 years	12.400
PFCs	2.600–50.000 years	11.100
NF ₃	740 years	16.100
SF ₆	3.200 years	23.500

Table 1.1: Life time and GWP of fluorinated gases

Differently from the CO₂ emissions, the emissions of these gases appear to have increased in recent years (Figure 1.2). Given their high Global Warming Potential (GWP) and extended atmospheric lifetimes, there is a pressing need to reduce the usage of these gases.

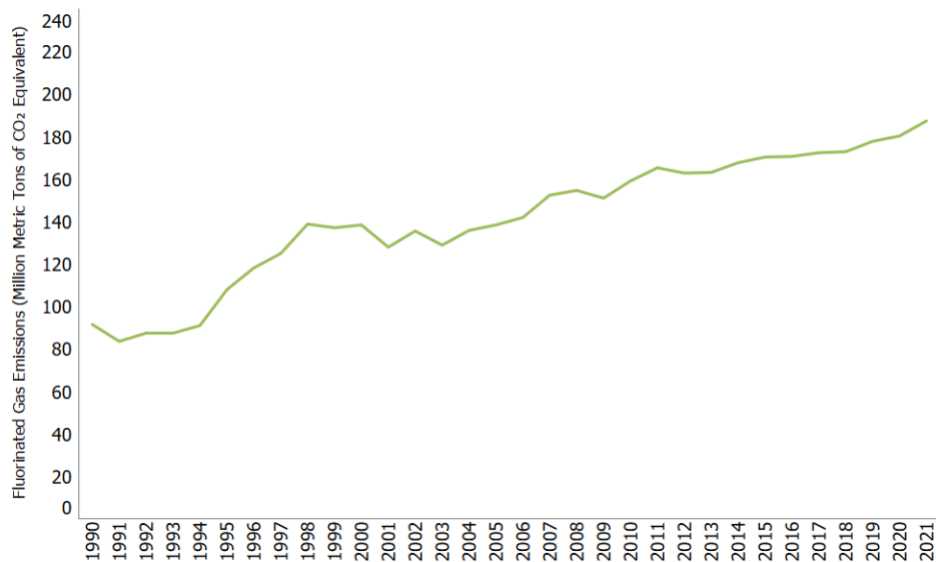


Figure 1.2: Fluorinated gas emission in US from 1990 till 2021

Here at CERN, fluorinated gases such as Freon and SF_6 are utilized in the detectors across various experiments. The goal is to construct recovery systems to prevent these gases from being released into the atmosphere. In my thesis, I will detail the design and implementation of a recovery system for SF_6 , located in CMS experiment.

1.2 Green house gases emissions at CERN

CERN's direct greenhouse gas emissions, categorized as scope 1, predominantly stem from the industrial infrastructure and on-site activities of the laboratory (figure 1.3)

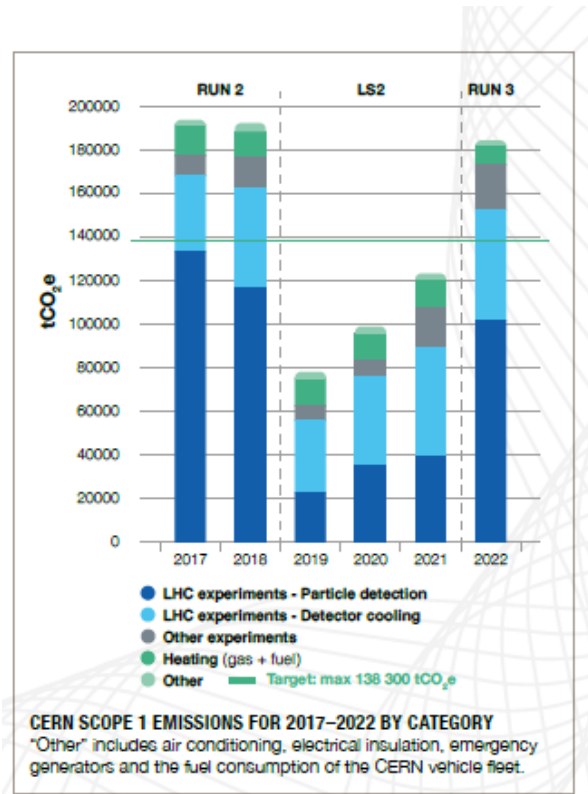


Figure 1.3: CERN Scope 1 Emissions for 2017-2022 by Category

A significant portion, approximately 90%, is attributed to the institution's experiments [5]. These experiments extensively employ diverse gas mixtures for particle detection and detector cooling, notably fluorinated gases (F-gases) with elevated global warming potential (GWP). F-gases contribute substantially, accounting for about 78% of CERN's total direct emissions. The table presented below outlines the emissions of fluorinated gases for the years 2021 and 2022. 1.2

GROUP	GASES	tCO ₂ e 2021	tCO ₂ e 2022
Perfluorocarbons (PFCs)	CF ₄ , C ₂ F ₆ , C ₃ F ₈ , C ₄ F ₁₀ , C ₆ F ₁₄	55,921	68,989
(HFCs)	HFC-23 (CHF ₃), HFC-32 (CH ₂ F ₂), HFC-134a (C ₂ H ₂ F ₄), HFC-404a, HFC-407c, HFC-410a, HFC-507	36,557	86,211
Other F-gases (HFO)/HFCs	SF ₆ , NF ₃ R-449, R1234ze, NOVEC 649	16,838 86	18,355 199
Total emissions		123,174	184,173

Table 1.2: Fluorinated Gas Emissions (in tons of CO₂ equivalent)

The organization focuses its mitigation efforts primarily on large experiments, where HFCs, PFCs, and SF₆ are utilized for particle detection, PFCs and HFCs for detector cooling, and HFOs/HFCs for standard air conditioning systems, including SF₆ for electrical insulation in power supply systems. The resumption of the accelerator complex in 2021 for Run 3 of the LHC led to increased emissions, contrasting with the period of inactivity in 2019–2020. Emissions totaled 123,174 and 184,173 tonnes of CO₂ equivalent (tCO₂e) in 2021 and 2022, respectively. CERN is actively enhancing its F-gas management, traceability, and monitoring, notably through the influence of the Working Group on F-Gases. Large experiments have refined their strategies to minimize emissions, while test facilities and smaller experiments now contribute to the comprehensive calculation of scope 1 emissions for 2021 and 2022. Moreover, at CMS, a specific concern has arisen regarding elevated pollution levels, particularly in the gas room, where emissions of at least 16,000 tons of equivalent CO₂ have been detected. The primary objective is to recover these fluorinated gases, mitigating their release into the atmosphere and aligning with CERN’s overarching commitment to environmental responsibility.

1.3 Fluorinated Green house gases use in CMS

The CMS Muon system includes four gas detector systems, with the Cathode Strip Chamber (CSC) and Resistive Plate Chamber (RPC) systems utilizing fluorinated gases, while the Drift Tube (DT) and Gas Electron Multiplier (GEM) systems employ Ar+CO₂ gas mixtures. Specifically, the CSC system operates with a gas mixture composed of 40% argon, 50% carbon dioxide, and 10% tetrafluoromethane (CF₄). On the other hand, the RPC system uses a mixture consisting of 95.2% tetrafluoroethane (C₂H₂F₄), 4.5% isobutane (iC₄H₁₀), and 0.3% sulfur hexafluoride (SF₆).

The fluorinated greenhouse gases (F-GHGs) utilized by the CSCs and RPCs, along with their global warming impact, are detailed in Table (1.3). The specific gases included in the CSC and RPC mixtures are crucial for ensuring operational stability and longevity of the detectors. CF₄ is particularly valuable in the CSC system for three key reasons: it prevents the detector from aging, it boosts the electron drift velocity (which is essential for accurately identifying the bunch crossing associated with a muon track), and it acts as a quenching agent, enhancing the stability of the CSC operation ([22]).

In the RPC system, C₂H₂F₄ serves as an effective photon quencher, while SF₆, being a highly electronegative gas, plays a critical role in stabilizing the RPC operation during the avalanche process.

Species	Lifetime (years)	GWP 100y	Molar mass (g/mol)
CF ₄	50000	6500	88
C ₂ H ₂ F ₄	10.6	1300	102
SF ₆	3200	23900	144

Table 1.3: Lifetime in atmosphere, Global Warming Potential (GWP) and Mass of GHG contained in CMS CSC and RPC detector gas mixtures. Source: [[11]]

1.4 CSC and RPC gas system design, and gas consumption and emission in Run 1, Run 2 and Run 3

Both the CSC and RPC gas systems operate as closed-loop systems with recirculation and purification, maintaining a fresh gas replenishment rate of 10-12% (based on Run 2 data). This recirculation process reduces the CMS GHG consumption by approximately 90% compared to an open gas system.

The CSC gas system has a total volume of 70 m³. The nominal gas mixture flow rate is 6 m³/h, with a 10% replenishment flow rate of 650 l/h (2017-18 data). In the CSC system, 10% of the extracted gas undergoes a CF₄ recovery and reinjection process before being vented to the air. Since 2012, this CF₄ recovery system has operated with an average efficiency of 50% during Run 2. Consequently, the total F-GHG emissions from CSCs are now 5% of the initial CF₄ gas flow (approximately 600 l/h), resulting in about 30 l/h. The gas recirculation and CF₄ recovery systems thus further reduce the GHG consumption by an additional 50%. The fraction of gas mixture that escapes due to micro leaks in the chambers is minimal (< 1%) and remains stable over time, currently about 50 l/h at the end of Run 2, with only 5 l/h being CF₄.

The RPC gas system has a total volume of 13 m³. The nominal gas mixture flow rate is 9 m³/h, with a 12% replenishment flow rate of approximately 1100 l/h (2017-18 data). Unlike the CSC system, the RPC system is less hermetic. Some chambers, accounting for about 6% of the total system, have developed leaks over time, primarily due to the rupture of delicate polyethylene gas pipes and junctions, possibly caused by pressure instabilities in the CMS underground cavern's ventilation system. Due to the significant leak rate, currently about 1000 l/h (end of Run 2), which matches the 12% replenishment rate, there is no measurable gas flow at the system exhaust.

Figure 1.4 presents a diagram detailing the specification and operation of the CSC and RPC gas systems.

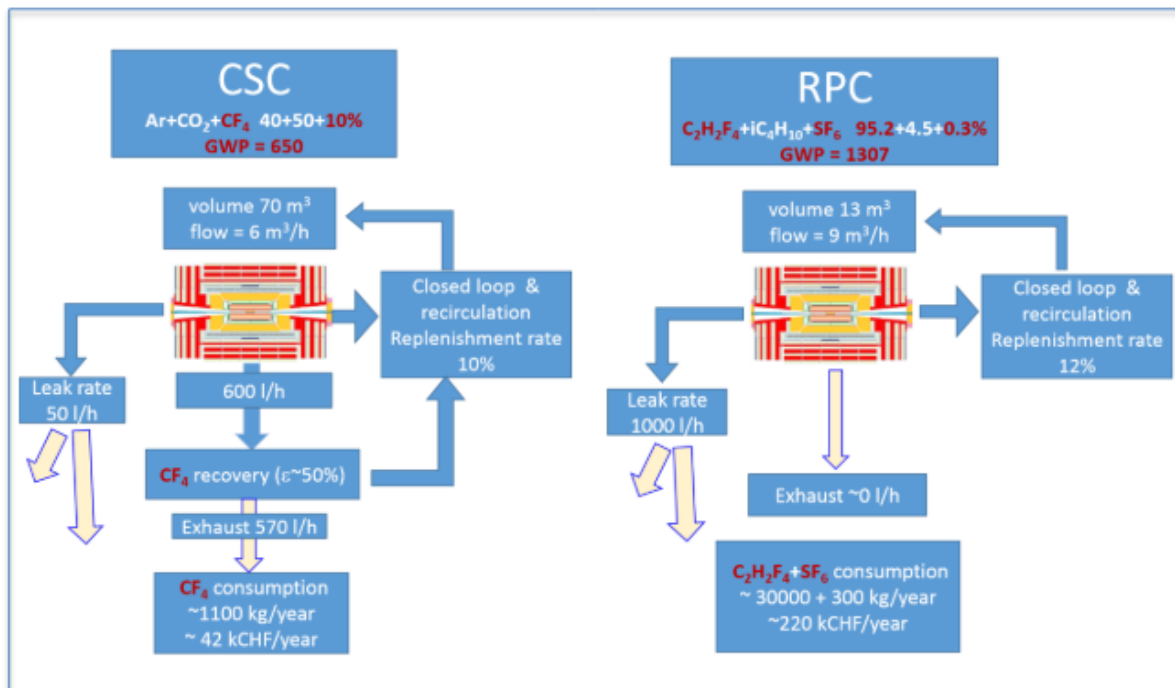


Figure 1.4: Flow diagram of the CSC (left) and RPC (right) gas systems of CMS. Indicated flow rates and consumption figures are from the 2018 (Run 2) LHC running

Gas consumption in Run 2 has increased compared to Run 1 due to a higher leak rate in the RPCs and the addition of new muon chambers during LS1 (2013-14). Specifically, the CSC system was expanded with the ME4/2 chambers, resulting in a 15% increase in system volume, while the RPC endcap was enhanced with the RE4/2 chambers, leading to a 5% increase in system volume.

During Run 2, the average F-gas consumption over 9 months of LHC operation per year was approx-

Gas	Volume (l/h)	CO ₂ -eq (kg/h)	Weight (kg/y)	CO ₂ -eq (t/y)
CF ₄	35	817	1,100	7,150
C ₂ H ₂ F ₄	1,000	5,410	30,000	39,000
SF ₆	3.2	450	300	7,170
Total	1,038.2	6,677	31,400	53,320

Table 1.4: F-GHG emissions in CMS at the end of Run 2 (2018) and their CO₂ equivalent masses.

imately 115 kg/day, with 110 kg/day for the C₂H₂F₄ and SF₆ used in the RPCs, and around 4 kg/day for the CF₄ used in the CSCs. Table 2.2 provides a summary of the annual gas consumption since the beginning of Run 1.

Consumption/year	CF ₄ (CSC)	C ₂ H ₂ F ₄ +SF ₆ (RPC)
Run1 (2012)	2800	29000 + 250 kg
2015	2200	25700 + 300 kg
2016	2000	38500 +240 kg
2017	1200	38000+300 kg
2018	1300	30400 + 0 kg

Table 1.5: F-GHG average annual consumption in CMS in Run 1 and Run 2 estimated from supplier procurements. SF₆ in 2018 profited from previous year carry-over.

The average annual emissions and gas consumption for Run 2, considering 9 months of LHC operation per year, show a reasonable agreement, as detailed in Table 1.6.

	Emissions	Consumption	Cost/year
CF ₄	3 kg/day	4 kg/day	46 kCHF
C ₂ H ₂ F ₄ + SF ₆	90 kg/day	110 kg/day	250 kCHF

Table 1.6: F-GHG emissions and consumptions averaged over 2017-2018. One must note that gas storage batteries are usually not completely emptied by the end of a given year of operation

While for Run 3 (which will end at July 2025) we report here the results in terms of consumption and emission till June 2024 (1.7).

	Emissions	Consumption	Cost/year
CF ₄	3 kg/day	4 kg/day	54 kCHF
C ₂ H ₂ F ₄ + SF ₆	80 kg/day	85 kg/day	300 kCHF

Table 1.7: F-GHG emissions and consumptions averaged over July 2022 till June 2024.

1.4.1 Estimated gas consumption and costs for Run 4

The increased instantaneous and cumulative luminosities anticipated at the HL-LHC (Run 4) will necessitate adjustments to the gas system operations. The settings for detector gas flow and replenishment may need to be revised due to higher currents drawn by the detectors and the creation of new contaminants, leading to a quicker rise in pollution rates within the circulated mixture. Radiation tests simulating higher instantaneous luminosity suggest, for instance, that the RPC gas mixture flow might need to be increased from 9 m³/h to 15 m³/h over 5 years of Run 4 to avert the occurrence of uncontrollable ohmic-current discharges resulting from the heightened particle flux. This would lead to an increase in F-gas consumption (approximately 220 tons over 5 years) and operating expenses.

Conversely, CSCs operate in proportional mode, keeping ionization currents manageable. Therefore, the CSC gas flow should remain constant, provided the CF₄ proportion in the mixture does not fall significantly below the current 10% (as CF₄ has beneficial anti-aging effects).

Regarding gas procurement, additional EU regulations aimed at reducing F-GHG emissions could result in higher costs and limited availability of F-gases. If consumption cannot be decreased, CMS might consider pre-purchasing and stockpiling the necessary F-gases to run the CSC and RPC systems until the LHC program concludes. An initial estimate of the gas volumes and associated costs required for a continuous five-year operation is presented in Table (1.8). Without a reduction in F-GHG consumption, CMS will need approximately 2 MCHF to cover gas costs for operating CSCs and RPCs over a five-year span. These plans depend on there not being an outright ban on the use of F-GHG gases.

Detector	Fluorinated gases	Weight/5y (t)	Cost/5y (MCHF)
CSC	CF ₄	5.5	0.2
RPC	C ₂ H ₂ F ₄ + SF ₆	220	1.8

Table 1.8: F-gas volumes and cost predictions for 5 years running at the LHC during Run 4. Volumes are calculated assuming a gas flow of 13 m³/h (RPC), averaged over 5 years, and 6 m³/h (CSC). Cost figures are based on 2024 gas prices.

1.5 CERN strategies to minimize emissions

In pursuit of its commitment to environmental sustainability, CERN has set ambitious targets for reducing greenhouse gas emissions. Originally slated for 2024, these objectives, including a 28% reduction in scope 1 emissions by the end of Run 3, have been adjusted in accordance with the evolving accelerator schedule [5]. The current strategy focuses on optimizing gas usage in experiments, emphasizing key pillars such as gas recirculation, gas recovery, and the exploration of more eco-friendly alternatives to existing gases. Noteworthy achievements include the implementation of a recovery system at the CMS facility for R134a recovery, that operates with a recovery efficiency of (80%). As part of its dedication to mitigating climate impact, CERN has conducted systematic leak-repair campaigns, addressing a major contributor to F-gas emissions – small leaks in detectors due to their lightweight construction. Recent efforts during the second long shutdown (LS2) demonstrated progress in containing and minimizing leaks, with a commitment to further campaigns in upcoming shutdowns. Additionally, the organization actively invests in research and development, testing new gases with lower Global Warming Potential (GWP) and exploring the partial replacement of HFC-134a with CO₂ for future applications, exemplified by ongoing activities in the ATLAS and CMS experiments. These initiatives underscore CERN’s proactive approach in aligning with evolving environmental standards and fostering sustainable practices within the scientific community.

1.5.1 Solutions to decrease F-GHG gas consumption in CMS

Closed loop gas systems, such as the CSC and RPC systems, can reduce gas consumption by approximately 90%, provided the detectors are sufficiently hermetic.

- **It is essential to minimize the current gas leakage in the RPCs, thus restoring a gas stream at the exhaust through a dedicated repair campaign and implementing long-term leak prevention measures. Alternatively, consider progressively deactivating the most leaky chambers after evaluating the impact on trigger and reconstruction.**

Table 1.8 presents the F-gas volume and cost estimates for 5 years of operation at the LHC during Run 4. Volumes are calculated assuming an average gas flow of 13 m³/h for RPCs and 6 m³/h for CSCs, with cost figures based on 2019 gas prices.

Since its implementation in 2012, the CSC recuperation system has reduced CF₄ consumption by about 50% to 70% on average.

- **Enhance the operational efficiency of the CF₄ gas recovery system to approximately 80%.**

Improving efficiency of a C₂H₂F₄ recuperation and implentig of an SF₆ recovery system for RPCs would reduce F-GHG consumption proportionally to the efficiency of the recovery-reuse plant.

- **The new R134a recovery system was installed in 2022 and operates with an efficiency of 80 % almost, the next step is to increase this value of efficiency to 90%. Design and install a system for high efficiency (>80%) SF₆ recuperation and reinjection. For this recovery system R&D is ongoing.**

The CSC group has conducted a series of tests on CSC detectors filled with an Ar+CO₂ gas mixture containing reduced percentages of CF₄ gas, specifically 5% and 2%. Preliminary results from aging tests at GIF++ indicate that CSCs can endure the integrated luminosity expected at the HL-LHC with a safety factor of 3, with a moderate performance degradation (less than 5%) in efficiency and spatial resolution.

- **Operate the CSC system with a lower CF₄ fraction, reducing it from 10% to 5%, provided that performance and longevity are maintained.**

If these actions are implemented in the coming years, CMS would gradually reduce F-GHG consumption and the overall emission footprint. By Run 4, it is conceivable to achieve a reduction in F-GHG emissions by as much as 60% compared to Run 1 emissions. A more straightforward approach to reducing F-GHG consumption and emissions would be to substitute CF₄, R134a, and SF₆ with environmentally friendly gases. In addition to being non-CO₂ emitting (as defined by the EPA), these alternative gases should be commercially available and cost-effective. They must also meet the following criteria:

- Ensure the operational stability of the current CSC and RPC detectors;
- Provide adequate performance in terms of resolution, efficiency, and timing;
- Possess anti-aging properties to guarantee the longevity of the detectors throughout the entire LHC program.

Each of these strategies is currently under study and undergoing improvements. A final economic analysis will be presented in Chapter 9, demonstrating why recovery systems are preferred over the installation of abatement systems. This analysis will definitively justify the decision to build recovery systems.

Chapter 2

CERN, The epicenter of Science

2.1 Introducing to CERN

The European Organization for Nuclear Research, commonly known as CERN, was established in 1954 and stands as the foremost institution in Europe dedicated to the exploration of particle physics. CERN is in close proximity to Geneva, near the border between Switzerland and France. Notably, it is the home of the Large Hadron Collider (LHC) and various particle accelerators designed for proton collision experiments. Through the collision of antiparallel, high-energy, and high-intensity proton beams, the LHC enables a profound comprehension of the phenomena that transpired during the early moments of the Universe's existence. The CERN facility is extensive, commencing with the Linear Accelerator (LINAC), which accelerates primary protons. To enter the Proton Synchrotron Booster (PSB), where hydrogen electrons are stripped away from negative hydrogen ions, leaving only protons, these protons must attain an energy level of 160 MeV [2]. The PSB increases the protons' energy to the requisite 2 GeV for the subsequent accelerator, the Proton Synchrotron (PS), where protons reach energy levels of up to 26 GeV. Subsequently, they are introduced into the Super Proton Synchrotron (SPS), where they undergo an additional acceleration, reaching speeds of up to 450 GeV. The LHC employs two beam pipes, one rotating clockwise and the other counterclockwise, to transport the protons. Within the LHC, they circulate for several hours until they attain their maximum energy of 6.5 TeV. At this point, the two beams collide at four specific locations along the ring: ALICE, ATLAS, CMS, and LHCb [3].

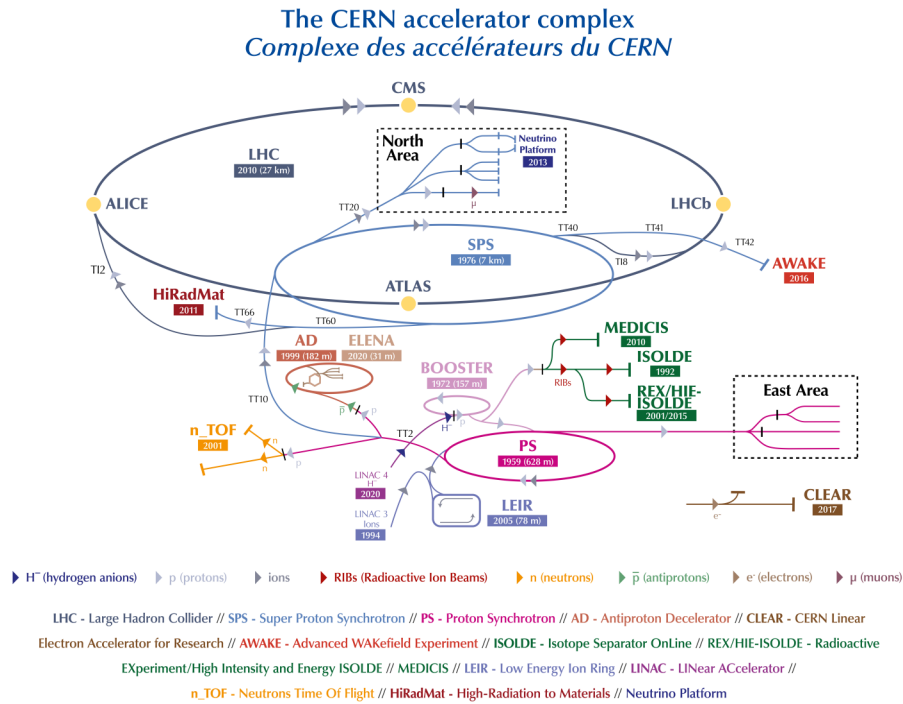


Figure 2.1: CERN accelerator complex

2.2 CMS-Compact Muon Solenoid

The Compact Muon Solenoid (CMS), one of the four major experiments at CERN’s Large Hadron Collider (LHC), is situated approximately 100 meters underground, adjacent to Cessy, France. Despite its name, “Compact,” its dimensions are substantial, measuring 21 meters in length, 15 meters in width, and 15 meters in height. Although slightly smaller than its counterpart, ATLAS, CMS’s moniker “Compact” is derived from its design philosophy rather than its physical size.

At the heart of CMS lies a formidable solenoid with a cylindrical structure, generating a magnetic field of 4 Tesla—over 100,000 times the Earth’s magnetic field. This solenoid plays a pivotal role in momentum measurements. The principle involves bending the path of charged particles with a magnetic field. Silicon sensors capture the electrical signals left by these particles along their trajectories. The interaction with strip sensors or pixels provides the precise position of a particle, enabling the reconstruction of its path. The curvature radius of the track facilitates the estimation of the particle’s momentum using the formula (2.1):

$$p = 0.3RB \quad (2.1)$$

Here, p represents the particle momentum in GeV/ c , B is the magnetic strength in Tesla, and R is the radius of curvature in meters.

CMS, akin to ATLAS, is optimized for the detection and measurement of muons due to their distinctive characteristics and their exclusive origin from the decay of heavy particles—central to collision research. Muon detectors are strategically positioned in the outer area of CMS, as illustrated in Figure (2.2).

This figure, portrays the schematic layout of CMS, highlighting the four types of gaseous detectors employed: Drift Tube (DT) chambers in the barrel, Cathode Strip

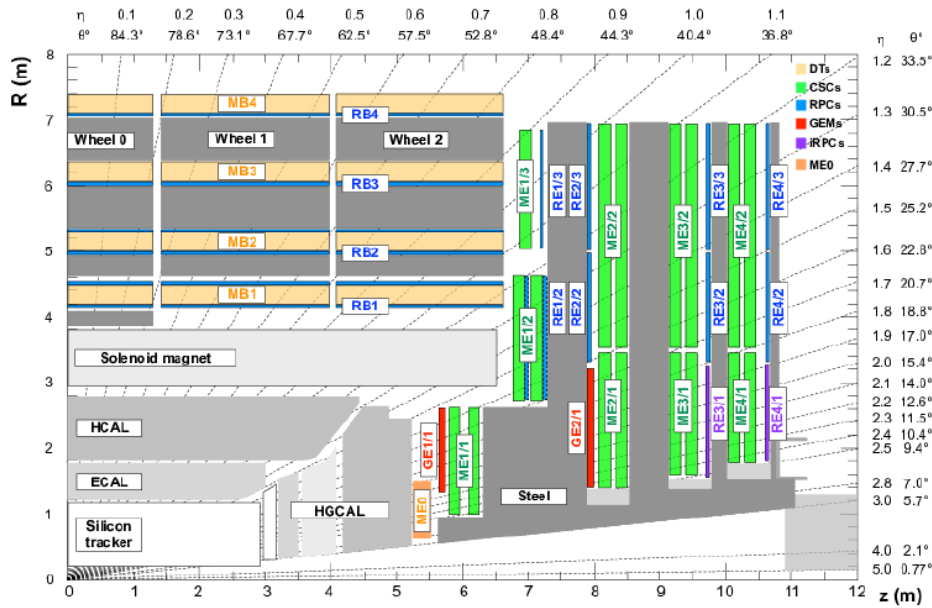


Figure 2.2: MUON system on CMS

Chambers (CSC) in the endcaps, both complemented by a Resistive Plate Chambers (RPC) system, and the gas electron multiplier (GEM).

The detectors considerable size and strategic placement are justified by the unique behavior of muons, which, unlike other charged particles, can traverse significant distances. The schematic cross-section of CMS, represented in the following image, illustrates the paths of various charged particles, with none surpassing the super-conducting solenoid except for muons.

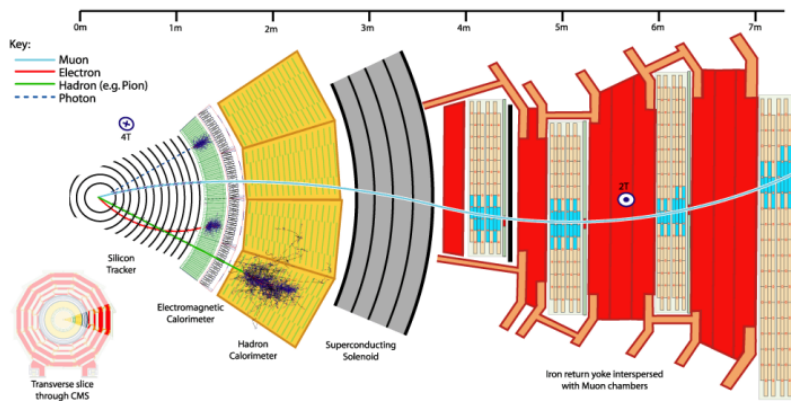


Figure 2.3: Cross section of CMS detectors

2.3 RPC-Resistive Plate Chambers

The RPCs (as shown in Figure 2.4), the detectors utilized at CERN for the examined gas mixture, function as gas detectors specialized in muon detection. In a broader context, a gas detector is a device designed to identify the presence of particles. When a particle traverses a gas and possesses sufficient energy to ionize the gas, electron-ion pairs are generated along the particle's trajectory. These pairs can be collected and further amplified through a potent electric field, facilitating the migration of electrons towards the positive anode and ions towards the negative cathode.

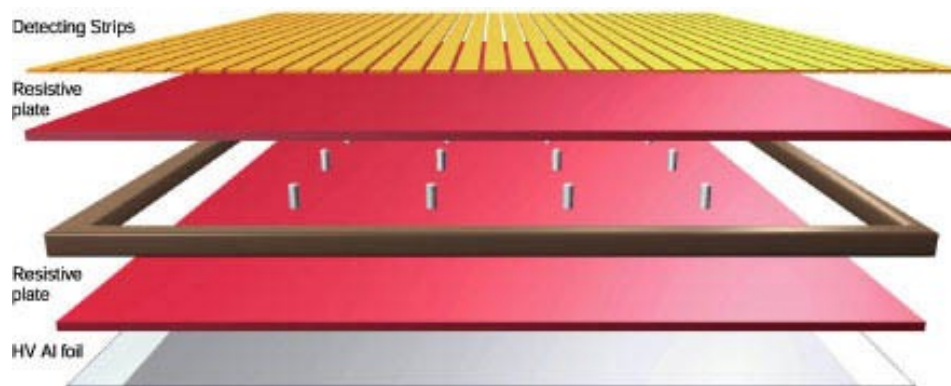


Figure 2.4: Resistive Plate Chambers

To delve into specifics, RPCs are gas detectors comprising two parallel electrodes separated by a chamber housing a specific gas mixture, meticulously chosen to optimize detector performance. The electrodes are subjected to different potentials, creating a robust electric field within the chamber. As a particle traverses the chamber, it ionizes a gas molecule, instigating the formation of an electron-ion pair (primary ionization). The resultant electron and ion experience acceleration due to the electric field, drifting towards the anode and cathode, respectively. The lighter electron undergoes greater acceleration, and during its drift, collisions with other gas molecules may occur, instigating the creation of additional electron-ion pairs (secondary ionization). These primary and secondary electrons are once again accelerated, perpetuating the drift through a multiplication process. The electrons must possess sufficient energy, contingent on the electric field's intensity, to initiate the formation of the electron avalanche. Given the disparate drift velocities of ions compared to electrons (approximately a factor of 103), the avalanche generates a charge distribution resembling a droplet, engendering an electric field opposing that of the detector. When these opposing electric fields achieve parity, the multiplication ceases, and ions and electrons recombine, emitting photons (UV) that may further ionize the gas, triggering additional ionization phenomena. Ionized molecules reach the electrode, producing a total charge substantial enough to be captured by a reading system consisting of metal strips. These strips are engaged across multiple detectors in the muon spectrometer, yielding a measurement of the muon's momentum. This data is pivotal for the trigger system, aiding in the determination of the significance of the acquired information and enabling event reconstruction based on momentum and energy. The gas mixture significantly shapes the charge multiplication process. Components with pronounced electronegativity that absorb electrons can impede the charge emitted during the ionization process. A notable consequence of this issue is a reduction in the detector's lifespan, exemplified by potential damage to the electrodes through the production of flu-

orides. The composition of the gas mixture characteristic of the CMS RPCs is detailed 2.1 .

Component	Concentration (%V)	Boiling point (°C)
IC ₄ H ₁₀	4.5%	-12
R134a	95.2%	-26.3
SF ₆	0.3%	-64

Table 2.1: Components of the gas mixture in CMS RPCs (with respective volumetric percentages and boiling temperatures).

Tetrafluoroethane (C₂H₂F₄, R134a), containing fluorine atoms, is highly electronegative with a low ionization potential, facilitating the supply of electrons needed for primary ionization. Isobutane (iC₄H₁₀) serves as a quencher for UV photons generated during the recombination of ions and electrons in electron avalanche development. These photons induce a high number of secondary avalanches, increasing the total charge within the detector and causing interference in the signal acquisition of muonic particles. Lastly, sulfur hexafluoride (SF₆), due to its high electronegativity, captures low-energy electrons and spatially limits the avalanche. The gas is distributed to the detectors through a gas mixture distribution system. While specific to each detector and experiment, these systems consist of modular units tailored to specific functions that are common across all systems. Dedicated systems provide the appropriate gas mixture to the detectors, requiring high reliability in terms of both stability and gas mixture quality.

The distribution system components are situated on three different levels:

- SG (Surface Area): Surface area where primary gas supply cylinders, specific to the required mixture for detectors, are located. Gases are mixed in the required proportions using a "mixer" module with flow regulators (Mass Flow Controllers, MFC) controlled by parameter management software (WinCC-OA). All units requiring immediate access are located in the surface area.
- US (Underground Service Area): Underground service area providing the initial division of the mixture into multiple lines (pre-distribution).
- UX (Experimental Cavern): The actual distribution to each detector is carried out in the experimental cavern

Here below there is a figure illustrating the proper arrangement. Figure(2.5).

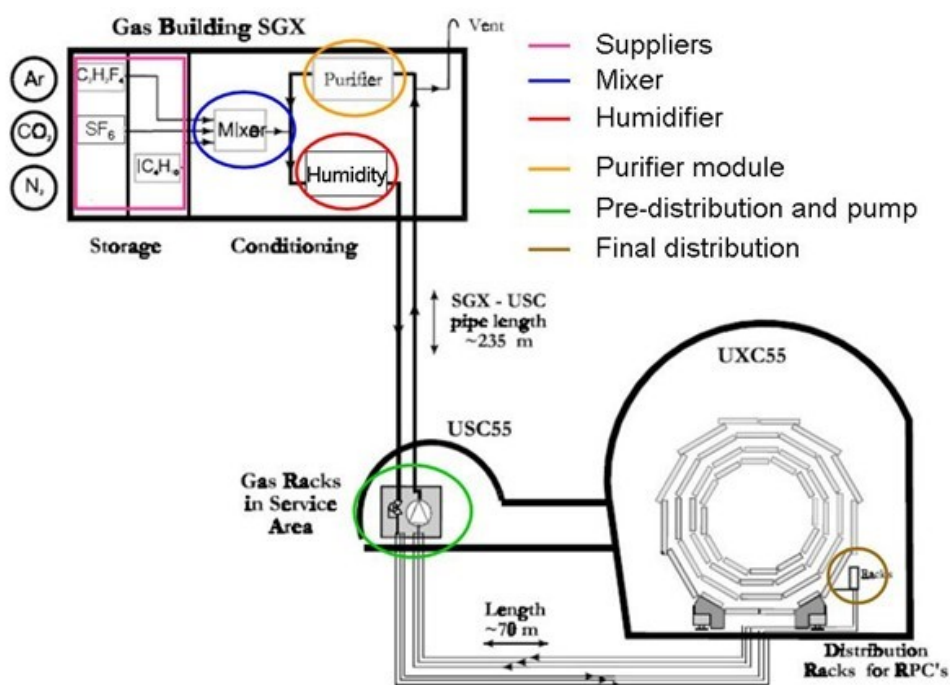


Figure 2.5: RPC gas system structure

Chapter 3

RPC gas system

At the conclusion of Chapter 2, we elucidated the concept of RPCs and their organization across three distinct levels. In this chapter, we will explore the intricacies of these three distribution levels in greater detail, examining their internal structures. The following section provides a comprehensive explanation.

3.1 Mixer

The mixer module is equipped with three input lines (as depicted in Figure 3.1) and is tasked with supplying the gas system and particle detectors with the appropriate gas mixture during the operational phase. Additionally, there may be specific phases where it becomes necessary to introduce different gases—for instance, purging the detector during the evacuation of the standard gas mixture, such as at the onset of an extended shutdown period, or delivering a standard mixture at a very high flow during detector restarts after prolonged shutdowns (filling mode). The injection of the gas mixture is finely tuned through mass flow controllers, ensuring an absolute precision of 0.3% [4]. This precise control is crucial to meet the required replacement rate, address potential leaks in the detector, or compensate for variations in atmospheric pressure. Notably, a significant number of detectors operate at a constant relative pressure, causing the gas volume within the detector to adjust to changes in atmospheric pressure [12]. Furthermore, the system is designed to automatically halt the gas flow if the concentration of iC_4H_{10} exceeds the flammability limit [6]. At 20 °C and atmospheric pressure, the lower and upper flammable limits are 1.86% and 8.41% by volume of air, respectively [19].

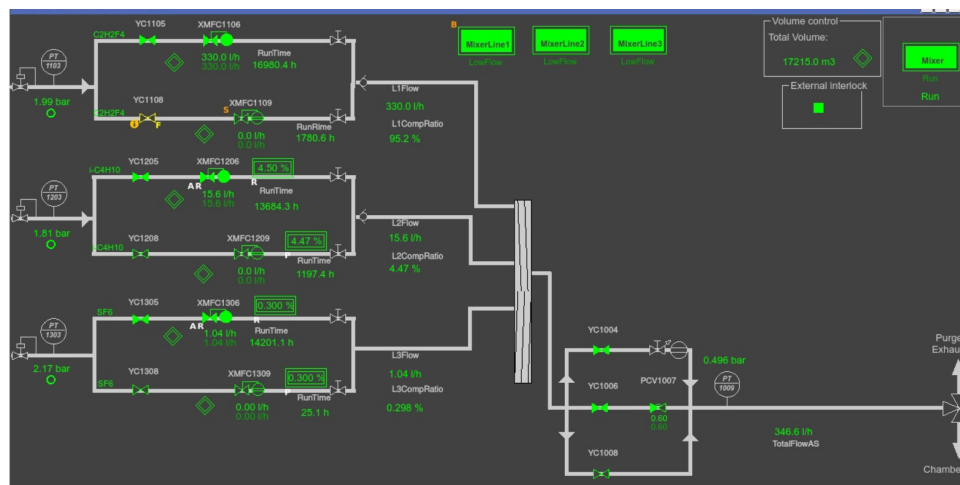


Figure 3.1: : RPC gas mixer with the WinCC OA software layout. Starting from the top to the bottom input lines , the following gas are injected: R134a, isobutane, and SF₆

3.2 Humidifier

After the initial gas mixture of RPCs is regulated at the mixer, it is directed to the humidifier. Here, the gas is imbued with the precise humidity required to enhance the avalanche effect in detectors operating at elevated temperatures. However, utmost care must be taken to maintain the correct relative humidity (around 40% at the RPC's operating temperature) [24] and avoid surpassing this threshold. This precaution is necessary because humidity has been found to impact the resistivity of the bakelite, which, over time, can detrimentally affect performance. In the humidifier module (Figure 3.2), the gas is split in two flows to modulate the humidity: one gas line flows through a water volume, while the other is maintained dry. Downstream, the two lines are mixed together and a water content analyser measures the mixture humidity, using the measured value as a feedback signal for splitting the input flow into the wet and dry channels [13].

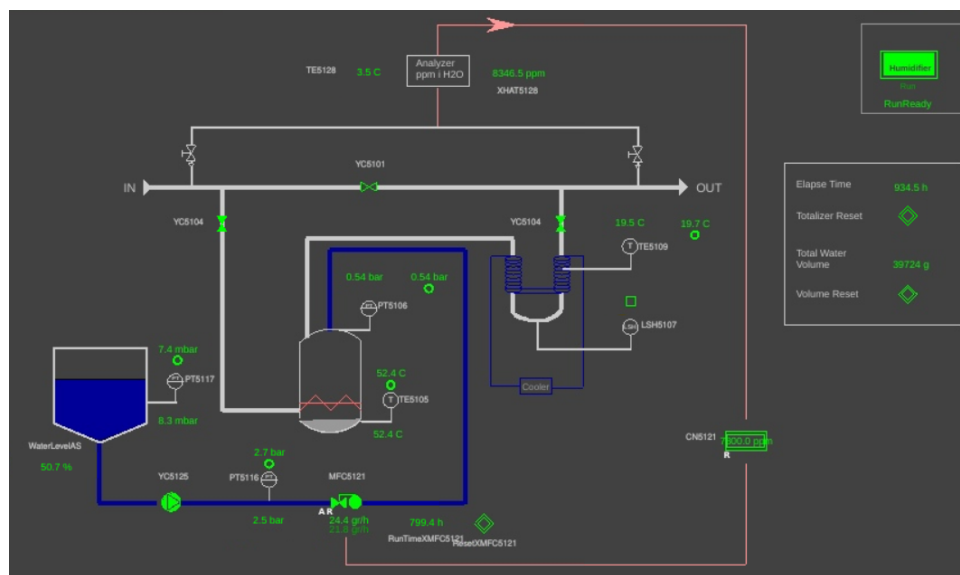


Figure 3.2: Gas Humidifier module with WinCC OA software layout.

3.3 Pump Module

After being processed by the humidifier, the gas mixture needs to be transported between the surface gas building and the distribution racks, in both directions. This requires the utilization of the pump system, situated 235 meters underground. The pump module comprises three parallel lines, (Figure 3.3). Each line is equipped with a pump dedicated to gas transportation, operating independently. In case of a malfunction in one pump, the other two are ready to step in.

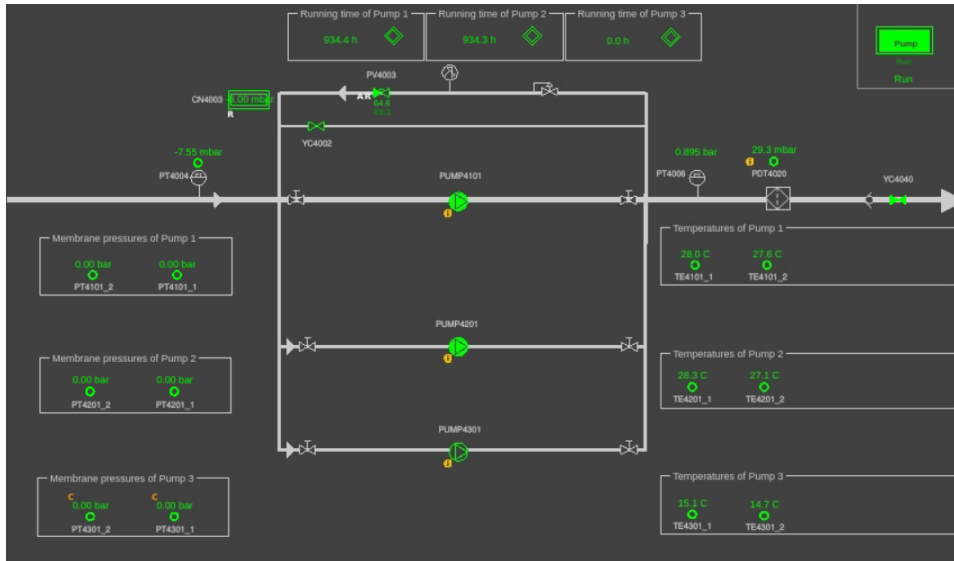


Figure 3.3: Pump module with WinCC OA software layout

3.4 Gas Purifier

After the gas mixture has been distributed to the RPCs, it is retrieved and pumped back to the surface building for recycling via the pump module. However, direct reuse is not possible due to the accumulation of impurities within the RPC chambers, which can significantly impact detector performance underground. The primary impurities include O₂ and H₂O, while others may arise from the breakdown and fragmentation of gas molecules caused by intense radiation and electric fields. Hence, to reuse a portion of the gas and mitigate these impurities, a gas purifier is installed in the surface building. The purifier unit (depicted in Figure 3.4) comprises two 24-liter cartridges filled with appropriate purifying agents. Typically, molecular sieves are utilized for water extraction, while metallic catalysts or other specific materials are employed for oxygen absorption. During regular operation, the gas mixture traverses one of the two columns, while the other undergoes regeneration or has just completed the regeneration cycle and is ready for use. Typically, regeneration procedures involve vacuum and high-temperature treatments (around 200 °C) for molecular sieves, and the application of high flows of Ar/H₂ mixtures at atmospheric pressure for metallic catalysts [24].

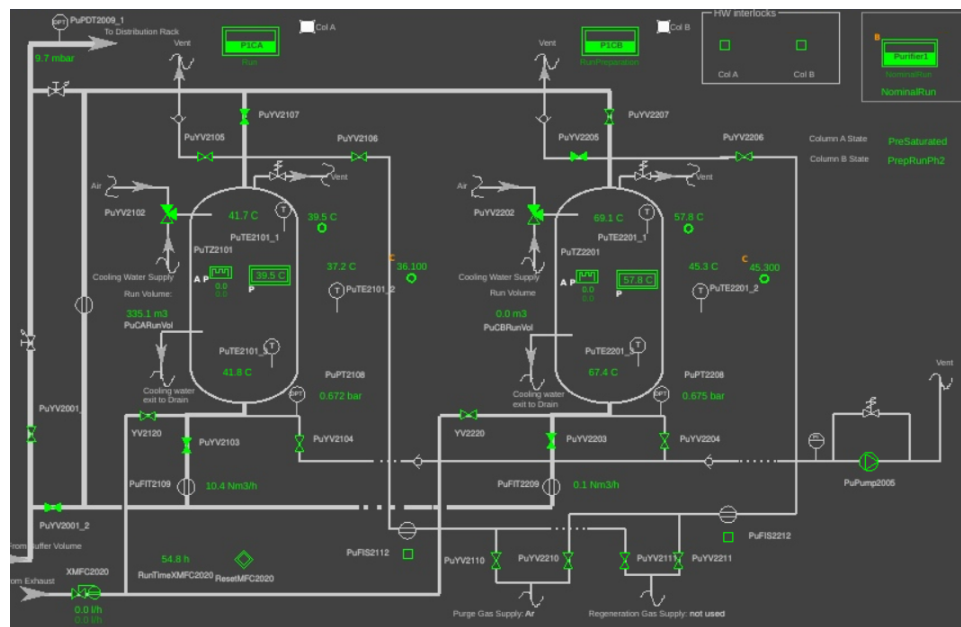


Figure 3.4: Gas Purifier with WinCC OA software layout. [24]

In the context of the RPC system, stringent purity requirements focus on nitrogen (j 1%) and oxygen (j 1%). The quantity of oxygen to be eliminated depends on the leakage rate of the chambers: the higher the rate, the greater the concentration of O₂ introduced from the external environment. Conversely, nitrogen, being an inert gas, can be removed solely by a recovery plant, such as the R134a recovery system [2].

Chapter 4

R134a recovery system

In this chapter we are going to give a detailed description on the R134a recovery system which is located in the gas room of the CMS facility. The recovery system is the result of a previous prototype which was previously built at ATLAS experiment in December 2018.

4.1 Prototype II configuration

The recovery system comprises three primary components (Figure 4.1): a vertical cold buffers and an horizontal hot buffer. Each buffer has distinct dimensions, with the first and third measuring 20 cm, while the second is 10 cm tall. In Appendix C.1 and D.1 we can clearly see the dimensions of these buffers. Additionally, an extra horizontal buffer is dedicated to stabilizing negative pressure before reaching the compressor, which is set at -500 mbar.

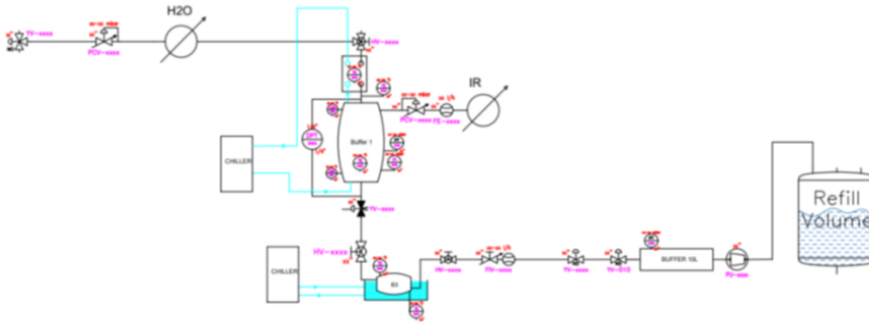


Figure 4.1: Prototype II of R134a recovery system

The system intakes a mixture of R134a (95.2%), iC_4H_{10} (4.5%), and SF_6 (0.3%) at $20^\circ C$ from the purifier 3.4. Before entering the first heat exchanger, this mixture undergoes by the Vaisala sensor to monitor H_2O concentration and ensure purity.

Upon exiting the first heat exchanger, the liquefied mixture fills buffer1, where its liquid level is controlled by a differential pressure transmitter. Given the discrepancy between the boiling temperature of SF_6 ($-67.6^\circ C$ at 1 bar) and the temperature of buffer1 ($-35.5^\circ C$), it's evident that SF_6 cannot condense and exits the system via the exhaust line. Additionally, a fraction of iC_4H_{10} and R134a exits the system as an azeotropic mixture, representing the most volatile component due to its lower boiling point compared to pure R134a ($-32.3^\circ C$ and $-26.4^\circ C$ respectively, at 1 bar).

The liquefied mixture then descends to buffer3, where the temperature exceeds 0°C, causing evaporation. Finally, the pumping unit extracts the recovered mixture by compressing it into the refill volume.

4.2 New R134a recovery system

The new recovery system was installed in the surface gas room and consists in four main units: the electric rack, the distillation unit, the pumping unit, and the storage units [1]. The system P&ID is reported in Appendix A.

4.2.1 Electric rack

The electric rack, depicted in Figure 4.2, serves as the housing for all electrical and electronic components essential for system automation, facilitated through the PLC (Programmable Logic Controller). This rack enables remote monitoring via the WinCC Open Architecture, a Supervisory Control and Data Acquisition (SCADA) system, and Human-Machine Interface (HMI) system from Siemens [25](Appendix B).

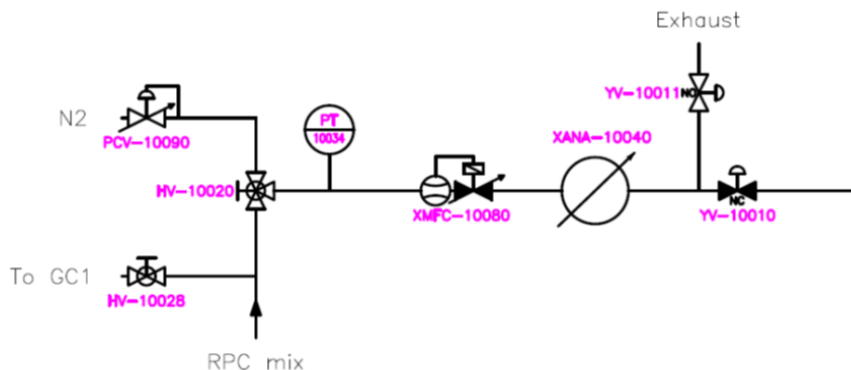


Figure 4.2: Electric rack P&ID

Within the electric rack, critical components include the mass flow controller, responsible for regulating the flowrate of the input mixture. Additionally, the Vaisala Dewpoint Transmitter is integrated to measure the dew point, ensuring the absence of water in the input stream—a crucial safety measure, as the dew point temperature should ideally not exceed -40°C.

Moreover, a three-way valve is strategically placed upstream of the Vaisala to facilitate the diversion of input flow from the mixture to the nitrogen line. This feature allows for versatile functionality, such as system purging operations.

4.2.2 Distillation Unit

The distillation unit is comprised of two enclosed racks, operating within an ATEX environment. Each rack houses two vertical columns dedicated to the separation process of the input mixture. These columns are equipped with both top and bottom buffers to facilitate the separation process. Additionally, the system is integrated with two refrigeration units: the HUBER UNISTAT 915w, responsible for setting the temperature of the top buffer cooling circuit (see Appendix 4) for technical data, and the Huber Ministat 125, which controls the temperature of the bottom buffers circuit.

The dimensions of the buffers vary depending on the column they belong to. For instance, columns 1 and 2 feature top buffers measuring 30 cm in height and bottom buffers measuring 10 cm in height (see Appendix E.1). Conversely, columns 3 and 4 have both top and bottom buffers measuring 20 cm in height. Despite these variations, all buffers share identical internal and external diameters, designed as coaxial cylinders, measuring 114.3 mm and 139.7 mm respectively (see Appendix F.1 D.1 for further details).

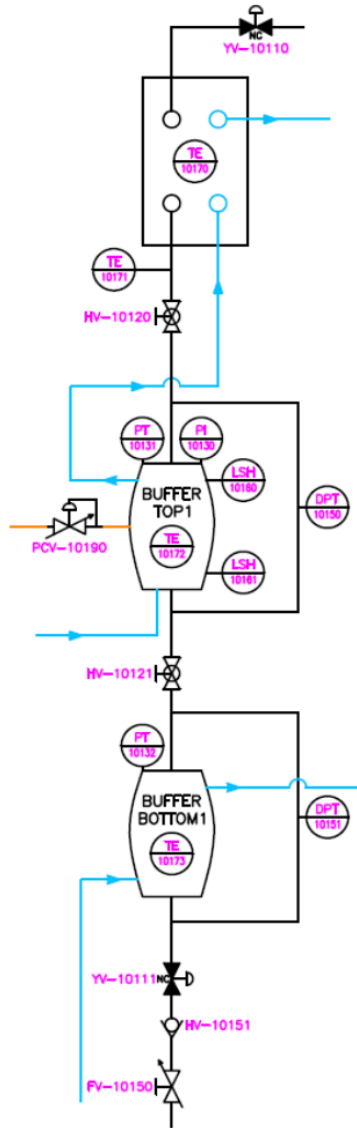


Figure 4.3: Column 1 P&ID. All columns have the same structure since they are designed in parallel.

Operating with four columns in parallel, each is filled individually. During the filling phase, the gas mixture is liquefied in a flat plate counter-current heat exchanger before entering the top buffer, where the separation process occurs. The top buffers must be cooled to a temperature within the range of the azeotropic and R134a boiling temperatures (-32.3°C and -26.4°C respectively, at 1 bar) to facilitate distillation.

As the liquid mixture flows down from the top to the bottom buffer through a 10 mm tube, gravity guides its movement. The bottom buffer, maintained at a warm temperature between 14°C and 23°C, allows for rapid evaporation of the mixture. The resulting vapor phase ascends due to buoyancy forces and condenses in the top buffer. The release of condensation heat gradually increases the temperature, causing the more volatile components to evaporate and exit through the exhaust line.

Once the filling phase concludes, the emptying phase commences with the opening of the pneumatic valve YV-10011. The recovered mixture flows through non-return and needle valves to regulate the emptying flowrate and prevent backflow issues.

Here, below a table is shown for a more clear comprehension of all the components presented in the P&ID (table 4.1):

Component	Index
Normally close pneumatic valve (column input)	YV-10x10
Normally close pneumatic valve (column output)	YV-10x11
Temperature sensor on heat exchanger	TE-10x70
Temperature sensor at the heat exchanger output	TE-10x71
Temperature sensor on the top buffer	TE-10x72
Temperature sensor on the bottom buffer	TE-10x73
Pressure transmitter on the top buffer	PT-10x31
Pressure transmitter on the bottom buffer	PT-10x32
Pressure indicator on the top buffer	PI-10x30
Lower liquid level sensor	LSH-10x61
Upper liquid level sensor	LSH-10x60
Top buffer differential pressure transmitter (for monitoring liquid level)	DPT-10x50
Bottom buffer differential pressure transmitter (for monitoring liquid level)	DPT-10x51
Zimmerli at the exhaust line	PCV-10x90
Manual valve connecting top and bottom buffers	HV-10x21
Non-return valve (to avoid backflows)	HV-10x51
Needle valve (to regulate emptying flowrate)	FV-10x50

Table 4.1: Component and Index of Distillation unit

4.2.3 Pumping and storage units

Following the completion of the filling phase, the emptying process commences. During this stage, the gas extractor, a double-stage gas booster compressor, is engaged to extract and convey the gas to the storage unit (refer to Figure 4.4). The rate of gas extraction is precisely controlled by a rotameter positioned downstream of the two racks. At the inlet of the compressor, a moderate vacuum is established to facilitate gas extraction. This is achieved by installing a 10 L buffer upstream of the compressor [7], and the air driving pressure is modulated to keep the buffer at a constant value of -300 mbar.

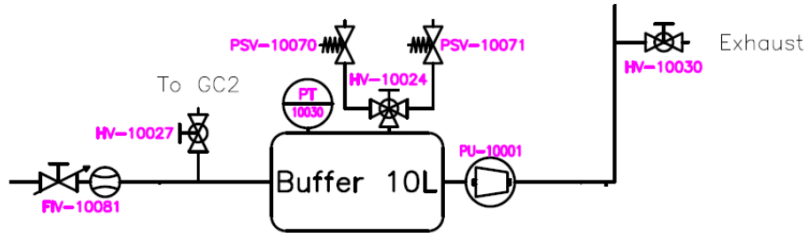


Figure 4.4: Pumping unit P&ID

The storage unit, depicted in Figure 4.5, takes the form of a stainless-steel cylindrical tank capable of holding up to 400 kg. It's essential to ensure that the pressure within the tank does not exceed the R134a saturation point (5.7 bara at 20°C [20]) to prevent the formation of liquid. Subsequently, a controlled flow of recovered gas is dispensed from the output of the storage unit into the RPC mixer at a pressure of 1.8/2.0 barg.

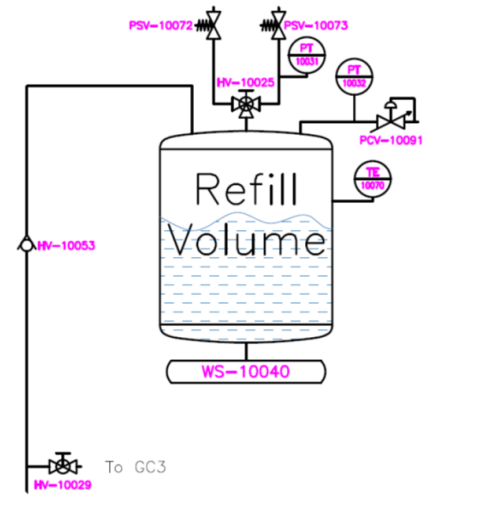


Figure 4.5: Storage unit P&ID

Component	Index
Rotameter (column output)	FIV-10081
Manual valve (before pump GC analysis)	HV-10027
Manual valve (exhaust line after pump)	HV-10030
Manual valve (after pump GC analysis)	HV-10029
Pressure transmitter (Buffer 10 L)	PT-10030
Pressure transmitter (inside storage tank)	PT-10031
Pressure transmitter (output storage tank)	PT-10032
Pressure safety valves (Buffer 10 L)	PSV-10070(1)
Pressure safety valves (Storage tank)	PSV-10072(3)
Non-return valve (avoid backflow to the compressor)	HV-10053
Pressure control valve (Tescom, storage tank output)	PCV-10091
Temperature sensor (monitoring the storage tank heating)	TE-10070
Weight scale	TE-10040

Table 4.2: Component and Index of Pumping and storage unit

4.3 Exhaust line of R134a recovery system

In this section, we'll thoroughly examine the exhaust line of the R134a recovery system (refer to figure 4.6 for detailed illustration). Subsequently, we'll discuss the most effective physical method for extracting SF_6 from our compound mixture. The exhaust line, positioned at the exit of the TOPx Buffers immediately after the PCV-10x90 valves, is identifiable by its orange color, as depicted in the AppendixA.1.

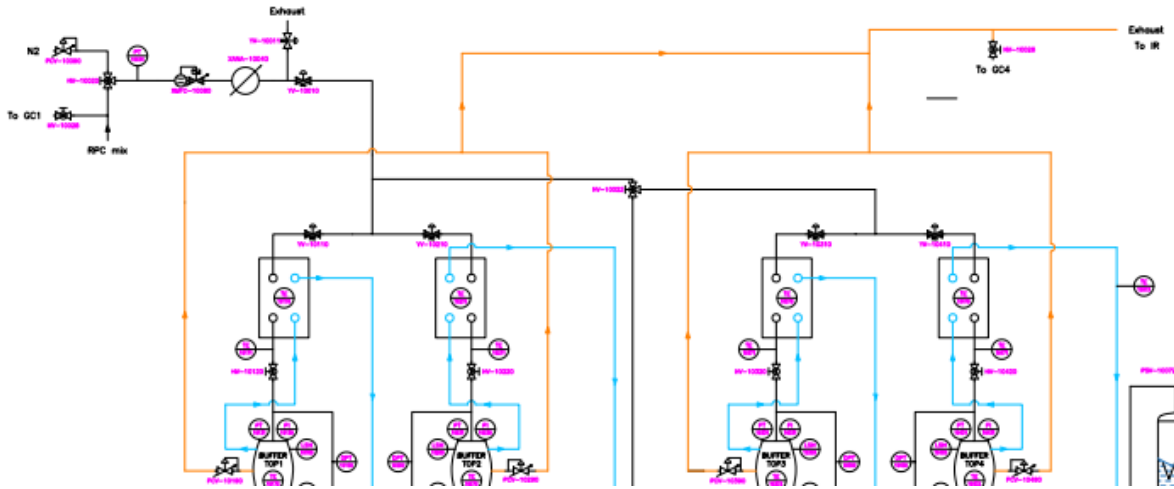


Figure 4.6: P&ID of the Exhaust line.

Considering the composition of the RPC mixture (refer to Table 2.1) and the maximum operational capacity of the freon recovery system set at 400 l/h, with an 80% recovery efficiency, the exhaust line will transport a gas blend at an average flowrate of 130 l/h. Unfortunately, we currently lack a means to directly verify the accuracy of this average flow rate due to the absence of a flowmeter on the exhaust line of the R134a recovery system. The decision to omit a flowmeter was made to sustain slightly higher pressure levels and to prevent the loss of the pressure differential of 10-20 mbarg over atmospheric pressure.

This blend will consist predominantly of 79% R134a, 19% isobutane, with smaller proportions of 1.3% SF_6 , and 0.36% N_2 . The temperature of this mixture will be maintained at 20°C, while the pressure will range between 10-20 mbarg. These specifications are crucial for designing a new SF_6 recovery system.

Chapter 5

Recovery of SF₆ with prototype 0

Prior to delving into the discussion and commentary regarding the design of the new SF₆ plant, we will first address the separation of the aforementioned mixture within an existing rack equivalent to Prototype II as described in Section 4.1. Here, the idea is to separate SF₆,N₂ from freon and isobutane, by performing a single stage criogenic distillation. The final aim of the test is to test the separation performances and the chemical physical proprieties of the gas via equilibrium diagrams.

5.1 Single stage simulation with Aspen Plus

In this section we are going to discuss on how the simulation with Aspen Plus for the existing rack where performed

5.1.1 Selection of thermodynamic method

For our simulation, we've chosen to utilize REFPROP as a thermodynamic method. This particular method is highly recommended for scenarios involving refrigerant fluids. Given that we primarily deal with a substantial quantity of R134a in our case, opting for this method is the most suitable choice.

5.1.2 Setting on the simulation

After setting the thermodynamic method, the simulation setup follows, which should be configured to mimic the real conditions as closely as possible. Prototype 0 has been constructed with the principle of single-stage separation in mind; therefore, the simulation should be adjusted accordingly. After establishing the thermodynamic method, the simulation setup proceeds by selecting a single flash separator in Aspen (see figure 5.1), followed by setting the molar fractions (see Table 5.1) and the inlet Temperature at 20 (°C) and a pressure of 1 (bar). Once the conditions are set, we set The flash separator at A temperature of -40 (°C) and a pressure of 1 (bar) as depicted in the figure, a non-optimized simulation can be run.

In the subsequent subsection, we will discuss how the simulation will be optimized.

Component	Concentration (%V)
IC ₄ H ₁₀	19%
R134a	79.3%
SF ₆	1.3%
N ₂	0.36%

Table 5.1: Components of the gas mixture in the exhaust line of R134a recovery system at CMS. (with respective volumetric percentages and feeding conditions).

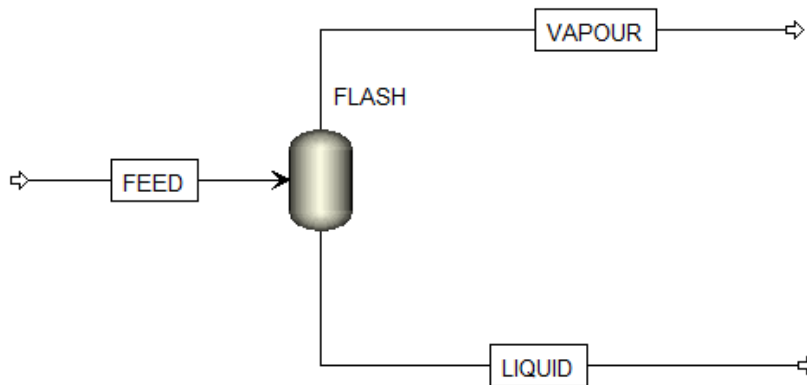


Figure 5.1: Aspen Plus, single stage FLASH separation

5.1.3 Sensitivity Analysis

A sensitivity analysis in Aspen Plus involves systematically varying input parameters or conditions within a simulation to assess their impact on the output results. This analysis helps in understanding the sensitivity of the model to different factors and can provide insights into which parameters have the most significant influence on the process [21]. Specifically, for our simulation, we aim to vary the inlet flow rate, inlet pressure, buffer temperature, and buffer pressure relative to the molar purity of component SF₆ in the vapor stream (refer to figure 5.1). The results of the analysis are presented the graphs below.

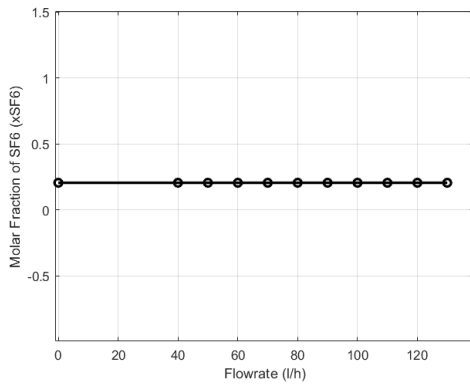
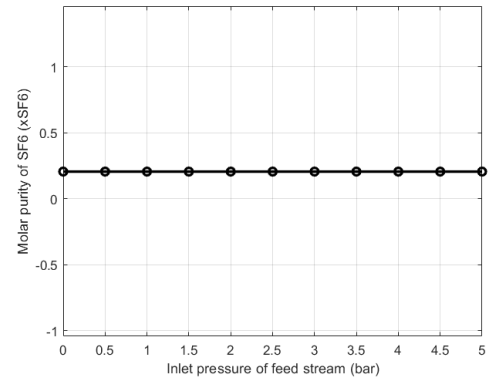
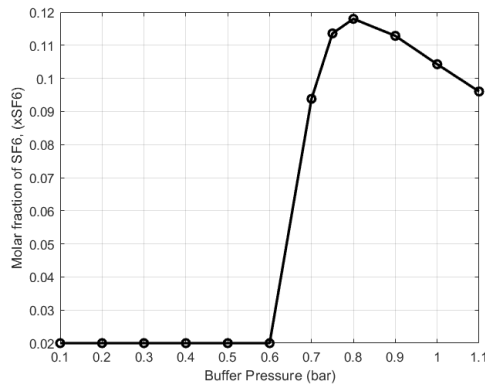
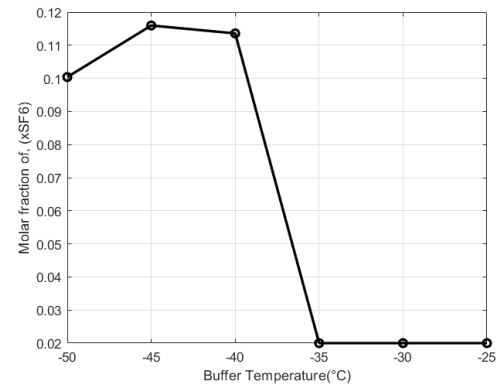
(a) Effect of variation of the inlet feed flowrate respect to the molar purity of SF₆(b) Effect of variation of the inlet pressure in (bar), respect to the molar purity of SF₆(a) Effect of variation of the Buffer pressure respect to the molar fraction of SF₆, (x_{SF₆})(b) Effect of variation of the Buffer Temperature in (°C), respect to the molar fraction of SF₆, (x_{SF₆})

Figure 5.3: First stage, sensitivity Analysis results

Based on the results of the sensitivity analysis, it's evident that the flow rate and inlet pressure of the feed stream to the buffer have no influence on the molar fraction of SF₆ (see Figure 5.2a and 5.2b). However, by varying the pressure and temperature of the buffer, we observe how these parameters affect the molar fraction of SF₆, (as shown in Figure 5.3a and 5.3b), consequently improving purity.

At this point, it becomes clear that we will set our flash to the optimal conditions to achieve the highest molar purity. In Table 5.2, the chosen values of inlet flow rate, pressure, and temperature in the buffer are reported.

Inlet feed stream (l/h)	Pressure in the buffer (bar)	Temperature in the Buffer (°C)
80	0,75	-45

Table 5.2: Optimal Feed Flowrate, Pressure and Temperature in Buffer 5.1

Unfortunately, even when utilizing the optimal configuration, it is evident that the SF_6 concentration in the vapor stream (5.1), remains low, reaching only 11% with a single separation stage (5.3).

Component	Concentration (%V)
iC ₄ H ₁₀	21.8%
R134a	59.1%
SF₆	11.4%
N ₂	0.08%

Table 5.3: Distillate composition of stream VAPOUR(see figure 5.1). Results of the single stage separation with Aspen Plus simulation).

Furthermore, it is important to consider that the outlet flow rate from the vapor stream is very low (only 4 out of 80 l/h at the inlet). By calculating the distillate-to-feed ratio (D/F) and the molar recovery (m_r) using the equations provided below (5.1 and 5.2), where \dot{D} and \dot{F} represent the distillate and feed flow rates, respectively, and y_c is the molar fraction of SF_6 in the gas mixture, the results shown in the table are obtained.

$$\frac{D}{F} = \frac{\dot{D}(l/h)}{\dot{F}(l/h)} \quad (5.1)$$

$$m_r = \frac{\dot{D} * y_c}{\dot{F} * y_c} \quad (5.2)$$

Distillate-to-feed-ratio	Molar recovery	Vapour Temperature (°C)	Duty of Buffer (KW)
0.05	0,44	-45	-0,0239

Table 5.4: Result of the Distillate-to-feed-ratio, molar recovery outlet Temperature and thermal duty of the Vapour stream 5.1

From the results of the calculations, it is evident that the distillate-to-feed ratio is very low, and the molar recovery is only 44%. Consequently, for design purposes, it will be necessary to consider recycling the bottom stream to achieve higher productivity. We will discuss this in more detail in Chapter (7). In the next subsection, a double-stage separation will be simulated to assess potential enhancements in the molar purity of SF_6 .

5.2 Double stage separation with Aspen Plus

In this section, we will discuss how to set up the simulation for a double-stage separation. Regarding the first stage, the steps and results to consider are the same as those outlined in the Single stage simulation section 5.1. In the following section, we will delve into more detail about the second stage, presenting the results of the simulation of the second stage, placed in series.

5.2.1 Simulation of the second stage

From the calculations conducted in Section 5.1.3, it is apparent that the second serial buffer receives a distillate with a minimal flow rate of only 4 [l/h]. For a clearer understanding, refer to Figure 5.4.

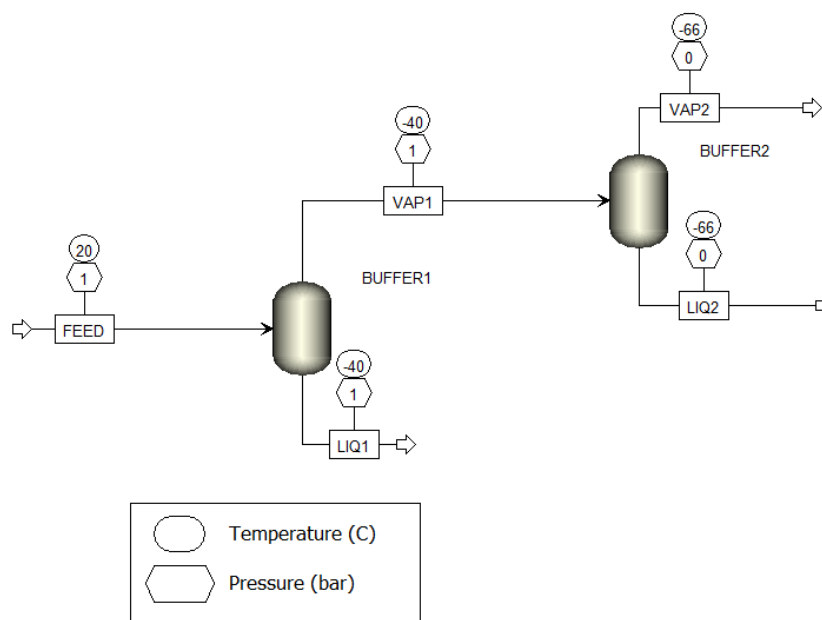


Figure 5.4: Aspen Plus, double stage FLASH separation

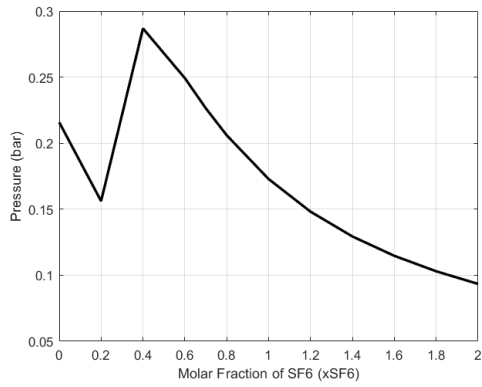
The composition at the inlet of BUFFER2 is the same as that reported in Table 5.3. Meanwhile, the inlet conditions in BUFFER2 are specified in the table below (5.5).

Feed flowrate (l/h)	Inlet Temperature(°C)	Inlet Pressure (bar)
4	-40	1

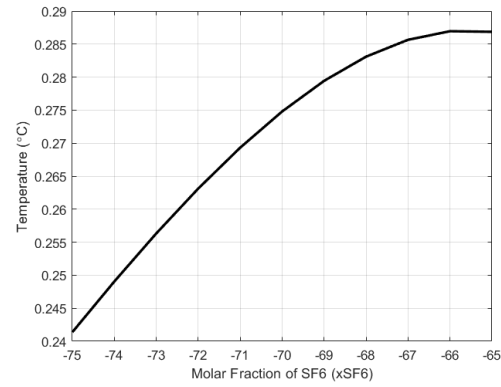
Table 5.5: Inlet conditions of BUFFER2 5.2a

Subsequently, sensitivity analyses were performed to determine which parameters are most influential in improving the concentration of SF₆ in the distillate of the second column. In our case, we will conduct a sensitivity analysis varying the temperature and pressure in BUFFER2, as a function of SF₆ molar fraction in VAP2 stream 5.4.

Based on the results of the sensitivity analysis, by varying the pressure and temperature of the buffer, we observe how these parameters affect the molar fraction of SF₆, (as



(a) Effect of variation of the Buffer pressure respect to the molar fraction of SF₆, (x_{SF_6})



(b) Effect of variation of the Buffer Temperature in (°C), respect to the molar fraction of SF₆, (x_{SF_6})

Figure 5.5: Second stage, sensitivity Analysis results

shown in Figure 5.5a and 5.5b), consequently improving purity.

At this point, it becomes clear that we will set our BUFFER2 to the optimal conditions to achieve the highest molar purity. In Table 5.6, the chosen values of inlet flow rate, pressure, and temperature in the buffer of the second stage are reported.

Feed flowrate (1/h)	Temperature in Buffer 2(°C)	Pressure in Buffer 2(bar)
4	-66	0.4

Table 5.6: Inlet conditions of BUFFER2 (5.4)

So, by setting the condition listed in table 5.6, the distillate stream of the second buffer has this composition (5.4) Once the simulation results are obtained, the calculation of

Component	Concentration (%V)
IC ₄ H ₁₀	10.4%
R134a	22.5%
SF₆	28.7%
N ₂	38.5%

Table 5.7: Distillate composition of stream VAP2 (see figure 5.4). Results of the double stage separation with Aspen Plus simulation.

the molar recovery and distillate-to-feed ratio for the second stage follows, using the same equations (5.1 and 5.2) as outlined above. Additionally, the thermal duty required for the separation is also reported in the table 5.8.

Distillate-to-feed-ratio	Molar recovery	Vapour Temperature (°C)	Duty of Buffer (KW)
0.33	0.84	-66	-0,00087

Table 5.8: Result of the Distillate-to-feed-ratio, molar recovery, outlet Temperature and thermal duty 5.4

From the obtained values, it can be deduced that both the distillate-to-feed ratio and molar recovery for the second stage are significantly improved. However, the flow rates remain very low (just over 1 l/h), as indicated by the negligible thermal expenditure required for the separation (see Table 5.8).

Finally, by analyzing all the results obtained, the productivity (equation 5.3) and total plant recovery values are calculated. Where \dot{V}_2 and \dot{F} , are respectively, the distillate of the second stage (which is 1,36 l/h) and the feed of the first stage (which is 80 l/h).

$$Productivity\% = \frac{\dot{V}_2(l/h)}{\dot{F}(l/h)} * 100 \quad (5.3)$$

These results are presented in Table 5.9.

Productivity	Total Molar Recovery
1.6%	37%

Table 5.9: Productivity and molar recovery of entire Separation, results. Conducted by Aspen plus simulator

Based on the obtained results, proceeding with experimentation for a second stage seems discouraging, as both the productivity and total recovery would be very low. Therefore, in the context of a new project, reconsideration of recovering the bottom stream is necessary to mitigate the negative impact on productivity. The experiments conducted at CMS will serve to evaluate the reliability of the simulator and its proximity to real conditions.

5.3 Prototype 0

In this section, we will briefly discuss Prototype 0, designed to experimentally test the separation of SF₆ from a mixture of R134a, iC₄H₁₀, and N₂. This system was initially constructed and implemented for the first recovery of R134a. After its initial use, the system was halted when a new R134a recovery setup was introduced. Subsequently, some minor modifications were made to reconfigure the system for the new testing requirements.

The recovery system consists of three primary components (Figure 5.6): a heat exchanger, a vertical cold buffer, and a horizontal hot buffer. The system intakes a mixture of R134a (79%), iC₄H₁₀ (19%), and SF₆ (1.3%) at 20°C from the exhaust line.

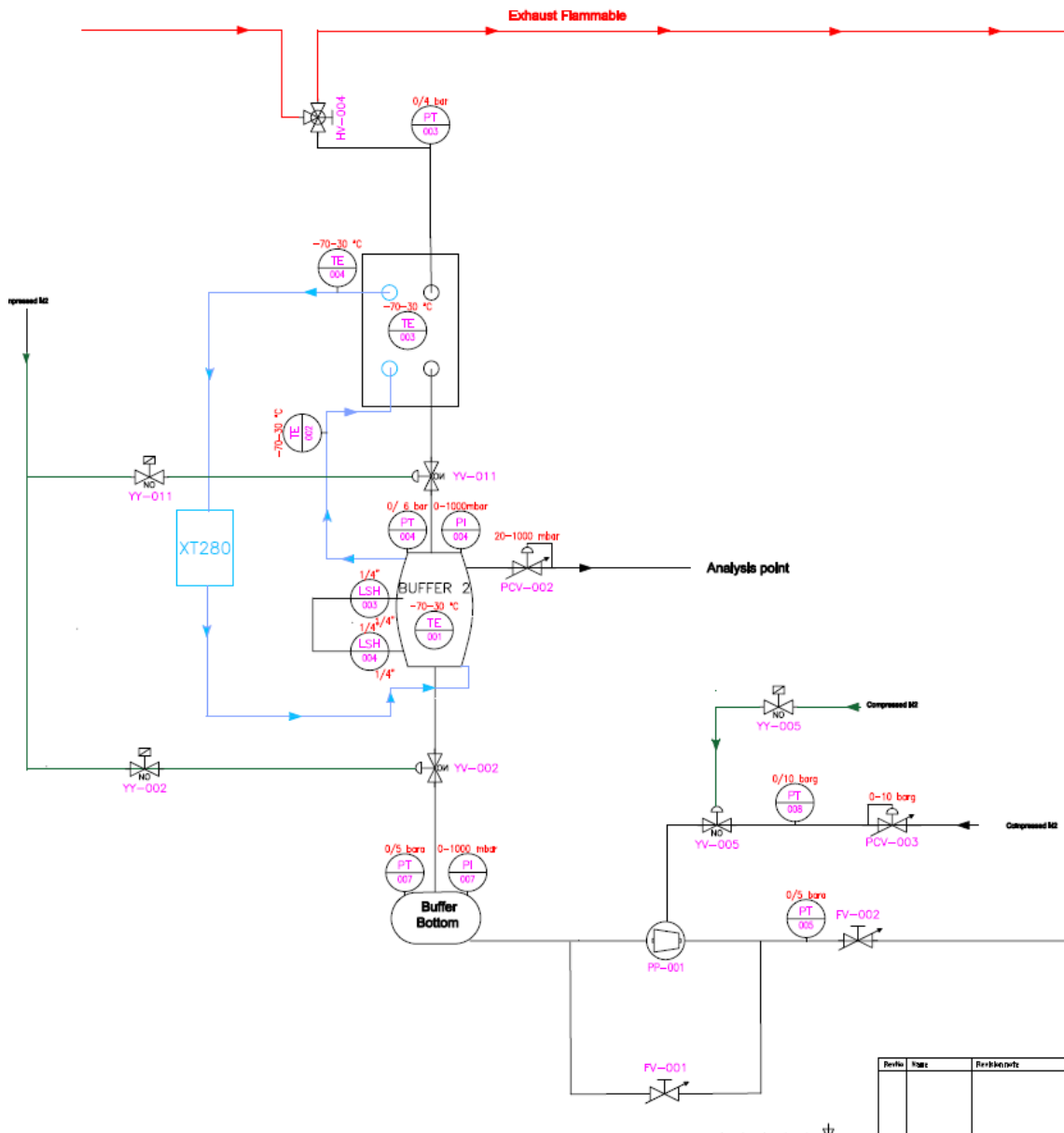


Figure 5.6: Prototype 0 for SF₆ separation in the gas room of the CMS experiment.

Upon exiting the first heat exchanger, the liquefied mixture fills Buffer 2, where its liquid level is controlled by a level sensor. Due to the discrepancy between the boiling points of SF₆ (-67.6°C at 1 bar) and the other two components, R134a (-26°C at 1 bar) and iC₄H₁₀ (-11°C at 1 bar), the temperature of Buffer 1 is set at -45°C. We expect that all components except SF₆ will condense, so SF₆ will exit the system via the Zimmerli valve, PCV-002 (see Appendix 5.6 for reference). Additionally, a fraction of isobutane and R134a exits the system as an azeotropic mixture, representing the most volatile component due to its lower boiling point compared to pure R134a (-32.3°C and -26.4°C, respectively, at 1 bar).

Monitoring the composition is essential, so a sample point with a GC line will be installed at the outlet of the Zimmerli valve PCV-002.

The liquefied mixture then descends to the bottom of the buffer, where the temperature exceeds 0°C, causing evaporation. Finally, the compressor unit pumps the separated gas into the exhaust flammable line. For a clearer understanding, refer to the P&ID in Appendix G.1.

Component	Index
Manual valve (Three way valve)	HV-004
Pressur Transmitter (before heat exchanger)	PT-003
Temperature sensor (monitoring the refrigerant temperature at the inlet of Heat exchanger)	TE-002
Temperature sensor (monitoring the refrigerant temperature inside of the Heat exchanger)	TE-003
Temperature sensor (monitoring the refrigerant temperature at the outlet of Heat exchanger)	TE-004
Pneumatic valve (after heat exchanger)	YV-011
Pressure transmitter (at the Top of buffer 2)	PT-004
Pressure indicator (at the Top of buffer 2)	PI-004
Zimmerly valve (output of top buffer)	PCV-002
Upper liquid Level sensor	LSH-003
Lower liquid level sensor	LSH-004
Pneumatic valve (between buffer 2 and buffer bottom)	YV-002
Pressure transmitter (inside storage tank)	PT-004
Pressure transmitter (input buffer bottom)	PT-007
Compressor gas Booster	PP-001
Needle hand valve	FV-001
Pressure control valve (compressed nitrogen line)	PCV-003
Pressure Transmitter (compressed nitrogen line)	PT-008
Pneumatic valve (compressed nitrogen line)	YV-005
Pressure Transmitter (after compressor)	PT-005
Needle valve (after compressor)	FV-002

Table 5.10: Component and Index of Prototype 0

Chapter 6

Investigation on gas mixture's distillation

Before delving into the description and design of the new SF₆ recovery plant, it is of fundamental importance to study thermodynamic properties and binary diagrams to partially understand the interactions and quantities of liquid and vapor formed, along with their respective compositions. A simplification is made by considering only binary interactions and neglecting mutual interactions among all four components. This simplification arises due to the complexity of studying chemical interactions among four components, coupled with the absence of relevant literature data on this specific mixture.

Given this, our approach involves examining phase diagrams for key binary pairs among the four components in our mixture. Subsequently, we will employ a McCabe-Thiele method to determine the theoretical number of stages required for designing a simplified distillation column. Our focus will be primarily on SF₆ and R134a, as these are the dominant components in the mixture. Furthermore, we are introducing Isobutane as the third component and we are analyzing the ternary diagram formed for this three components and all the possible suitable solution, that we could adopt for separating this mixture.

6.1 VLE equilibria

To study our system accurately, it is crucial to examine a thermodynamic model that can satisfy the liquid-vapor equilibrium of a mixture composed of SF₆ and R134a. In our case, a REFPROP thermodynamic model was assumed. The condition of vapor-liquid equilibrium (VLE) is expressed through the equality of the chemical potentials (μ) in the two phases, therefore, for the j^{th} component in the mixture, one can write:

$$\mu_j^l = \mu_j^v \quad (6.1)$$

And the chemical potential associated with the liquid and gas phase (??), can be, respectively express as :

$$\mu_j^l = x_j P_{s,j} \quad \mu_j^v = y_j P \phi_j \quad (6.2)$$

Where μ_j^l and μ_j^v are the chemical potentials of the j^{th} component respectively in liquid and vapor phase. P and $P_{s,j}$ are the pressure of the system and the vapor pressure of the j^{th} component. The term γ_j and ϕ_j is a term as follows:

$$\phi_j = \frac{\phi_j}{\phi_{\text{sat},j}} e^{\frac{v_i^l(P-P_{s,i,j})}{RT}} \quad (6.3)$$

Where ϕ_j is the fugacity coefficient of j^{th} species in the mixture at T,P condition, $\phi_{\text{sat},j}$ at saturation conditions and, lastly the exponential term is the Poynting Factor ([8]). Most of the time, the fugacity coefficient is believed unitary in system with low pressure. On the other hand, it is a very strong assumption to neglect the activity coefficients. In fact, the second assumption suggests that there is absolutely no interaction between the molecules in the liquid phase and this could be a wrong assumption, therefore it is necessary to study activity coefficient at 3 bar of pressure (see figure 6.1)

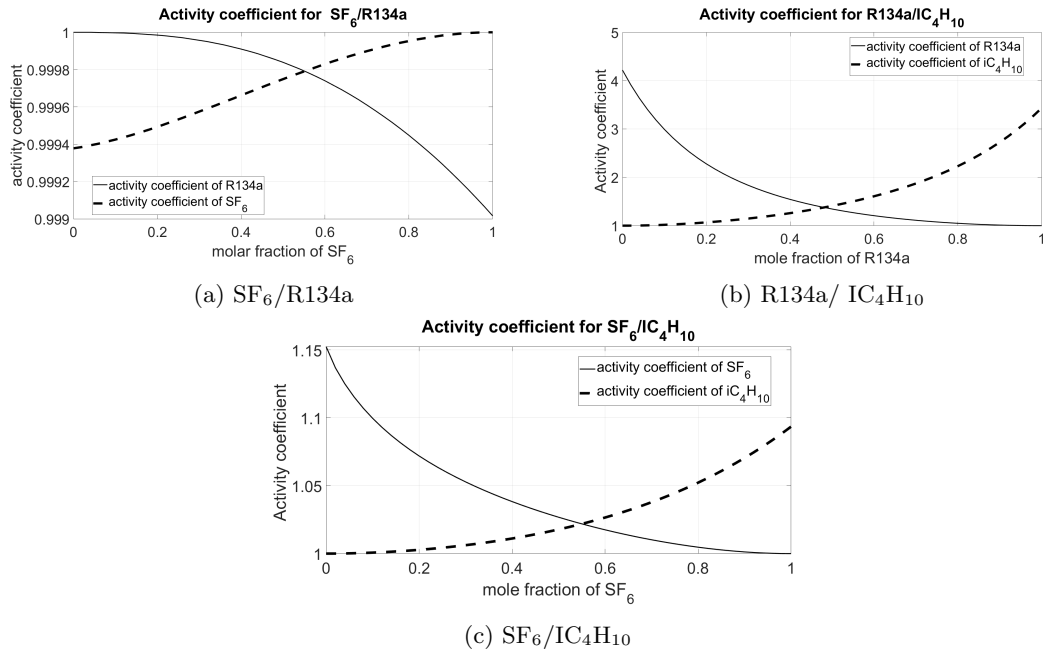


Figure 6.1: Activity coefficient for binary mixtures at 3 bar

It is clearly seen from the graph 6.1, that the activity coefficients can be assumed to be unity. Consequently, for the system under consideration, an ideal behavior can be assumed for SF_6 and R134a (6.1a), the same could be said for SF_6 and IC_4H_{10} (6.1c), while the activity coefficient are clearly non ideal for R134a/ IC_4H_{10} (6.1b). In fact, this last two components form a minimum boiling azeotrope, wich is typical for non ideal components.

Let's now analyze the binary diagram for SF₆/R134a. In this case, we will plot the Txy curves at various pressures (see Figure 6.2). Once the optimal working pressure is chosen, the other Txy curves of the other binary pairs will be represented directly at the selected optimal pressure.

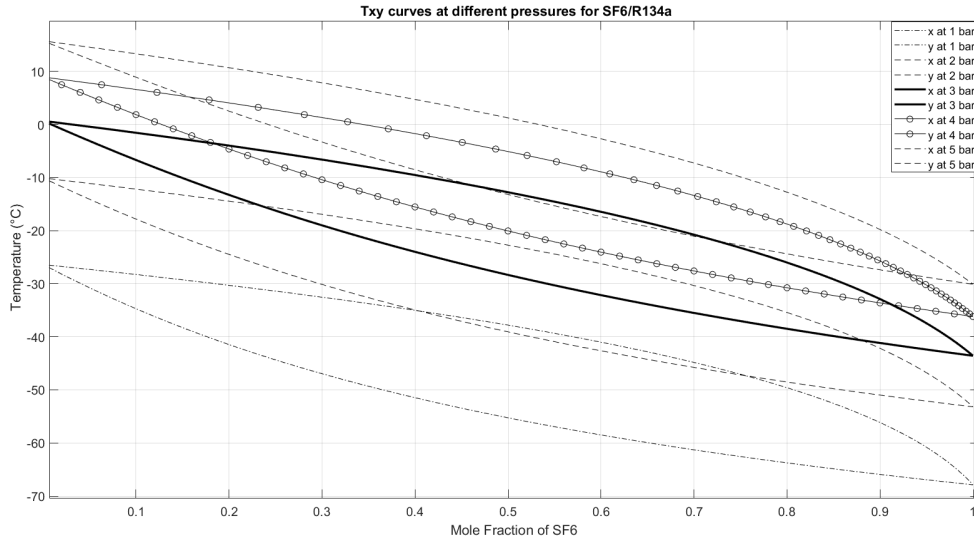


Figure 6.2: Txy diagrams for SF₆/R134a at different pressures

The analysis starts with the binary diagram of the key component to be distilled and the other component present in greater quantity, in our case SF₆ and R134a. Upon examining Figure 6.2, it became evident that the temperature ranges from 0 to -70°C at a pressure of 1 bar. Achieving these temperatures would require a larger amount of cooling, resulting in high operational costs. To mitigate this issue, a working pressure of 3 bar was selected. Knowing that the composition of the incoming mixture was mentioned in the previous chapter, (refer to Table 5.1 for reference). For the binary analysis, we scale the new compositions by considering the sum of the two compositions (79% R134a and 1.3% SF₆), thus scaling them on a basis of 80.3%. Resulting in 1.6% in SF₆ and 98.4% of R134a. Considering the binary diagram at this composition we can see that at 1.6% at a temperature of -7.5(°C), we are in the biphasic region with the below mentioned composition:6.1: We can then split the liquid and vapour fraction at this temperature to

Phase	Component	Concentration (%V)
Liquid	SF ₆	11.3
	R134a	88.7
Vapour	SF ₆	33.2
	R134a	66.8

Table 6.1: Liquid and Vapour phase equilibria at Temperature of -7.5 °C at pressure of 3 bar

have a liquid and vapour phase at this equilibrium composition. The vapour stream is more reach in SF₆ compared to the liquid one, this means that when acting the biphasic separation of this two component gas phase will be of our interest.

6.1.1 McCabe-Thiele Approach for the determination of Theoretical number of stages for a biphasic separation of SF₆ and R134a

In the following section, we will outline a simplified approach for determining the number of ideal stages for our distillation process using the approximate method of McCabe-Thiele. For our distillation, we consider the incoming mixture with feeding conditions as detailed in Table (6.2). Our target is to achieve a distillate purity of SF₆ (x_d) of 99%, with an acceptable recovery, of 60%. Subsequently, we assume that the incoming

Component	Concentration (%V)	Feed Flowrate (l/h)	Temperature(°C)	Pressure (bar)
IC ₄ H ₁₀	19.3%	0.52	25	3
R134a	79.3%	31.736	25	3
SF ₆	1.3%	7.6	25	3

Table 6.2: Feeding condition for the distillation column

mixture behaves as a saturated vapor mixture, hence setting $q = 0$. For brevity, only some equations will be mentioned in the following description. A comprehensive explanation can be found in the referenced article ([17]).

Given the SF₆-R134a mixture's ideal nature, McCabe-Thiele employs a constant relative volatility ($\alpha = 5.107$) assumption throughout the column. This α value was derived from equation (6.8), then after calculating it for all the j th components, an average value was taken. By utilizing equation (6.7), we determine y (vapor molar fraction) as a function of x (liquid molar fraction), facilitating the representation of the equilibrium curve, (refer to Figure 6.3). Employing the linear equation of the rectifying section (6.4), we

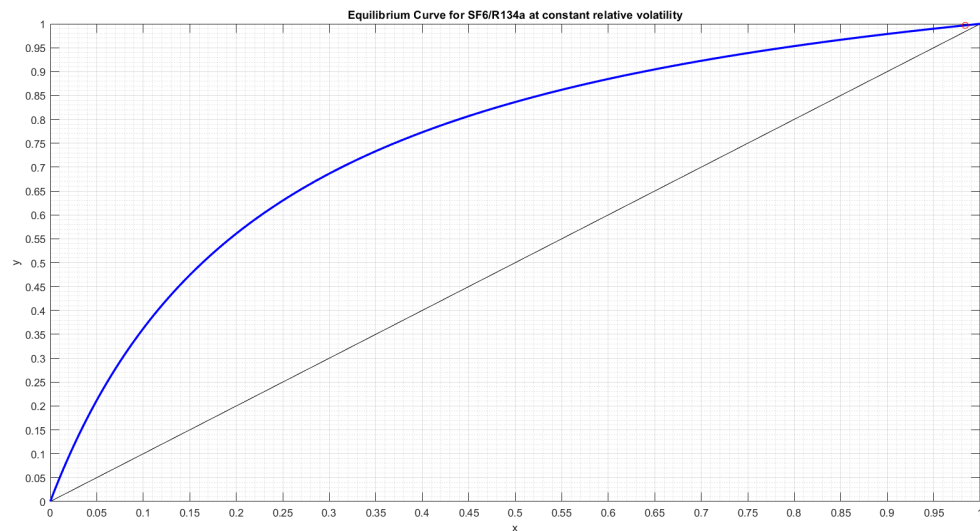


Figure 6.3: Equilibrium curve for SF₆/R134a at temperature of -20 °C and pressure of 1 bar

initiate from the distillate composition x_d , intersecting it with the feed line. Similarly, starting from x_b , we intersect the stripping line (6.5) and connect it with the feed condition. With a stage efficiency of 0.5 taken into account, we proceed accordingly. Starting from x_d , we draw a horizontal line intersecting the equilibrium curve. From the equilibrium curve, we intersect the rectifying line by drawing a vertical segment and

repeat the process. The number of stages is thus determined.

$$y = \frac{L}{V}x + \frac{x_D D}{V} \quad (6.4)$$

$$y = \frac{\bar{L}}{\bar{V}}x + \frac{x_B B}{\bar{V}} \quad (6.5)$$

$$y = \frac{q}{q-1}x - \frac{zf}{q-1} \quad (6.6)$$

$$y = \frac{\alpha x}{1 + (\alpha - 1)x} \quad (6.7)$$

$$\alpha_{i,j} = \frac{K_i}{K_j} = \frac{y_i(1-x_j)}{x_i(1-y_j)} \quad (6.8)$$

For our specific distillation case, a MATLAB code was developed to determine the number of ideal stages (see Appendix G.1 for reference). In total, 7 ideal stages were determined: 6 in the rectification section and 1 in the stripping section, with feeding at the 6th stage (see figure 6.4).

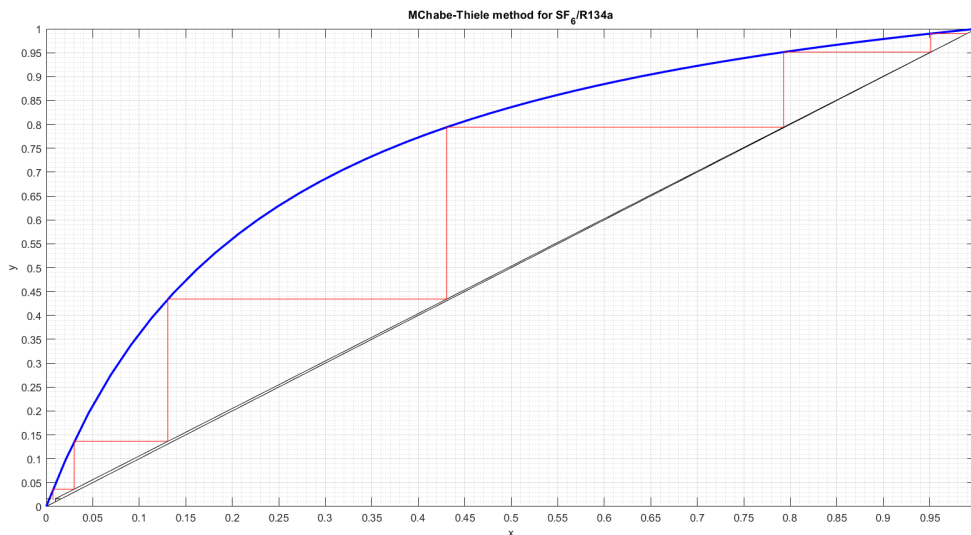


Figure 6.4: Evaluation of theoretical Plate for SF₆/R134a using McCabe Thiele method

Obviously, the obtained result of six ideal stages (considering 100% efficiency) helps us understand what the number of stages in a hypothetical distillation column would be if the separation were ideal and only the two key components were involved. For a multicomponent system like ours, the approximation used by McCabe-Thiele is not exhaustive but serves as a good starting point for studying the binary separation of these two components.

6.2 Azeotropic distillation

An azeotrope, or azeotropic mixture, consists of two or more liquid substances or vapors that cannot be separated by distillation due to their identical vapor composition, denoted as $y = x$, at the desired temperature [8]. When the temperature at which the compositions match exceeds the boiling point of the two components, it's termed a maximum boiling azeotrope see figure (6.5); conversely, if it's below, it's known as a minimum boiling azeotrope (figure 6.5).

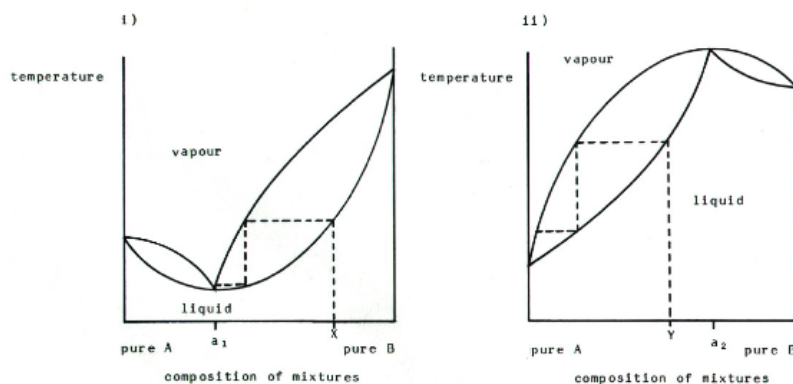


Figure 6.5: Minimum and maximum boiling azeotrope

Azeotropic distillation is a method used in industries like chemicals and petrochemicals to separate mixtures that are difficult to separate by simple distillation [8]. These mixtures might contain an agent called an "entrainer" that helps with separation, either already in the mix or added separately. Azeotropic distillation can handle tricky mixtures that have components with similar boiling points or mixtures that form azeotropes. Different methods are used to make azeotropic distillation work well, like picking the right entrainer or changing the pressure. In the next subsection, we are going to give a short description of them.

6.2.1 Homogenous Azeotropic distillation

Homogeneous azeotropic distillation involves using a specific flow sheet structure to achieve separation in one or more distillation columns. This method either takes advantage of or avoids azeotrope formation in the system. The structure of the separation process depends on the shape of the residue curve map or distillation region diagram for the mixture and entrainer. There are two main approaches: choosing an entrainer so that all desired products are in the same distillation region, or selecting an entrainer that allows separation of products in different regions by crossing distillation boundaries.

For breaking homogeneous binary azeotropes, certain residue curve maps are suitable depending on whether the original components have a distillation boundary connected to the azeotrope. Entrainers must meet specific criteria regarding boiling point and azeotrope formation. For example, for dehydrating organics that form azeotropes with water, finding a suitable entrainer can be challenging due to the need to avoid azeotrope formation with water [15]. Unfortunately, here at CERN, this option is not applicable because we did not want to contaminate our gas mixture that is going on RPC so, due to this the pressure sensitivity approach is adopted.

6.2.2 Pressure sensitivity azeotrope

Pressure can affect the composition of many azeotropes, and pressure-swing distillation can exploit this effect to separate azeotropic mixtures. In our case we are going to exploit if the azeotropic distillation of R134a-isobutane is pressure sensitive or not, by simply plotting the binary diagram at two different pressures.

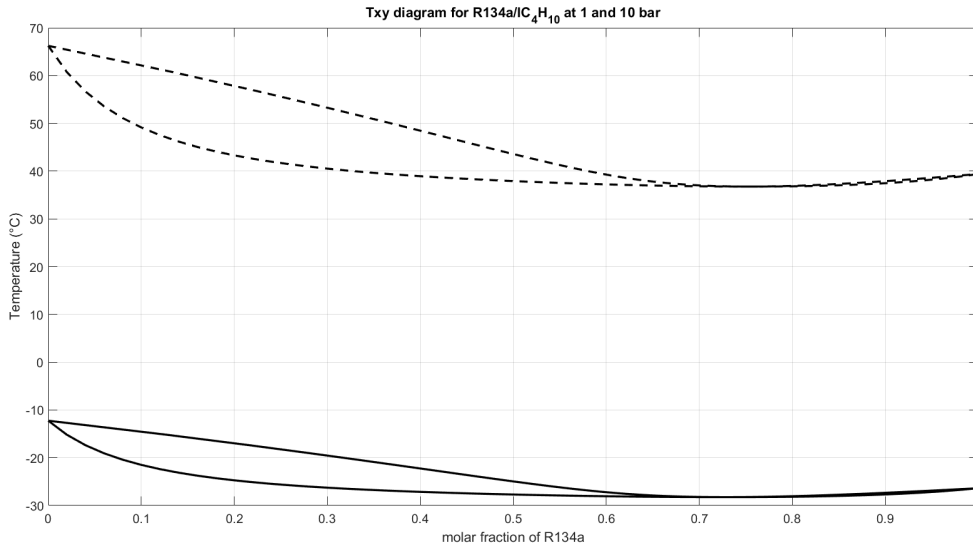


Figure 6.6: Txy curves of R134a-IC₄H₁₀ at 1 and 10 bar

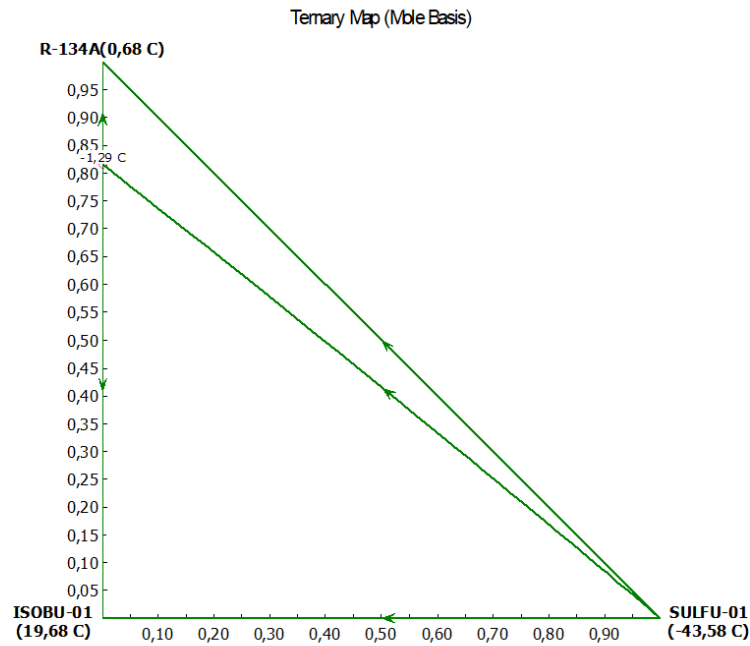
From figure 6.6, it is evident that even with a variation of 10 bars in pressure, the azeotrope only shifts by 5%. We transition from a 65-35 to a 70-30 composition, which implies only a slight movement of the distillation boundary. In fact, as mentioned by the author Kirk, only a few azeotropes are significantly influenced by the pressure effect, such as the tetrahydrofuran-water and hydrogen chloride-water systems [8]. Many others, however, are not affected by pressure, necessitating investigation into an appropriate entrainer that can shift or separate the azeotrope to facilitate its separation. In this thesis, we are not going to exploit this alternative because there is no experimental data and test could not be performed.

6.2.3 Ternary diagram for SF₆/R134a/isobutane

In this section, we are going to represent the ternary diagram for the three components which are SF₆/R134a/isobutane, unfortunately, the presence of the azeotrope, poses our boundary limits for the construction of the ternary diagram. The reading and comprehension of this ternary diagram could let us understand what are the limits that we have in our azeotropic distillation. Here below there the graph is represented by using aspen PLUS software and using UNIFAC as a thermodynamic method.

Positioned at the vertex of the ternary diagram is R134a, which stands as the component with a boiling temperature situated between the other two. Isobutane occupies the bottom-left vertex with the highest boiling point, while SF₆ is situated at the bottom-right with intermediate boiling point.

Subsequently, we mark another significant point on the R134a-isobutane line at the composition of the azeotrope. From this point, a straight line is drawn until it intersects with the light key component at the bottom-right corner of the ternary diagram (refer

Figure 6.7: Ternary diagram and boundary limits for $\text{SF}_6/\text{R134A}/\text{IC}_4\text{H}_{10}$

to Figure 6.7). Then we place our homogeneous low boiling known azeotrope in our ternary diagram, which has a composition of 81,6-18,4 %. Then we identify our stable nodes, saddles, and unstable nodes. For our diagram a VLL equilibria is considered. Here, we have two stable nodes, one saddle, and one unstable node. In the table below a clearer classification of the type of nodes is here mentioned 6.3:

Temperature (°C)	Classification	Type	Number of components	SF_6	IC_4H_{10}	R134a
-43.576	Unstable node	Homogeneous	1	1	0	0
-1.293	Saddle	Homogeneous	2	0	0.184	0.816
0.684	Stable node	Homogeneous	1	0	0	1
19.681	Stable node	Homogeneous	1	0	1	0

Table 6.3: Azeotrop investigation: Classification of nodes

Following this, we plot the various residue curves identified by the Aspen Plus software. These curves illustrate the evolution of the liquid composition throughout the boiling process of the mixture, under the assumption of batch distillation, see figure 6.8 for reference.

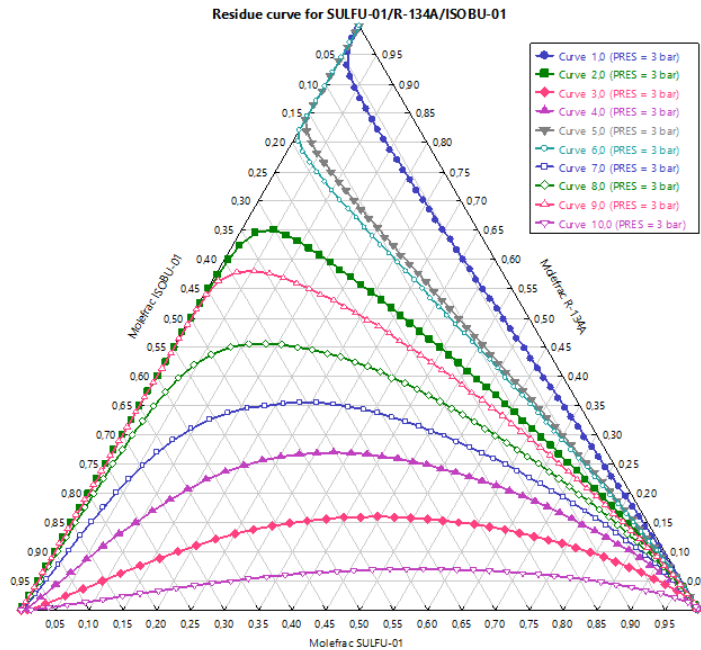


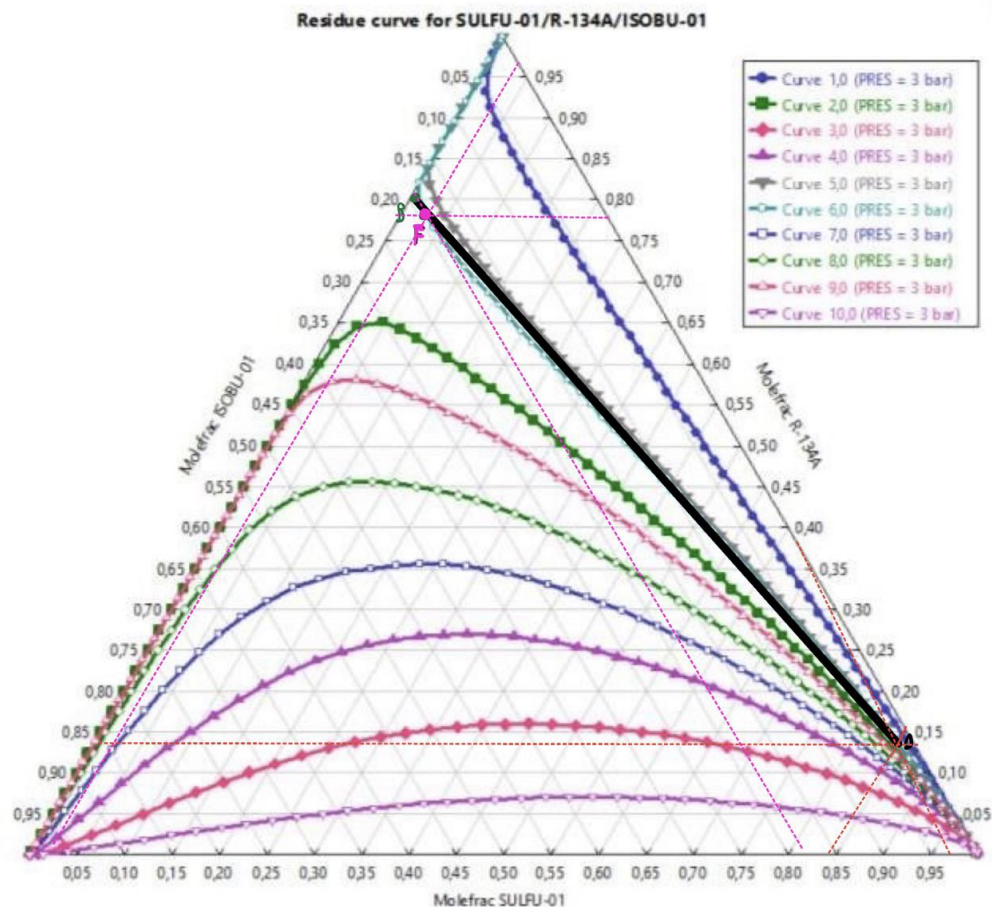
Figure 6.8: Residue curves and boundary limits for SF₆/R134A/iC₄H₁₀

Identifying the appropriate residue curve enables us to establish the composition of the distillate according to our requirements. For instance, for the three components in our system, we have a gas mixture with a feed composition detailed in Table 6.8.

Component	Concentration (%V)
iC ₄ H ₁₀	19.3%
R134a	79.3%
SF ₆	1.3%

Table 6.4: Components of the gas mixture in the exhaust line of R134a recovery system at CMS. (with respective volumetric percentages).

Therefore, we position our feeding point along the appropriate residue curve and set our outlet distillate composition, ensuring that these two points lie on the same residue curve. We then connect these two points and extend the line until it intersects the boundary defined by the diagram. This ensures that the composition of the bottom product is also determined along the intersection of the operational line and the same residue curve(see figure 6.9)

Figure 6.9: Residue curves and boundary limits for $\text{SF}_6/\text{R134A}/\text{IC}_4\text{H}_{10}$

Some important information could be deduced from our residue curves first of all we can clearly see that the feed is really near to the the bottom (see figure 6.9) this implies that our feed stream should be positioned near the reboiler of our distillation column. This placement is logical because as Henry Z. Kister mentioned in his book *"Distillation Design"* [16], the closer the feed is to the reboiler, the more challenging the separation, and positioning the feed stream closer aids in achieving better separation. Below is the anticipated composition of our expected bottom and distillate, as presented in the table:

Component	Distillate Concentration (%V)	Bottom Concentration (%V)
iC_4H_{10}	1.2%	19.0%
R134a	10.6%	80.1%
SF_6	88.12%	0.8%

Table 6.5: Distillate and Bottom concentration expectation

From the table provided above, it's clear that the compositions of both the reboiler (ref. Table 6.5) and the feed (ref. Table 6.4) are remarkably similar. This alignment is expected since the feed should ideally be introduced near the reboiler. Hence, this aspect must be duly considered during the design and sizing phases of the distillation column.

Chapter 7

Design and simulation of an SF₆ recovery System

From the previous chapter we have almost understand that it was quite difficult to asses the separation because we are recovering a very small fraction (1%) from a (99%) of other components. The goal of the project, is to develop a recovery system of SF₆, with an acceptable level of purity of SF₆ (P_{SF_6}), (7.1) with a reasonable recovery rate (\dot{m}_{SF_6})(5.2).

$$P_{SF_6} = x_{SF_6} * 100 \quad (7.1)$$

Due to this circumstances, it is of fundamental importance to do some experimental campagne for the recovery of SF₆, and by accesing the data of the experiments, the plant is then built.

Nowadays, process engineering, which focuses on component separation, has consistently operated more efficiently under steady-state conditions. Achieving stability is not only necessary to ensure consistent adherence to specifications, but it is also vital for designing and managing control and protection systems. Indeed, multiple layers of control and protection are implemented to restore the system to steady-state conditions (also referred to as nominal or design conditions). Their primary function is to monitor the variables requiring control and, when necessary, enact systemic adjustments to bring deviating parameters within a specified range or to an agreed-upon setpoint. Thus, the fundamental necessity for any separation apparatus is the maintenance of steady-state conditions. The design of the new SF₆ recovery system will lack this attribute because it will be directly connected to the R134a exhaust line (4.5). Here, it's evident that the composition of various components isn't constant, as it's contingent upon the thermodynamic conditions within the Freon system's buffers. In this setup, cooling occurs sequentially across the four columns, causing temperature (T) fluctuations from column 1 to column 4 (4.2). Additionally, the Zimmerli connections to the exhaust line is maintained at a specific pressure (P). Consequently, both T and P are variable, impacting vapor-liquid equilibrium and thus, the composition reaching the exhaust is subject to change. This means that our product purity and recovery will still fluctuate. Moreover, for a significant percentage of the operating time the product would not meet specifications.

7.1 Design of the new plant

For the design of our facility, we opted for a thermodynamic model known as REFPROP, the reason that stands among this choice is detailed in Chapter 5. As evidenced by the findings in Chapter 5, simple condensation alone cannot facilitate effective separation to a lower temperature due to excessive dilution of the mixture. The comprehensive analyses presented in preceding chapters have been instrumental in comprehending this aspect. Furthermore, it is assumed that chemical separations are not available for our project, as they would contaminate the gas sent in the RPC mixture. Additionally, it's imperative not to degrade SF₆, as doing so would cost more than 500kCHF/year doing this, and moreover would contradict CERN's objectives of maximizing gas recovery while reducing emissions.

These are all compelling reasons why SF₆, our primary component, must be recovered rather than degraded, even at such minimal concentrations in our mixture. The physical separation chosen for our design it's a criogenic distillation.

In order to guarantee the system's reliability, these two unique solutions have been designed simultaneously. Unfortunately, the change of composition and flow rate that characterizes the current stage of condensation affects both equally. The research of an equalization tank had been planned in order to guarantee a feed stream with a constant flow rate and composition. This tank collects the gaseous stream that exits from the zimmerly valves at the exhaust of the R134a recovery system. The plant can be divided into two distinct temporal periods—accumulation and separation— due to the presence of the tank. Finally, a small pumping station was installed in the facility to allow for fluid compression and movement. The next sub-chapters are dedicated to the description, design, and simulations of the four subsystems (accumulation tank and pumping station, distillation columns, storage unit, membrane separation). Before proceeding with the reading, it is recommended to refer to Appendix I.1, where the P&ID of the entire system is provided along with a brief explanation of its general operation.

7.2 Design of the accumulation tank and pumping station

This section describes the process of gas accumulation and pumping from an exhaust source in a facility. The accumulation area extends from line L0 to line L3, while the pumping area spans from line L4 to line L10.

In the accumulation section, the gas from the exhaust is directed towards a three-way valve (HV-10110). Here, it is possible to select whether to send the gas to the recovery system or to the flammable gas line. The three-way valve acts as a distributor, allowing for the management of gas flow according to the system's requirements.

It is important to note that this configuration offers operational flexibility, enabling the gas to be directed based on recovery or safe disposal needs, depending on the conditions and specifications of the facility.

Before entering the accumulation tank, the gas flow encounters two branches: one designated for GC analysis (LINE L1), and the other for purging purposes (LINE L2). The latter is utilized for cleaning the entire line with nitrogen when necessary. The accumulation tank, serves as an equalization vessel for the mixture's composition.

It's important to note that both pressure and temperature sensors are continuously monitoring these variables, both via software and visually. A three-way valve (HV-10114) connects two safety valves (PSV-10130 and PSV-10131) to vent compressed gas in the event of internal overpressure. It's crucial to highlight that, for convenient and safe maintenance activities, two safety valves are installed. This allows the three-way valve to easily isolate the one that requires repair or replacement.

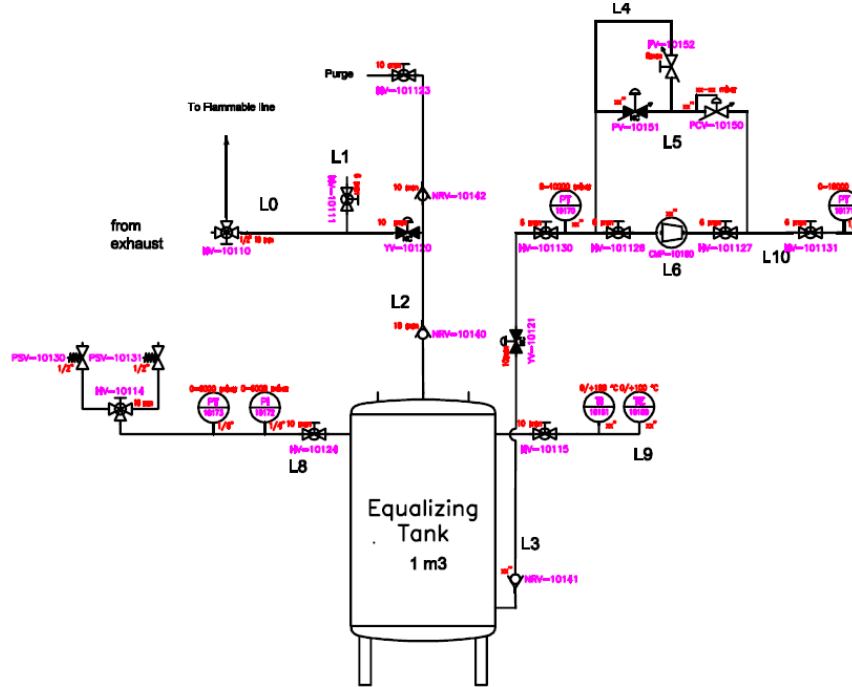


Figure 7.1: Pumping and accumulation section

After the accumulation tank, we enter the pumping section. The loop comprises a single-cylinder piston compressor (CMP-10150) and two pressure sensors (PT-10170 and PT-10171). These sensors are crucial for measuring and transmitting the pressure difference upstream and downstream of the compressor, allowing for precise regulation of the opening of various pneumatic valves within the system.

Specifically, the two sensors play a vital role in regulating the gas flow exiting the loop through the recycle stream located in the upper part of the diagram. The recycle stream includes a back pressure valve (PCV-10140), which opens when the pressure in the inlet duct exceeds the sum of the pressure exerted by a manually adjusted spring and the pressure exerted by the connected compressed air.

The primary function of this PCV is to stabilize the pressure upstream of the pneumatic control valve (PV-10151), which is highly sensitive to pressure fluctuations. Let's now briefly discuss the different phases.

- *Accumulation phase* : The gaseous mixture, with a variable composition, is initially directed from line L0 towards the equalizing tank. Ordinarily, a compressor would be indispensable for pushing the gas into the tank. However, in this scenario, such an installation is unfeasible due to the direct connection of line L0 with the exhaust of the R134a recovery system.

Increasing the pressure upstream of the tank would consequently impact the suction pressure ahead of the compressor. This would prompt the compressor to draw the

gas expelled from the Zimmerly of the R134a recovery system. Consequently, when the Zimmerly 10x12 reaches its set point value, it will open, allowing all injected gas into the Freon recovery system to pass directly into the exhaust line, facilitated by the compressor's suction.

For the gas to inject into the tank successfully, its pressure must exceed that within the tank. However, a potential issue arises. The Zimmerlys are configured to operate within a pressure range of 20 to 50 mbarg. These pressures may prove insufficient to propel the gas into the tanks, particularly due to pressure drops experienced along the L0-L2 lines attributed to the three-way valve (HV-10110), the pneumatic valve (YV-10120), and the non-return valve (NRV-10140). The gaseous mixture of variable composition arriving from line L0, is pushed into the tank following the path L0-L2. The pneumatic valve (YV-10120) is opened, while the non return valve (NRV-10140), is opened only if the gas pressure it's enough to overcome the force exerted by the spring.

- *Pumping section :*

After the accumulation tank, we enter the pumping section. The loop comprises a single-cylinder piston compressor (CMP-10180) and two pressure sensors (PT-10170 and PT-10171). These sensors are crucial for measuring and transmitting the pressure difference upstream and downstream of the compressor, allowing for precise regulation of the opening of various pneumatic valves within the system.

Specifically, the two sensors play a vital role in regulating the gas flow exiting the loop through the recycle stream located in the upper part of the diagram. The recycle stream includes a back pressure valve (PCV-10150), which opens when the pressure in the inlet duct exceeds the sum of the pressure exerted by a manually adjusted spring and the pressure exerted by the connected compressed air.

The primary function of this PCV is to stabilize the pressure upstream of the pneumatic control valve (PV-10151), which is highly sensitive to pressure fluctuations. In the operational phase, the accumulation tank is consistently filled at an average rate of 80 liters per hour, with variations ranging between 30 and 130 liters per hour.

Once the tank reaches its full capacity with gas, the pressure in the tank will be 3 bar, than, the pneumatic valve (YV-10121) is automatically opened, and the compressor (CMP-10160) is activated. This action is aimed at elevating the downstream pressure from 1 to 3 bar. The outlet flow from the tank is carefully regulated downstream by a mass flow regulator (XMFC-10180) to maintain a constant flowrate of 80 liters per hour.

7.3 Design of the two Distillation Columns

7.3.1 Introduction to the Distillation Process

One of the most used separation techniques in the process industry is distillation. Within a distillation column, a crucial mass transfer phenomenon unfolds between a liquid phase and a vapor phase. This transformation occurs by either adding or withdrawing heat from the initial mixture [10]. As the two phases move in opposite directions within the apparatus, they undergo a process known as counter-current flow. This movement aims to enrich the vapor phase with more volatile components while concurrently concentrating heavier species in the liquid phase.[28].

Efficiency in distillation hinges on the relative volatility of the components slated for separation. Essentially, the process operates most effectively when the key constituents possess significantly different boiling points relative to each other, given a particular operating pressure.

A distillation column comprises three fundamental components:

- *Reboiler*: Serving as a pivotal heat exchanger, the reboiler facilitates continuous vaporization of the liquid at the bottom of the column. A portion of this liquid is extracted as the bottom product, while the remainder undergoes vaporization, reintegrating into the column as boil-up vapor.
- *Condenser*: This critical heat exchanger is linked to a volume known as the reflux drum. Here, the overhead product is either wholly or partially condensed, depending on the type of condenser employed (total or partial, respectively). Subsequently, the condensed product divides into distillate and reflux. The reflux to distillate ratio (RR) emerges as a vital parameter in this context.
- *Column*: Acting as the backbone of the system, the column amplifies the surface contact area between the two phases, thereby enhancing mass and heat transfer efficiencies. To achieve this, the internals of the column are meticulously engineered, typically falling into two categories: plate columns and packed columns. Plate columns, being more prevalent, serve as the focus for the mathematical models discussed herein. In Figure 7.2, a simplified depiction of a trayed distillation column is presented.

7.3.2 Defining the Specifications and the Goals

Designing a separation system based on distillation necessitates understanding specific parameters. In this case, these parameters include the composition, flow rate, and thermal conditions of the feed. Once these are known, it's essential to fix other critical parameters to limit the degrees of freedom in the system. Typically, the operating pressure (referenced to the column's head), as well as the desired distillate (D) and bottom (B) flow rates, are chosen. Additionally, the reflux ratio or number of theoretical stages must be specified. The selection of which variable to fix depends on the objectives and specifications set for the system.

In this project, the primary goals are to maximize the purity of the distillate product and achieve the highest possible recovery. Therefore, among the various variables, fixing the bottom column flow rate, specifically the bottom to feed ratio (B/F), alongside the pressure at the column's top, is deemed beneficial. Setting the B/F equal to the molar fraction of SF₆ in the feed is considered a prudent choice, aiming for optimal recovery.

The determination of the number of equilibrium stages (N) and reflux ratio (RR) is conducted iteratively. Initially, the minimum number of stages is chosen, with subsequent iterations increasing this number. The impact of varying the reflux ratio on the purity and recovery of sulfur hexafluoride is observed through sensitivity analysis. This iterative process helps optimize the design parameters for the desired outcomes.

- *Operating pressure* : Regarding the selection of operating pressure, it plays a critical role in the process, with higher pressure making the separation more challenging.

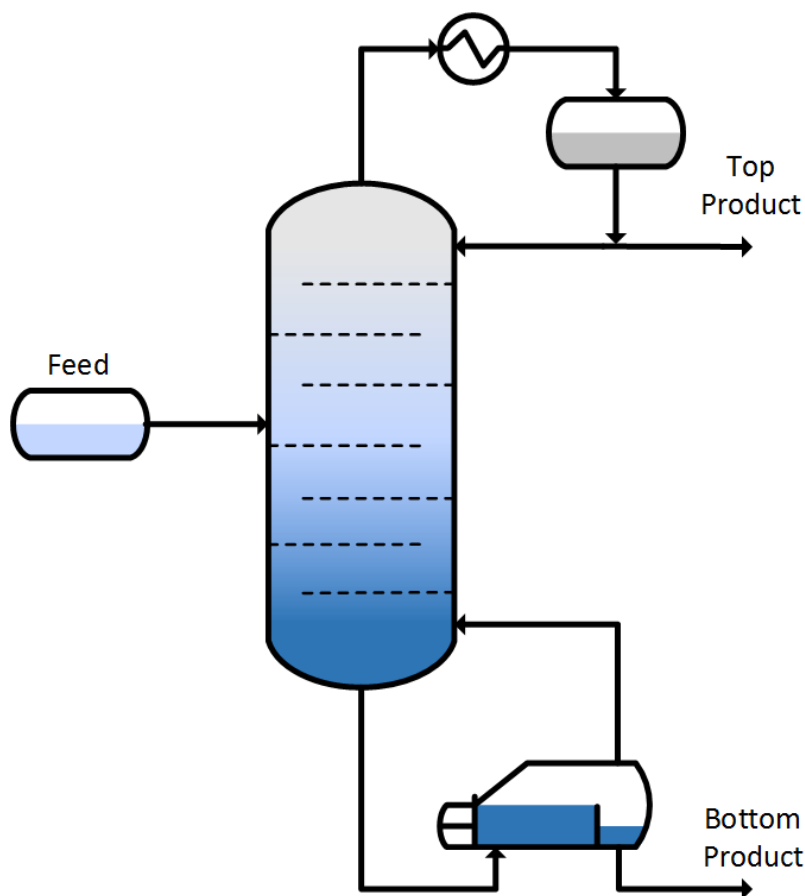


Figure 7.2: Diagram of a basic distillation column

Operating at low pressures, while incurring high energy costs, is often necessary when dealing with transition temperatures below zero degrees Celsius at atmospheric pressure. Thus, an initial pressure value of approximately 2.5 bara is set to facilitate effective condensation of the distillate and vaporization of the bottom product within practical temperature ranges.

- *Boilup Ratio* The boil up ratio is the amount of feed boiled over the one sent to the bottom, here a initial value of 0.8 is selected.
- *Number of equilibrium stages (N) and Reflux Ratio (R_R):*

The determination of the number of equilibrium stages follows an iterative process. Initially, the minimum number of stages is chosen, typically starting with three stages, where the first and third stages correspond to the condenser and reboiler, respectively. Subsequently, as the iterations progress, the number of stages is incrementally increased. During each iteration, the reflux ratio is adjusted, and the resulting impact on the purity and recovery of sulfur hexafluoride is observed through sensitivity analysis. The findings of this analysis are depicted in the accompanying figures 7.3a 7.3b, 7.4a, 7.4b.

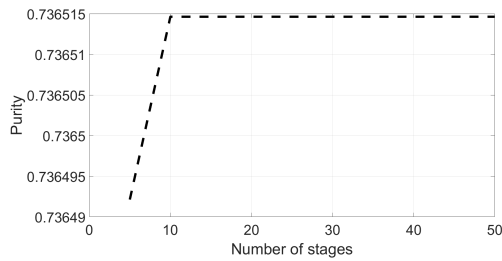
From the analysis depicted in Figure 7.3a, it's evident that the purity of SF₆ in the separation process reaches a plateau after 10 stages, indicating a stage-independent separation beyond this point. Thus, we opt for a configuration of 10 stages.

Further sensitivity analysis, focusing on the feeding stage's impact on molar purity,

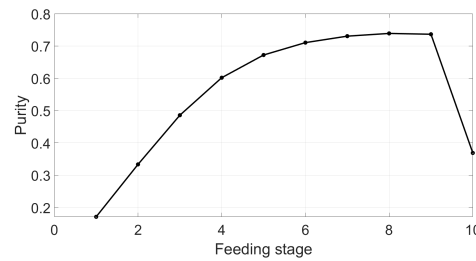
suggests that optimal performance is achieved when the gaseous mixture is introduced at the 9th stage.

Exploring the influence of the molar reflux ratio on both molar purity and molar recovery (as illustrated in Figure 7.6), we observe a significant impact. Increasing the reflux ratio elevates purity but reduces recovery. Due to the low SF_6 concentration in the mixture, a high reflux ratio (e.g., 144) akin to total reflux and non-distillation is chosen. However, it's crucial to note that such high ratios entail elevated utility consumption and operating costs.

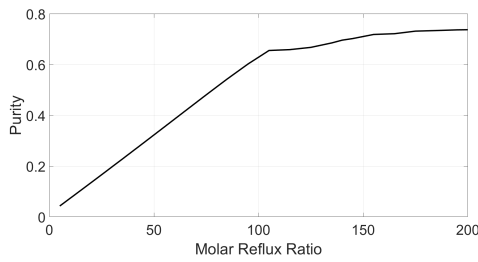
Considering the negligible impact of the stage count on heat exchanger duties, a linear relationship between the reflux ratio and the thermal power requirement (or removal in the case of the condenser) is apparent (refer to Figure 7.5).



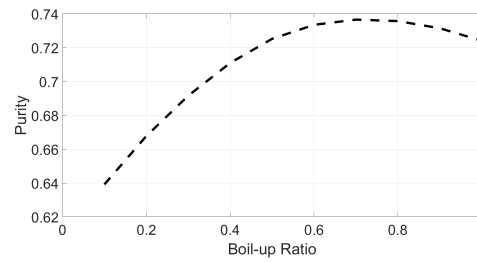
(a) Effect of variation of the number of stages to the molar purity of SF_6



(b) Effect of variation of the feeding stage, respect to the molar purity of SF_6



(a) Effect of variation of the Molar Reflux Ratio respect to the molar fraction of SF_6 , (x_{SF_6})



(b) Effect of variation of the Boilup Ratio, respect to the molar fraction of SF_6 , (x_{SF_6})

Figure 7.4: Sensitivity Analysis results respect to Molar Purity

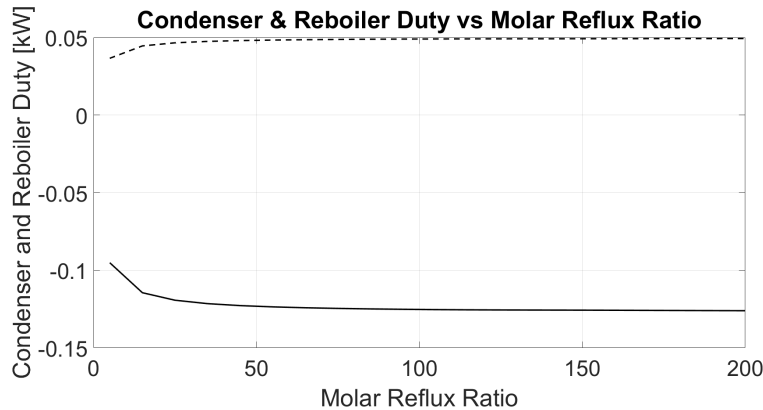


Figure 7.5: Condenser and Reboiler Duty respect to the Molar Reflux Ratio

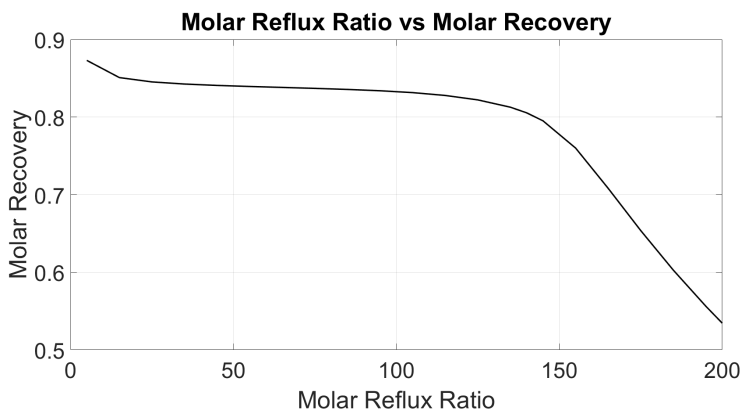


Figure 7.6: Molar Recovery vs Molar Reflux Ratio

Lastly, in the sensitivity analysis regarding boilup ratio versus distillation column purity, a positive correlation is observed. Higher boilup ratios correspond to improved purity.

Summarizing our distillation column's parameters:

Number of equilibrium stages	Optimum Reflux Ratio	Pressure (bara)	Distillate-to-Feed-Ratio	Recovery (R_{SF6})	Purity $P(SF_6)$
10	144	3	0.014	79.5%	73.7%

Table 7.1: Input parameters and simulated specifications

The results presented in the table highlight the significant challenge of achieving effective separation with a single distillation column. The notably high reflux ratios, as indicated by Henry Z. Kister in his book [16], far exceed the typical operational ranges of 5-10 observed in industry. This discrepancy underscores the impracticality of relying solely on a single column for such operations.

In light of this limitation, an alternative solution emerges: the utilization of two distillation columns arranged in series. This approach offers a promising avenue for addressing the challenges posed by the excessive reflux ratios encountered in the single-column configuration. By distributing the separation process across two columns, each operating within a more conventional reflux ratio range, the feasibility and efficiency of the distillation operation can be greatly enhanced.

7.3.3 Simulation and specifications findings with two distillation columns

In the previous paragraph, we understood that for the purpose of facilitating our separation process, distillation cannot be carried out using a single column, but at least two columns in series are required (7.7). In this context, a series of simulations have been executed to determine the optimal operational parameters. The plant's specifications and objectives align with those outlined in the preceding paragraph. Our focus lies in exploring a sensitivity analysis to identify the ideal input parameters for our columns.

In this sensitivity analysis, we scrutinize the variation of purity and molar recovery

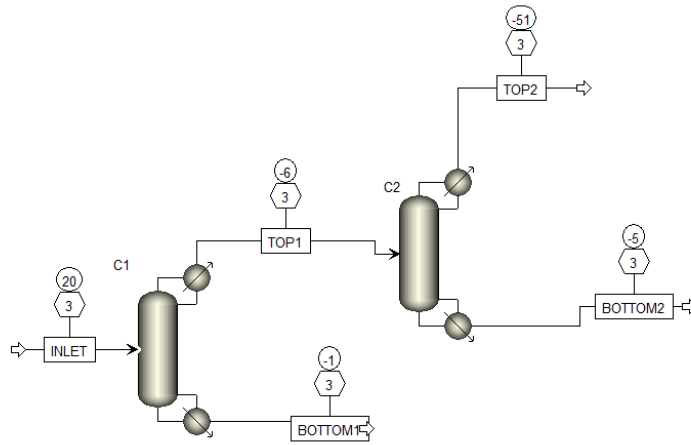


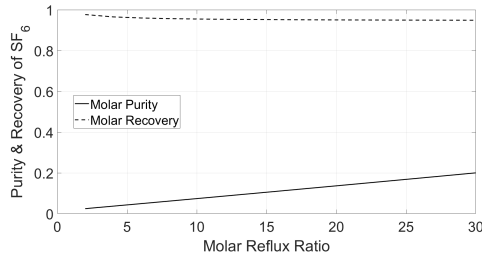
Figure 7.7: Main Flowsheet of the two distillation columns, made by Aspen Plus

concerning the molar reflux ratio (see Figure 7.10 and 7.11).

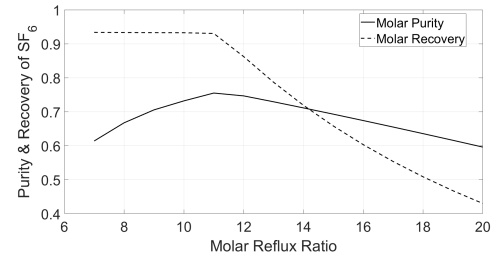
The analysis reveals that, for the first column, elevating the reflux ratio enhances the purity of SF_6 , while the molar recovery of our target component remains relatively stable, fluctuating between 94% and 97%. Consequently, we opt for a molar reflux ratio of 20, cautious not to exceed this threshold as it would lead to a steady escalation in operational costs.

Conversely, in the sensitivity analysis of molar recovery and purity for the second column, the dynamics are slightly different. Initially, augmenting the molar reflux ratio boosts the purity of our target component. However, as the molar reflux ratio approaches 15, the purity begins to decline. Meanwhile, the molar recovery of the second column remains largely consistent until reaching a molar reflux ratio of 15, after which it diminishes with further increases in the molar reflux ratio.

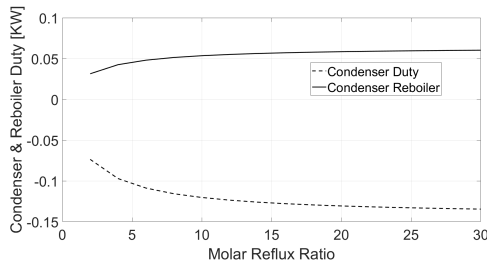
Additionally, we have conducted an analysis of the condenser and reboiler duty over the molar reflux ratio for both the first and second columns. Our findings indicate that in the first column, both the reboiler and condenser duty are higher, primarily due to higher flow rates. Furthermore, these duties exhibit a linear increase with the rising molar reflux ratio 7.9a and 7.9b. A last sensitivity analysis was performed involving the feeding stage with respect to the molar purity and recovery. For both parameters, we find that the optimal inlet feeding stage is the 9th stage, which is the one before the reboiler. Consequently, the feed for both columns will be introduced at stage 9 (7.10a and 7.10b).



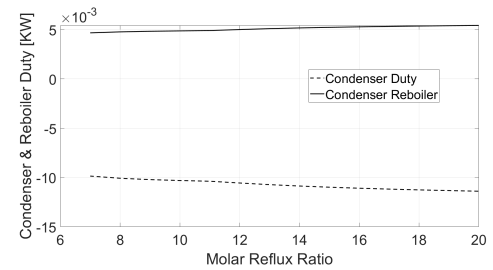
(a) Effect of variation of the Molar Reflux Ratio respect to the molar fraction of SF₆, (x_{SF_6}), Column 1



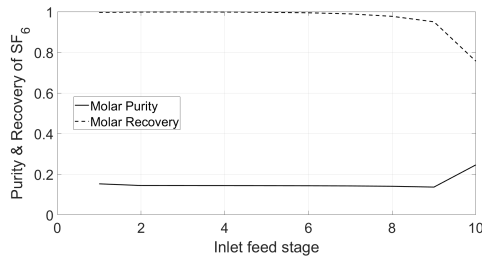
(b) Effect of variation of the Molar Reflux Ratio respect to the molar fraction of SF₆, (x_{SF_6}) Column 2



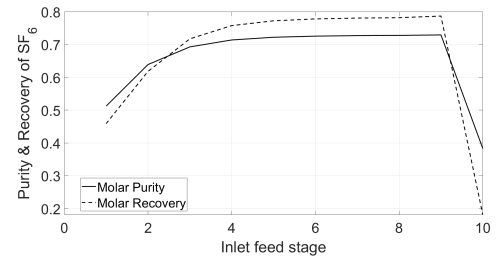
(a) Effect of variation of the Molar Reflux Ratio, respect to the condenser duty in column 1



(b) Effect of variation of the Molar Reflux Ratio, respect to the condenser and reboiler duty in column 2



(a) Effect of variation of the feeding stage, respect to the molar purity and recovery of SF₆, in column 1



(b) Effect of variation of the feeding stage, respect to the molar purity and recovery of SF₆, in column 2

Here below in the reference table are shown all the summarized parameters for the first 7.2 and the second column 7.3:

Number of equilibrium stages	Optimum Re-flux Ratio	Pressure (bara)	Distillate-to-Feed-Ratio	Recovery (R_{SF6})	Purity $P(SF6)$
10	20	3	0.09	94.9%	13.6%

Table 7.2: Input parameters and simulated specifications for first column

Number of equilibrium stages	Optimum Re-flux Ratio	Pressure (bara)	Distillate-to-Feed-Ratio	Recovery (R_{SF6})	Purity $P(SF6)$
10	13	3	0.14	78.6%	72.9%

Table 7.3: Input parameters and simulated specifications for second column

7.3.4 Sizing and Optimization of the Distillation Columns

In the preceding section, we identified the optimal parameters for our distillation columns, noting that the separation process is stage-independent and that the molar reflux ratio plays a crucial role in enhancing separation efficiency without significantly affecting recovery.

Now, in this section, we delve into the sizing and optimization of the distillation columns. Our first step is to define the conditions of the incoming feed. After delineating the inlet conditions (as shown in Table 7.4) and saturating all degrees of freedom (refer to Table 7.3), we proceed to determine the type of condenser and establish the hydraulic and pressure drop profile within the column.

We opt for a partial condenser, as there is no requirement to fully condense the vapor. This choice not only meets our operational needs but also reduces the thermal load removed by the refrigerant fluid.

Additionally, we initially assume a constant variation in the hydraulic and pressure drop profile, with a pressure drop of 50 mbar between the injection point and the column's top.

Volumetric Flowrate (l/h)	Molar Flowrate (mol/h)	Molar fraction of SF_6	Temperature ($^{\circ}C$)	Pressure (bara)
95	13.3	0.013	25	3

Table 7.4: Feed conditions of the first column

We then assume for the first column that it works in adiabatic conditions. Here, the duties of the reboiler and condenser are respectively 58.45 W and -130.72 W. Moreover, the thermal, pressure and composition profiles along the column are reported here below in Figures 7.11 and 7.12.

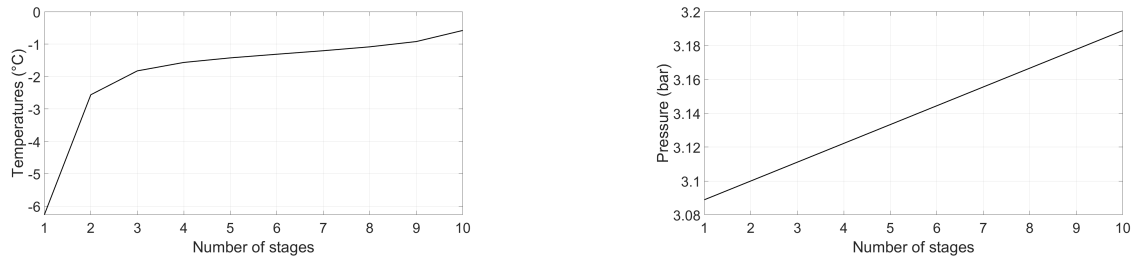


Figure 7.11: Temperature (left-side) and Pressure (right-side) profiles along the first column.

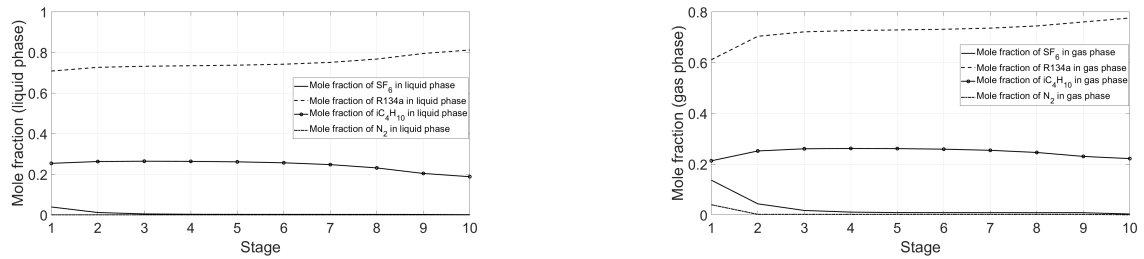


Figure 7.12: Liquid mole fraction (left-side) and Gas mole fraction (right-side) profiles along the first column.

Once steady-state conditions are achieved in the first column and operating with a reflux ratio of 20, the following composition is attained in the distillate stream (see Table 7.5).

Component	Concentration (%V)
IC ₄ H ₁₀	21.1%
R134a	61.1%
SF₆	13.7%
N ₂	0.04%

Table 7.5: Distillate composition of column 1

As depicted in Figure 7.7, the temperature at which partial condensation occurs stands at -6.07°C, a relatively moderate value. This implies that achieving this temperature is feasible with the use of a straightforward refrigeration unit, such as the LAUDA model.

Consequently, the distillate stream from Column 1 serves as the feed for the second column. Below is a table summarizing the inlet conditions for this latter column (see Table 7.6).

Volumetric Flowrate (l/h)	Molar Flowrate (mol/h)	Molar fraction of SF ₆	Temperature (°C)	Pressure (bara)
8.02	1.02	0.136	-6.3	3

Table 7.6: Feed conditions of the second column

The same assumption are made for the second column, so ideally it works in adiabatic conditions. The duty of reboiler and condenser are respectively 5.1 W and -10.72 W. For instance, the thermal, pressure and composition profiles along the column are reported here below in Figures 7.13 and 7.14.

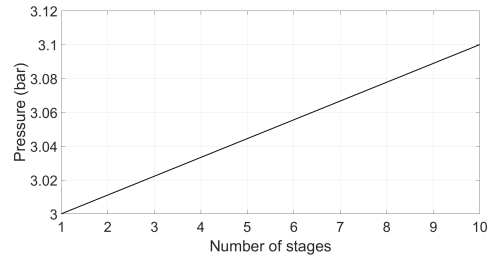
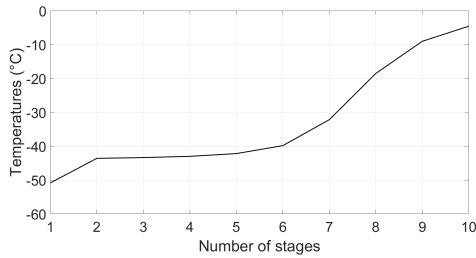


Figure 7.13: Temperature (left-side) and Pressure (right-side) profiles along the second column.

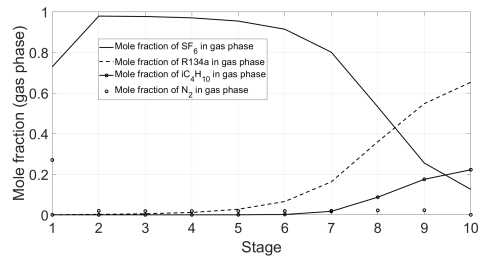
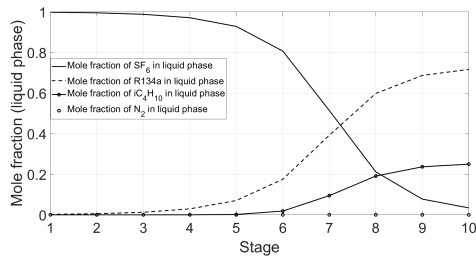


Figure 7.14: Liquid mole fraction (left-side) and Gas mole fraction (right-side) profiles along the second column.

As soon as we approach steady-state conditions are achieved in the second column, the following composition is attained in the distillate stream (see Table 7.7).

Component	Concentration (%V)
IC ₄ H ₁₀	1.67E-07%
R134a	0.0068%
SF₆	72.9%
N ₂	27.0%

Table 7.7: Distillate composition of column 2

With these considerations in mind, we are now poised to proceed with the sizing of our initial column. Our first step is to determine the type of column best suited for our needs. As elucidated in Section 7.3, distillation processes conventionally employ tray columns. However, given the relatively small scale of our system, with a column diameter on the order of centimeters, we have opted for the design of a packed column.

The design process unfolds in the following steps:

- Selection of an appropriate diameter and determination of specific vapor and liquid flow rates for each stage.
- Choosing the type of packing and analyzing the hydraulic and thermal characteristics of the column.
- Computing pressure drops, assessing packing efficiency under given hydraulic conditions, and estimating the column's height.

For our specific case, we've set the column diameter (D_c) at 3 centimeters. The specific volumetric flow rates of the liquid phase (V_s^l) and vapor phase (V_s^v), along with the F-factor (packing characteristic factor), are then calculated using the equations outlined in Equations 7.2, 7.3 and 7.4, respectively.

$$A_c = \frac{\pi D_c^2}{4} \quad (7.2)$$

$$V_s^l = \frac{V^l}{A_c} \quad \text{and} \quad V_s^v = \frac{V^v}{A_c} \quad (7.3)$$

$$F_{\text{factor}} = V_s^v \sqrt{\rho^v} \quad (7.4)$$

Where A_c and ρ^v represent the cross-sectional area of the column and the density of the vapor at temperature and pressure conditions within the column. Next, the selection of an appropriate packing material is a critical step in the project's implementation. The chosen packing material plays a crucial role in maximizing the interface between the two fluid phases moving in opposite directions within the column. This enhanced interface increases the surface area available for both mass and heat transfer, ultimately improving the overall performance of the distillation process.

Packing materials are broadly categorized into structured and random packings. These materials vary in characteristics such as packing size (d_p), void volume fraction (V_{void}), and specific surface area (A_p), which represents the surface area per cubic meter of the

column. Generally, reducing the packing size increases the specific surface area while decreasing the void fraction. However, this can also lead to higher pressure losses.

In our case, after careful consideration, we opted to utilize laboratory structured packings known as DX™, manufactured by Sulzer Chemtech AG (figure 7.15). These packings offer favorable features that align with our project requirements.



Figure 7.15: DX™ structured packing as reported by *Sulzer Chemtech AG*

Diameter Range, D_c , (mm)	Specific Surface Area, a_p , (m^2/m^3)	Void Fraction, V_{void} , (%)
30-125	900	93.3

Table 7.8: Specifics of the DX™ packing material

Figure 7.16 depicts the relationship between the HETP/m and the F-factor, which is a crucial aspect of design specifications. In practical terms, the number of theoretical stages (N) and the HETP/m value determine the height of the packing bed (Z). This process involves the following steps:

- Start with a reasonable initial value for the pressure drop.
- Calculate the F-factor for each theoretical stage.
- Determine the corresponding HETP value from Figure 7.16
- Compute the total packing height by summing the individual HETP values using Equation 7.5

$$Z = \sum_i (HETP)_i \quad (7.5)$$

Where i goes from 1 to N , where N represents the number of stages. Subsequently, utilizing the data provided in Figure 7.17 and maintaining consistent F-factor values, the pressure drops per meter at each stage are determined through similar calculations. These individual pressure drops per meter are then summed up to calculate the total pressure drop (ΔP). This total pressure drop is obtained by multiplying the pressure drops per meter ($\Delta P/Z$) by the total height of the packing bed (Z).

$$\Delta P = Z \sum_i (\Delta P/Z)_i \quad (7.6)$$

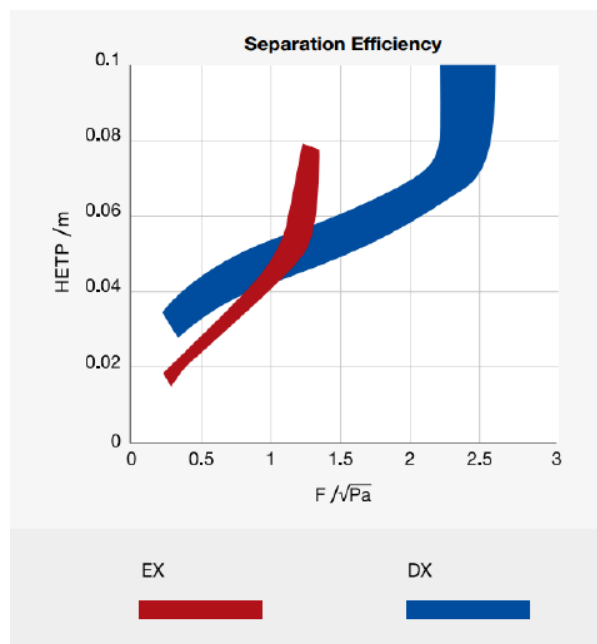


Figure 7.16: Normalized Height Equivalent to Theoretical Plate (HETP) as a function of normalized F-factor as reported by *Sulzer Chemtech AG*

The iterative process is essential due to the dependence of the F-factor on gas velocity and density, both influenced by pressure. Fortunately, the Aspen Plus simulator streamlines this process with its capability to update pressure drops by setting the head pressure at 3.09 bara. After inputting the characteristics of the selected packing material (refer to Table 7.8), an average F-factor value is computed. Subsequently, an HETP value is chosen from the blue region in Figure 4.32, with preference given to the lower limit of the blue band, representing a conservative estimate. In this instance, an average F-factor of 0.49 corresponds to an approximate HETP of 0.03-0.04 m^{-1} . With this in mind we can run our last simulation and summarize all the results for the first distillation column here in Table 7.9 .

Stages (N)	Molar fraction of SF_6 in liquid phase	Molar fraction of $R134a$ in liquid phase	Molar fraction of SF_6 in vapour phase	Molar fraction of $R134a$ in vapour phase
1	0.0386063	0.70789	0.136552	0.610886
2	0.0113281	0.726232	0.0432704	0.703271
3	0.00443647	0.731544	0.0172105	0.720813
4	0.00272638	0.734076	0.0106318	0.725886
5	0,00229749	0,736857	0,0089973	0,728303
6	0,00217523	0,741646	0,00858713	0,730955
7	0,00211067	0,750642	0,00847158	0,735519
8	0,00203024	0,767043	0,00841529	0,744088
9	0,00190279	0,794399	0,0083516	0,759705
10	0,000707997	0,811558	0,00323036	0,775334

Table 7.9: Molar liquid fraction and vapor fraction along the first column

The HETP value obtained from the simulation is approximately 0.065 m per stage, closely matching the data presented in Figure 7.17. Consequently, the theoretical total

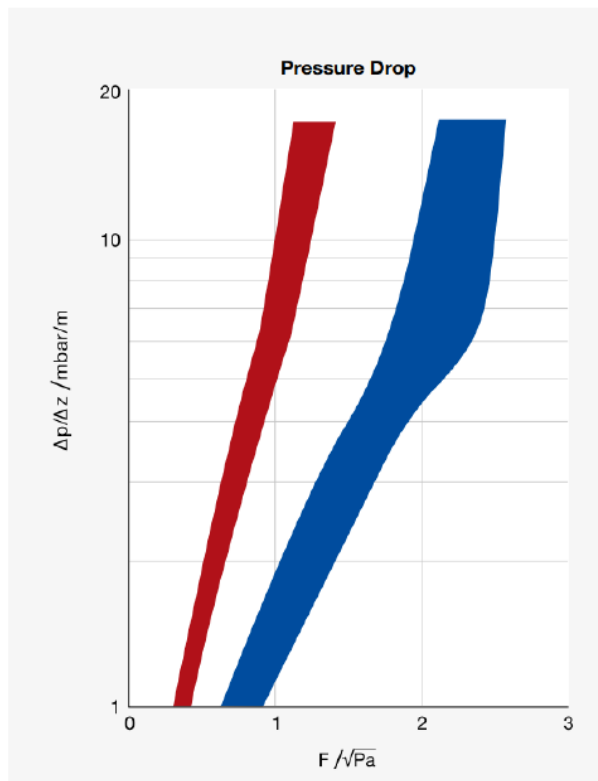


Figure 7.17: Normalized Pressure drops per meter of column, $\Delta P/Z$, as a function of normalized F-factor as reported by *Sulzer Chemtech AG*

Stages (N)	Stage Temperature ($^{\circ}\text{C}$)	Stage pressure (mbar)	Specific Liquid Flowrate ($\text{m}^3/\text{h}/\text{m}^2$)	Specific vapor flowrate ($\text{m}^3/\text{h}/\text{m}^2$)	F-factor ($((\text{m}/\text{s})\text{Pa}^{0.5})$)
1	-6.26671	3.08889	3.914392757	317.7842717	0.320226923
2	-2.56084	3.1	4.00450778	321.4865831	0.323957692
3	-1.82415	3.11111	4.017542206	321.0552829	0.323523077
4	-1.56385	3.12222	4.021339938	320.2213086	0.322682692
5	-1.42302	3.13333	4.020595659	319.2117608	0.321665385
6	-1.3109	3.14445	4.015309369	318.099159	0.320544231
7	-1.20247	3.15556	4.001893261	316.812892	0.319248077
8	-1.08235	3.16667	3.974202262	315.2346387	0.317657692
9	-0.919627	3.17778	3.711528994	315.6182287	0.318044231
10	-0.576435	3.18889	1.944648597	0	0

Table 7.10: Temperature profile ($^{\circ}\text{C}$), Pressure profile (bara), Specific liquid flowrate ($\text{m}^3/\text{h}/\text{m}^2$), Specific vapor flowrate ($\text{m}^3/\text{h}/\text{m}^2$), F-factor($((\text{m}/\text{s})\text{Pa}^{0.5})$), for the first column 7.7

height of the packing (Z) is determined to be 0.5 m.

To derive the total column height, several factors must be considered, as outlined in reference [14]

1. Firstly, it is essential to account for potential errors in the simulation and provide a safety margin. To address this, it was decided to double the theoretical height, resulting in a packing height of 1 m.

2. Additionally, to ensure optimal distribution of descending liquid and ascending gas within the column, an increase in height is recommended. Typically, an extra 1-2 meters is suggested for columns of this size. Therefore, an additional increase of 25% is deemed appropriate, bringing the packing height to 0.625 m.

3. Moreover, allowance must be made for various components such as the liquid distributor, packing support, and redistribution ones. Thus, an estimated 0.1 meters of column height is allocated for these elements.

4. The height corresponding to the hold-up of liquid at the bottom of the column is determined by multiplying the liquid flow rate at the ninth stage by a predefined residence time of 5 minutes. This calculation results in a liquid volume, which, when divided by the column's cross-section, yields a height of 0.3 m.

5. Finally, additional space is allocated above and below the packing zone. Approximately 0.3 meters is reserved for the liquid inlet and disengagement of any entrained liquid particles, ensuring uniform vapor flow from the reboiler.

In summary, a total of 0.925 meters is designated for the packing zone, with an additional 1 meter allocated for the free zone. Hence, the total column height (excluding the head and dished bottoms) amounts to 1.925 meters.

After completing the sizing of the first column, our focus shifts to sizing the second column. We present the mole fractions of both liquid and vapor phases at each stage of the second column in Table 7.11. Subsequently, Table 7.12 summarizes the temperature and pressure profiles, along with the volumetric flow rates of both phases and the corresponding F-Factor for each stage.

Stages (N)	Molar fraction of SF ₆ in liquid phase	Molar fraction of R134a in liquid phase	Molar fraction of SF ₆ in vapour phase	Molar fraction of R134a in vapour phase
1	0.998387	0.00161237	0.933164	0.000561476
2	0.996231	0.00376901	0.994686	0.00155273
3	0.991218	0.00877784	0.992825	0.00359578
4	0.97928	0.0206658	0.988072	0.00833249
5	0.948928	0.0503457	0.976755	0.0195652
6	0.861405	0.130768	0.948039	0.0475395
7	0.622768	0.331657	0.865852	0.122698
8	0.299898	0.592311	0.646607	0.306229
9	0.118769	0.736648	0.358358	0.537683
10	0.0538578	0.789473	0.187039	0.681089

Table 7.11: Molar liquid fraction and vapor fraction along the second column in series 7.7

The HETP value obtained from the simulation is approximately 0.0321 m per stage, closely matching the data presented in Figure 7.17. Consequently, the theoretical total height of the packing (Z) is determined to be 0.4 m.

To derive the height of the second column steps 1-5 should be repeated (7.3.4).

Stages (N)	Stage Temperature ($^{\circ}\text{C}$)	Stage pressure (mbar)	Specific Liquid Flowrate ($\text{m}^3/\text{h}/\text{m}^2$)	Specific vapor flowrate ($\text{m}^3/\text{h}/\text{m}^2$)	F-factor ($((\text{m}/\text{s})\text{Pa}^{0.5})$)
1	-50.8855	3	5.385893362	429.7061541	0.452762172
2	-43.6153	3.01111	5.793694322	450.1332291	0.474285268
3	-43.3818	3.02222	5.784778212	448.438872	0.4725
4	-43.0151	3.03333	5.752579502	446.1520823	0.470090512
5	-42.2103	3.04444	5.649940559	442.3842111	0.466120474
6	-39.8548	3.05556	5.330263944	433.3288793	0.456579276
7	-32.1844	3.06667	4.842129128	415.0375237	0.437306492
8	-18.5243	3.07778	4.751812782	410.1647658	0.432172285
9	-9.02007	3.08889	4.888279625	417.389481	0.439784644
10	-4.56948	3.1	2.596996302	0	0

Table 7.12: Temperature profile ($^{\circ}\text{C}$), Pressure profile (bara), Specific liquid flowrate ($\text{m}^3/\text{h}/\text{m}^2$), Specific vapor flowrate ($\text{m}^3/\text{h}/\text{m}^2$), F-factor($((\text{m}/\text{s})\text{Pa}^{0.5})$), for the second column in series 7.7

In summary, a total of 0.6 meters is designated for the packing zone, with an additional 1 meter allocated for the free zone. Hence, the total column height (excluding the head and dished bottoms) amounts to 1.5 meters.

7.3.5 Reboiler and Condenser's Sizing

After completing the sizing of the column, we proceed with the sizing of the heating and cooling equipment. Our initial focus is on the condenser, where the incoming stream comprises vapor from the second stage, while the outgoing streams are the distillate and reflux. The temperature, composition, and flow rate conditions are detailed in Table 7.13. Additionally, a simplified schematic is depicted in Figure 7.18.

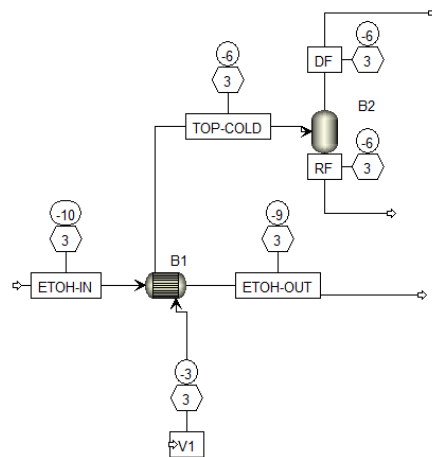


Figure 7.18: Heat exchanger and reflux drum at condensre stage for the first column

In table 7.13 the reflux flow rate of the first column was determined, and assuming a liquid residence time of 15 minutes in the reflux drum, we can estimate the volume occupied by the liquid under standard conditions. Assuming that the liquid volume fills

Streams	Molar Flowrate (mol/hr)	SF ₆ molar fraction	iC ₄ H ₁₀ molar fraction	R134A molar fraction	N ₂ molar fraction	Temperature (°C)
V1	25.2805	0.0432704	0.251564	0.703271	1.89×10^{-3}	-2,57
D1	1.264025	0.136552	0.212776	0.610886	0.0397852	-6,27
R1	24.016475	0.038360842	0.253605474	0.708133368	9.96421×10^{-5}	-6,27

Table 7.13: Condenser input and output, stream conditions for first column

approximately 30% of the total available volume under these conditions, we size the reflux drum using Equations 7.7 and 7.8. This involves setting the internal diameter of the reflux drum equal to the nominal closure flange diameter, while disregarding the volume of the bottom.

$$V_{\text{reflux}} = R\tau_{\text{RD}} \quad (7.7)$$

$$V_{\text{reflux}} = 0.3V_{\text{RD}} = \frac{\pi D_{\text{RD}}^2 H_{\text{RD}}}{4} \quad (7.8)$$

The volume of liquid in the reflux drum, denoted as V_{reflux} , is determined by the residence time (τ_{RD}) and the dimensions of the reflux drum, specifically its height (H_{RD}) and internal diameter (D_{RD}). This calculation utilizes the total volume of the reflux drum (V_{RD}) as listed in Table 7.14

In the event that the liquid refrigerant supplied to the heat exchanger proves inadequate, an additional volume of the cooling jacket is provided to ensure optimal cooling capacity.

ID stream	Vapour flowrate (mol/hr)	Volume of Reflux Drum (m^3)	Height of reflux drum (m)	Diameter of reflux drum (m)
R1	24.016475	6.67×10^{-3}	0.3	0.168
L9	22,9905	1.9×10^{-2}	0.5	0.221

Table 7.14: First column, Condenser and Reboiler sizing.

The identical procedure can be applied to size the condenser and reboiler of the second column. All required streams are consolidated in Table 7.15, which presents their respective compositions and operating temperatures.

Streams	Molar Flowrate (mol/hr)	SF ₆ molar fraction	iC ₄ H ₁₀ molar fraction	R134A molar fraction	N ₂ molar fraction	Temperature (°C)
V2	2.48291	0.978522	3.96×10^{-8}	0.00218659	0.019291	-43.6153
D2	0.177351	0.729315	1.64×10^{-9}	0.000628167	0.270057	-50.8855
R2	2.305559	0.997691802	4.25246×10^{-8}	0.002306469	1.27423×10^{-6}	-50.8855
L9	1.95032	0.077294	0.236445	0.686261	3.57×10^{-8}	-9.02007

Table 7.15: Condenser input and output, stream conditions for second column

Utilizing Equations 7.7 and 7.8, the outcomes for the volume (V), diameter (D), and height (H) of the condenser and reboiler for the second column are presented in Table 7.16.

ID stream	Vapour flowrate (mol/hr)	Volume of Reflux Drum (m^3)	Height of reflux drum (m)	Diameter of reflux drum (m)
R2	2.48	1.91×10^{-3}	0.2	0.111
L9	1.95	1.63×10^{-3}	0.2	0.101

Table 7.16: Second column, Condenser and Reboiler sizing.

After completing the sizing of the distillation column, we can now present performance results for our separation process. These results are conveniently summarized in the following table 7.17. The results clearly indicate a low productivity of the process,

Distillate to feed Ratio column 1	Distillate to feed Ratio column 2	Molar recovery of SF ₆ in the first column	Molar recovery of SF ₆ in the second column	Molar recovery of SF ₆ in the entire process	Efficiency of the entire process
8.42%	13.2%	84.21 %	70.92%	60%	1%

Table 7.17: Performances of the separation with the distillation column.

amounting to only 1%. This is primarily attributed to the extensive residence times and reflux ratios employed in both distillation columns to attain the desired purity of SF₆ in our separation. To enhance productivity, one potential solution is to recycle the bottoms of the two distillation columns and readjust their compositions to align with the requirements outlined in the RPC (Refer to Table 2.1). Such an adjustment is projected to increase productivity from 1% to 2.3%.

7.4 Accumulation tank and storage in cylinders

After exiting the condenser of the second distillation column, our focus shifts to storing the gas in an accumulation tank before transferring it into cylinders at a pressure of 50 bar 7.19.

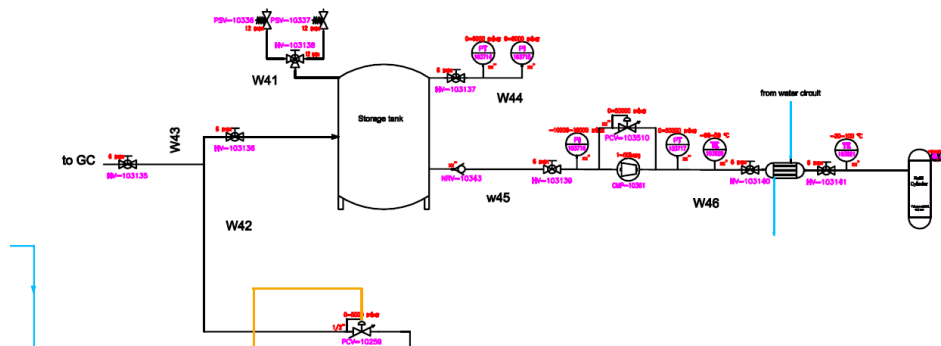


Figure 7.19: Accumulation and storage section of the SF₆ recovery Plant.

To accomplish this, an accumulation tank is positioned immediately after the condenser of the second column. Within this tank, pressure is monitored using the PT-103714 pressure sensor. In series with the tank, a high-pressure compressor is installed to elevate the gas pressure from 3 to 50 bar. Given the elevated pressure, precise pressure measurement is crucial, along with the installation of a check valve (NRV-10343) in line W45 to prevent backflow into the tank.

Furthermore, compressing gas to high pressures results in elevated temperatures. Therefore, a water-cooled heat exchanger is necessary to mitigate the gas's exit temperature. Subsequently, the gas is stored in cylinders at a pressure of 50 bar.

The stored gas mixture will roughly comprise a 70/30 ratio of SF₆/N₂, as detailed in Table 7.7. This mixture will later be reused and concentrated to achieve a purity level ranging between 95% and 99% using membrane technology.

7.5 Control logic of the plant

7.5.1 Control of the two distillation columns

Our description begins with the introduction of the first distillation column within our plant. The second column will be operated using the same control methodology, hence further elaboration is unnecessary. So we start our description from line L16 (see figure 7.20).

Upon entry into the system, the gas encounters the (XMFC-10180) mass flow regulator, which ensures a precise flow rate of 95 l/h. At this juncture, we establish an analysis line (W2) to thoroughly assess the composition of the feed before it enters the column.

The gas is introduced into the column at the 9th stage, characterized by a temperature of 25°C and an inlet pressure of 3 bar. Within the column, the temperature ranges, between -6°C and -0.5°C, meticulously monitored by multiple thermocouples strategically positioned throughout the column.

Pressure regulation within the column is facilitated by the pressure sensor (PI-10276) positioned at the column's apex. In the event of flooding or clogging within the column, potentially leading to overpressure, protective measures are enacted. To safeguard

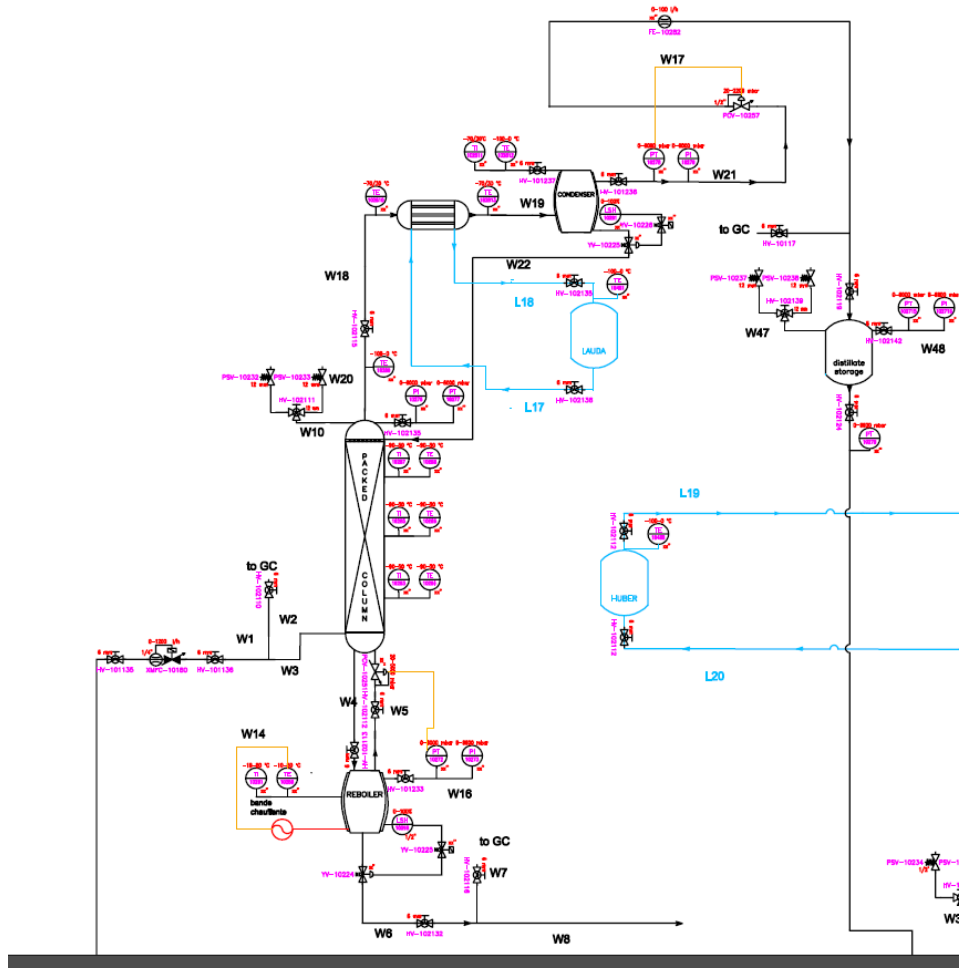


Figure 7.20: First distillation column, with controllers

against such occurrences, two safety valves are installed at the upper left section of the column: the pressure safety valves (PSV-10232) and (PSV-10233). These valves operate autonomously, triggered to open automatically upon reaching the pre-set pressure threshold.

Moving to the rectifying section, the gas from the distillation buffer is directed to the heat exchanger. Within this equipment, the gas mixture undergoes cooling from -3°C to -6°C . Temperature monitoring before and after the heat exchanger is ensured by two temperature emitters (TE-102810) and (TE-102813). Subsequently, the gas is directed into the condenser.

Regulating the molar reflux ratio to achieve the target composition involves two potential strategies:

- The first strategy entails continuous monitoring of the liquid stream's composition exiting the condenser. A composition analyzer and a gas chromatograph (GC) are installed to continuously monitor the composition of the reflux stream (line L22). Liquid reflux into the column continues until the desired composition is attained. Upon reaching the target composition, a pneumatic valve (YV-101236) is opened in the top stream (see Figure 7.21).
- The second configuration, depicted in Figure 7.20, involves control of the condenser

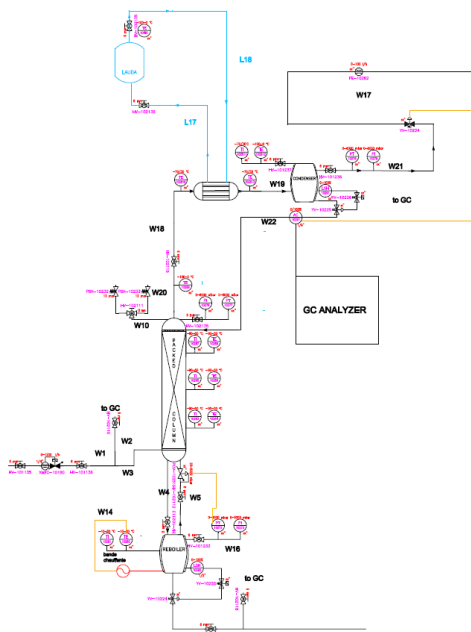


Figure 7.21: First distillation column, FIRST configuration with controllers

using a liquid level sensor (LSH-10281) and a Zimmerly valve (PCV-10257) placed in the condenser's exhaust line. Pressure monitoring is facilitated by the pressure transmitter (PT-10278). The logic here is to set the Zimmerly valve at a predetermined pressure threshold, prompting it to open at the specified pressure. This configuration aims to achieve a desired level of purity, necessitating regulation of the amount of liquid reinjected from the condenser to the distillation column. For this purpose, a mass flow regulator is required.

Upon comparison, it becomes evident that the first configuration (Figure 7.21) is more efficient for controlling the required composition, albeit at a higher cost. In contrast, the second configuration (Figure 7.20) is less efficient but more economical, with approximately a 30 kCHF cost difference. Given the total budget constraint of 200 kCHF for the entire plant, we opt for the second solution, despite its lower accuracy. Thus, the second control system (Figure 7.20) is adopted for regulating the distillation column. The description of the control system for the second column, situated in series, is omitted in this thesis, as it operates in an identical manner to the first column.

7.6 R&D of a membrane for the separation of SF₆/N₂ mixture

In the previous section, an extensive analysis was conducted on the sizing of the two distillation columns arranged in series within our plant, taking into account the project specifications outlined in the preceding section. It was established that at the end of the second stage in the series of the distillation column, 1 l/h of gas is obtained with the composition as listed in Table 7.7.

As evident, at the conclusion of the second distillation stage, a mixture of SF₆/N₂, albeit not pure, is obtained, necessitating further concentration. This section focuses on the R&D efforts undertaken in the laboratory to determine the feasibility of separating the SF₆/N₂ mixture using the hollow fiber polyimide membrane manufactured by UBE Corporation. In the next chapter further explanation will be provided about the experimental procedure and results.

While, in the next sections a MATLAB modelling of the membrane is explained and conducted to attempt simulating the separation process.

7.7 Theory of membrane separation

The membrane serves as a selective barrier allowing certain components to pass through while retaining others. Each membrane has a feed stream, the fluid passing through it is termed permeate, while the flow containing components that do not permeate the membrane is referred to as retentate or non-permeate. Refer to Figure 7.22 for a visual representation.

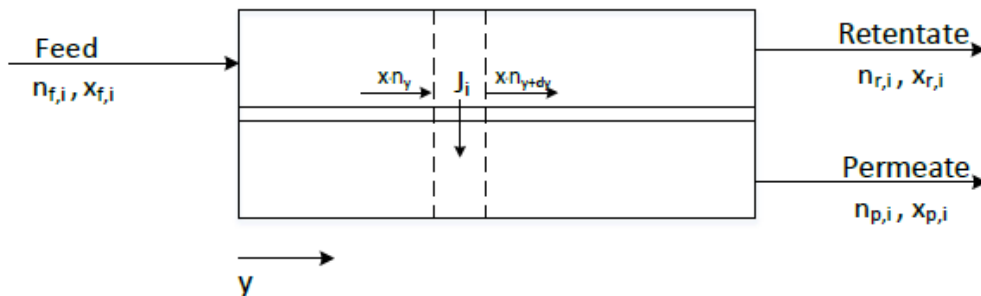


Figure 7.22: Membrane module configuration

Membranes can be used individually or in modules to achieve the desired concentration.

7.7.1 overall mass balance of a membrane module

By considering a control volume that includes the whole membrane module it is possible to impose the total and single species mass balance constraints.

Overall mass balance (hyp.: no chemical reactions)

$$\dot{n}_f = \dot{n}_p + \dot{n}_r = \sum_i \dot{n}_f x_{i,f} = \sum_i \dot{n}_p x_{i,p} + \sum_i \dot{n}_r x_{i,r} \quad (7.9)$$

where,

- \dot{n}_f , is the molar flowrate in the feed stream;

- \dot{n}_p , is the molar flowrate in the permeate stream;
- \dot{n}_r , is the molar flowrate in the retentate stream;
- x_i is the molar fraction of component i .

Single species overall mass balance

$$\dot{n}_f x_{i,f} = \dot{n}_p x_{i,p} + \dot{n}_r x_{i,r} \quad (7.10)$$

which is complemented by the molar fraction for each process stream:

$$\sum_i x_{i,f} = \sum_i x_{i,p} + \sum_i x_{i,r} \quad (7.11)$$

By considering a control volume that includes the whole membrane module it is possible to frame the total mass flux across the membrane into the mass balance

$$\dot{n}_f = \dot{n}_p + \dot{n}_r = \int_A J dA \quad (7.12)$$

where,

- $J = \sum J_i$ is the total molar flux of permeating species;
- J_i represents the molar flux equation for species i across the membrane;
- A represents the membrane section area where mass transfer occurs.

For a clearer understanding see figure 7.22. To quantitatively solve the membrane mass balance equations, adopting a local approach proves convenient. This entails considering an infinitesimally small arbitrary control volume within the membrane to describe the local separation process. Within this context, the single-species mass balance equation holds true.

$$(x_{i,r} \dot{n}_r)|_y - (x_{i,r} \dot{n}_r)|_{y+dy} = J_i dA \quad (7.13)$$

Through the use of this equation 7.13 it is possible to define the input data which represents the design specifications. (e. g. feed flow rate, composition and operative conditions), as well as the output variables (e. g. membrane area) involved in the process.

7.8 Membrane modelling for gas separation

Before delving into the description of the membrane modelling we first want to take a look at what is the pressure profile in the gas permeation module see figure 7.23.

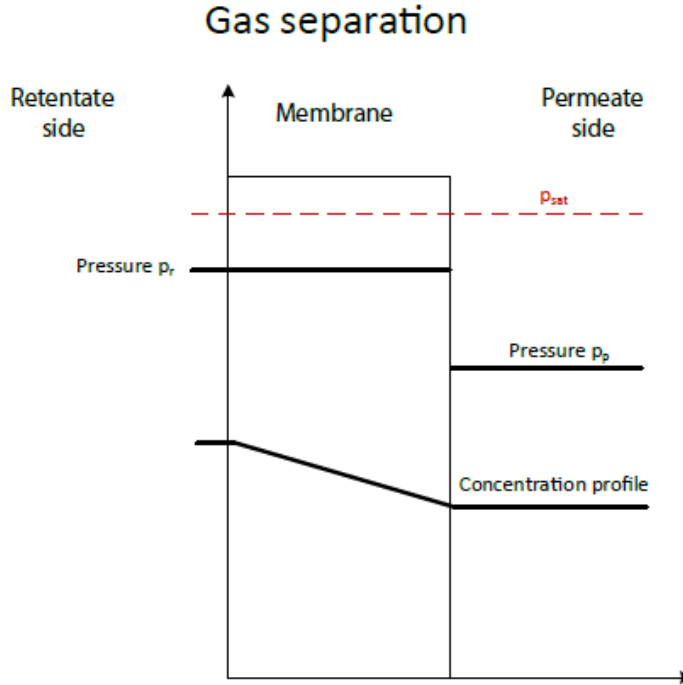


Figure 7.23: Pressure and concentration profiles in a gas separation process

a high pressure gas mixture at p_r is fed to the feed side of the membrane while the permeate is removed at a lower pressure p_p at the downstream side. The pressure profile within the membrane is assumed constant and equal to p_r . The diffusion through the cross section is neglected. Permeability, feed and retentate pressure are assumed to be constant through all the membrane Area. With all this hypothesis in mind we can now write the overall balance equation used for modelling the membrane

$$\begin{cases} dn_{N_2} = p_{N_2}(p_f \times x_f - p_p \times x_p)dA \\ dn_{SF_6} = p_{SF_6}(p_f \times y_f - p_p \times y_p)dA \end{cases} \quad (7.14)$$

$$\begin{cases} F.N_2(A + dA) = F.N_2(A) - n.N_2(A) \\ F.SF_6(A + dA) = F.SF_6(A) - n.SF_6(A) \end{cases} \quad (7.15)$$

where,

- dn_{N_2} is the differential molar flowrate of N_2 .
- dn_{SF_6} is the differential molar flowrate of SF_6 .
- F_{N_2} is the molar flowrate of N_2 expressed in $\frac{kmol}{h}$.
- F_{SF_6} is the molar flow rate of SF_6 expressed in $\frac{kmol}{h}$.
- p_{SF_6} is the permeability coefficient of SF_6 expressed in $\frac{kmol}{h \times bar \times m^2}$

- p_{N_2} is the permeability coefficient of N₂ expressed in $\frac{kmol}{h \times bar \times m^2}$
- dA is the differential area and it is express in (m^2)
- x_f and y_f are the molar composition respectively in the feed and in the permeate region.
- x_p and y_p are the are the molar composition respectively in the feed and in the permeate region.

For solving our modelling problem we need then to solve the system of linear differential equations 7.14, and for doing this we need to set our boundary conditions. Our boundary conditions will be the following :

- at $A = 0$ $n_{SF_6} = 0.00415 \frac{kmol}{h}$
- at $A = 0$ $n_{N_2} = 0.001247 \frac{kmol}{h}$

Here below a brief scheme for understanding how the membrane is discretized is provided 7.24.

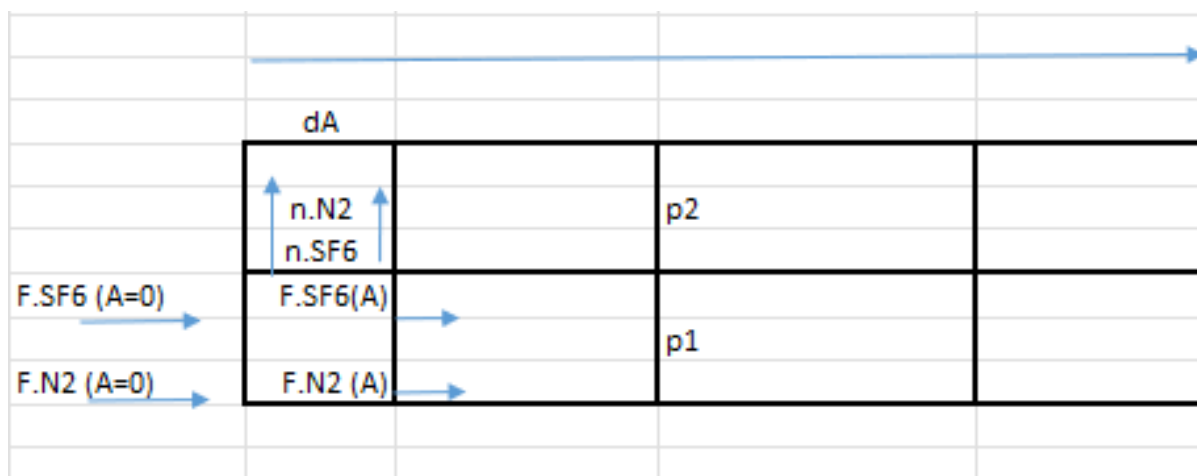


Figure 7.24: Schematic scheme of the discretization for the membrane modelling

Furthermore, to address this issue, it is imperative to ascertain the permeability values of the two gases through the membrane, denoted as p_{SF_6} and p_{N_2} . These values represent the total kilomoles permeated through the membrane in one hour per unit area, under a pressure of 1 bar, and are expressed as $\frac{kmol}{h \times bar \times m^2}$. Additionally, the feed pressure p_f and the permeate pressure p_p , along with the compositions of the gases at the feed and permeate sides, are essential parameters for solving this problem.

The permeability coefficients are obtained from literature [23], while all other parameters listed in the table are chosen to closely mimic real experimental conditions. A summary of this information is provided in Table 7.18.

Permeability coefficient ($\frac{kmol}{h \times bar \times m^2}$)	SF ₆ feed flowrate ($\frac{kmol}{hr}$)	N ₂ feed flowrate ($\frac{kmol}{hr}$)	Feeding pressure (bar)	Permeate pressure (bar)	molar fraction SF ₆ , x _{SF6}	molar fraction N ₂ , x _{N2}
1.02	0.00415	0.001247	1.5	0.4	0.7	0.3

Table 7.18: Inet parameter for membrane module.

With all this input data the simple separable first order differential equation 7.14 can now be numerically solved. The solution of the differential equation is referenced in figure 7.25:

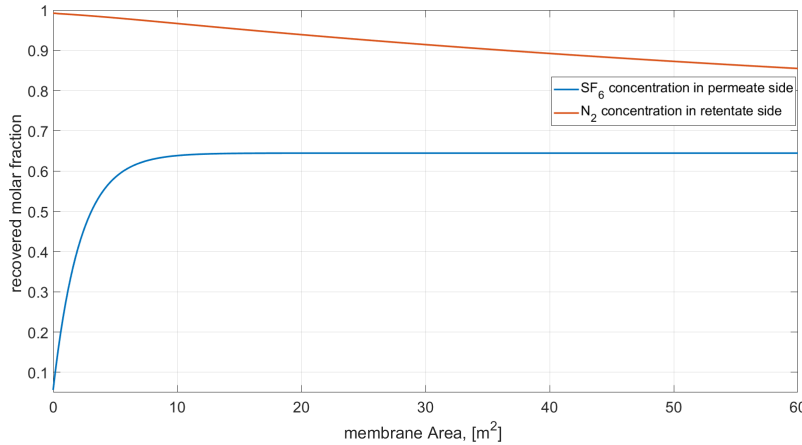


Figure 7.25: Results of ODE, SF₆ permeate side and N₂ retentate side.

The results clearly indicate that the efficiency of SF₆ gas recovery reaches almost 65% with a purity exceeding 92% at an equivalent area of 8 (m^2). Interestingly, further increasing the area up to 60 (m^2) does not yield a higher recovery efficiency. Meanwhile, the concentration of N₂ on the non-permeate side remains relatively constant, gradually decreasing only as the permeation area increases.

Considering these findings, it's evident that increasing the area does not significantly enhance the separation process. Therefore, for our application, we'll opt for an equivalent permeation area equal to that of the membrane itself.

In the upcoming chapter, we'll delve into the experimental tests conducted with the membrane, to compare the simulated data with the experimental findings.

Chapter 8

Experimental R&D of a separation membrane

In this section, we will describe the R&D activity done in laboratory for testing the separation performances of the membrane.

For the test a hollow fiber polyimide membrane was tested in our system. The goal of the experiment is to test if the UBE membrane separates a mixture of N_2 SF_6 , at constant ratio but at different feed flowrate and retentate pressure. The UBE membrane is the MINI- CO_2 separator here a picture is referenced 8.1.



Figure 8.1: Mini CO_2 separator

8.1 Introduction to experimental set-up

For conducting the tests, an experimental setup was first assembled. A P&ID of the setup is provided for clearer understanding (Figure 8.2).

In this setup, one cylinder contains SF_6 gas, while another line is directly connected to the gas supply for the injection of N_2 . The inlet gases are regulated using a Pressure Control Valve (PCV). Following the PCV, a rotameter is used to regulate the flow, and a flowmeter is placed to measure the flow rate.

The gases are mixed in a buffer before being sent into the membrane. Before the membrane inlet, a pressure transmitter is installed to monitor the pressure. At the outlet of the membrane, both a pressure transmitter and a flowmeter are placed to measure the pressure and flow respectively.

On the retentate side, a recirculation loop is implemented to recirculate the gas. To

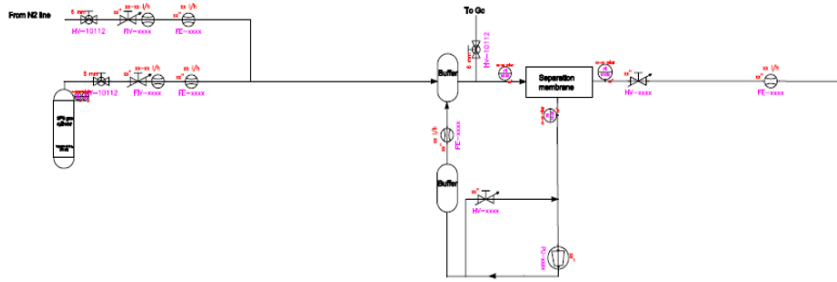


Figure 8.2: Membrane module configuration

create the necessary pressure differential (ΔP) between the inlet and retentate side, negative pressure is required. This negative pressure is generated by a vacuum pump located at the outlet of the retentate side. An equalizing buffer is placed at the exhaust of the pump to avoid fluctuations that might be registered by the flowmeter placed in series. The gas is then recirculated back into the mixing buffer.

Unfortunately, this initial configuration was ineffective. The issue was that the recirculation stream was connected from the exhaust line to the suction line to regulate the pressure on the retentate side. However, the suction of the pump was too strong, causing all the flow to be drawn into the vacuum pump. In the next subsection, the correct configuration adopted for the experimental test will be described .

8.1.1 Final Set-up Configuration

In Figure 8.3, the final configuration used in the laboratory is presented.

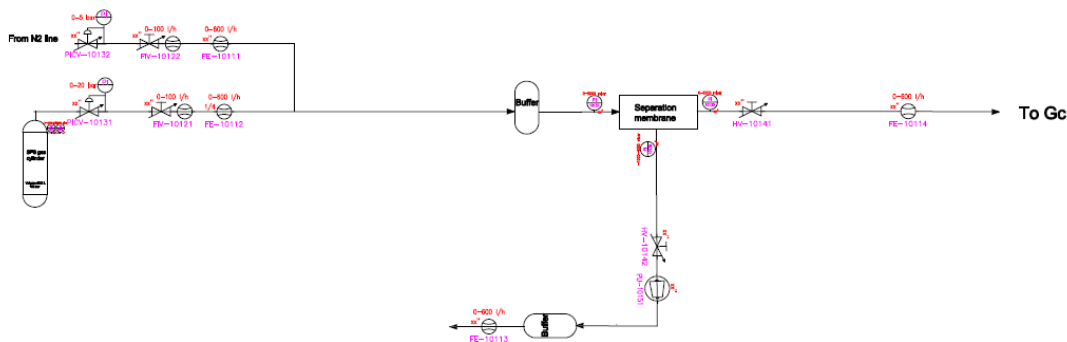


Figure 8.3: Membrane module configuration

This configuration resolved the issue of gas recirculation in the suction line by installing a very small needle valve (4 mm) in the retentate side, denoted as HV-10142. This valve is more sensitive to pressure regulation on the retentate side. The working principle remains almost the same, with the key difference being the absence of recirculation on the retentate side.

In this configuration, the mass balance of the three streams is maintained. Below is a

table that provides an understanding of the equipment present in the P&ID 8.1.

Component	Index
Pressure regulator with indicator	PICV-10131
Pressure regulator with indicator	PICV-10132
Mass flow regulator	FIV-10121
Mass flow regulator	FIV-10122
Flow meter	FE-10111
Flow meter	FE-10112
Buffer (Mixing volume for SF ₆ and N ₂)	BF-10151
Buffer (Equalizing volume)	BF-10152
Pressure Transmitter	PT-10130
Pressure Transmitter	PT-10131
Pressure Transmitter	PT-10132
Needle valve	HV-10141
Needle valve	HV-10142
Flow meter	FE-10113
Flow meter	FE-10114

Table 8.1: Component and Index of membrane set-up

For a clearer understanding a figure here is referenced of the setup mounted in lab. 8.4

In the next subsection, we will discuss the experimental tests performed with the membrane.

8.2 Experimental test

In this section, we will describe in details the experimental tests held with membrane. For the tests they were held at various flowrate, than at different ratio and than at different retentate pressures. With this we want to test what are the parameters that most affect the membrane separation, and if there are some parameters that are more influencing than others.

since the process of membrane is a rate controlled process we aspect that the ΔP (pressure gradient) between inlet and retentate side is the most affecting parameter, 8.2 let's see if this is experimentally verified.

8.2.1 Experimental Procedure

In this subsection experimental procedure of the tests it is explained, so in table 8.1, we have reported all the necessary element in the P&ID, than, here we are going to describe them more accurately In this subsection, the experimental procedure for the tests is explained. Table 8.1 lists all the necessary elements in the P&ID. Below, we provide a detailed description of these components:

- **Pressure Regulator with Indicator:** The function of these regulators is to control the gas pressure. The PICV-10132 is directly connected to the hydrogen line from a gas supply, while the PICV-10131 is directly connected to the SF₆ cylinder.
- **Rotameter-Flow Regulator:** These devices indicate and manually regulate the flow rate by adjusting the valve. Although all are calibrated in air, for more accurate flow rate measurement, a flowmeter is necessary. For the tests, an OMRON

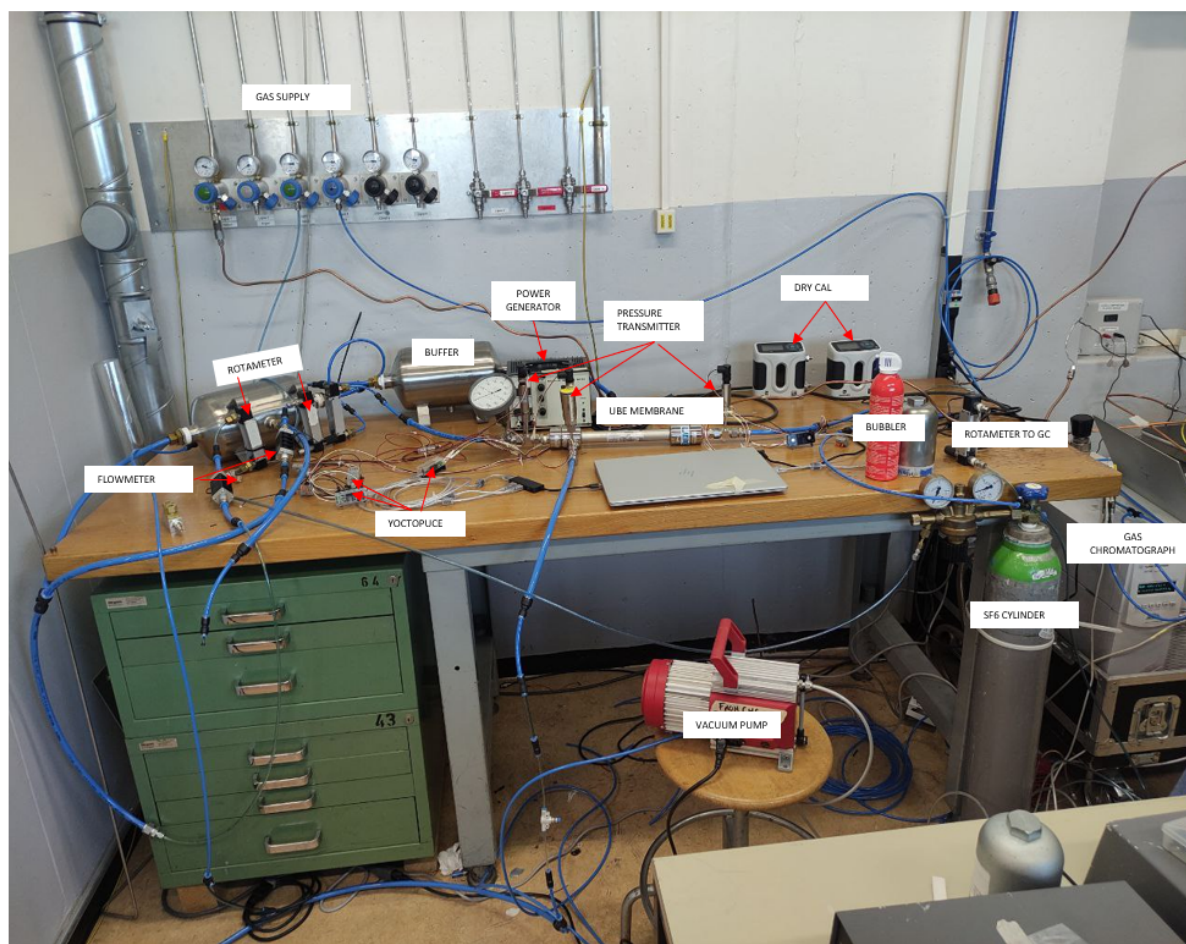


Figure 8.4: Laboratory setup description

flowmeter D6F-10A61-000, is used (see Appe. This latter, has a range of 0/50 l/min calibrated in air, and it is directly connected to a Yoctopuce, which sends an electric signal to a PC, allowing real-time monitoring of the flow rate. All flowmeters are calibrated in air, meaning that for accurate readings with different gases, calibration with a drycal is needed. A drycal provides an actual volume measurement of the injected gas regardless of its type. The Omron flowmeter, calibrated in air, requires multiple measurements at different flow rates to determine the volume of gas corresponding to the indicated flow rate. This trend is typically linear, and the calibration lines for SF_6 and N_2 are provided in the appendix (see Figures J.1 and J.2).

- **Buffers:** The system includes two buffers with different functions: the first buffer mixes the gases, while the second one dampens the vibrations caused by the vacuum pump on the retentate side.
- **Pressure Transmitters:** These devices detect pressure at specific points. When connected to a Yoctopuce device (essentially a Raspberry Pi), they detect variations in gas flow rate proportional to the current sent to them. If necessary, pressure variations can be monitored and recorded with Yocto-Visualization software.
- **Gas Chromatograph Analyzer:** When conducting experiments with two gases, a gas chromatograph is essential to determine the mutual composition of the gases.

In the laboratory, the instrument used for detecting variation in gas composition, when the binary mixture is sent, is a Gas Chromatograph.

8.3 Test held at constant flowrate

In this section, we will summarize all the experimental tests held at constant inlet flowrate but at different retentate pressure, to test the membrane performances, in the next subsection we are going to report all the test performed and the final findings from the data that we have got.

8.3.1 Test 0

In the following table 8.2, the experimental test held with the ube membrane for N₂ gas at 50 l/h is here reported.

Inlet flowrate (l/h)	Non permeate flowrate (l/h)	Permeate flowrate (l/h)	Inlet pressure (bar)	Outlet Pressure (bar)	Permeate Pressure (bar)
50	40	10	0.55	0.52	-0.9
50	46.1	9.43	0.49	0.47	-0.7
50	43.9	6.7	0.47	0.432	-0.5
50	44.2	4.5	0.51	0.498	-0.3

Table 8.2: N₂ gas in UBE membrane. Test 1 at Constant inlet flowrate : 50 l/h

As noted from the experimental results the mass balance (7.9) is not exactly respected, this is because there are some errors in the calibration of the mass flow meter and the lower the flow the highest the errors. We can than estimate really fastly what is the permeability of the membrane calculating the average flowrate at the feed 8.2 and permeate side 8.3.

$$\dot{V}_{p,av} = \frac{\sum_i \dot{V}_{p,i}}{N} \quad (8.1)$$

$$\dot{V}_{f,av} = \frac{\sum_i \dot{V}_{f,i}}{N} \quad (8.2)$$

where:

- $\dot{V}_{p,i}$ is the volumetric flowrate in the permeate side expressed in (l/h).
- $\dot{V}_{f,i}$ is the volumetric flowrate in the feed side expressed in (l/h).
- N is the total number of experimental data.

. In this table the average flowrate of the feed and permeate side are here summarized 8.3.

After that, the ratio of this two calculated flowrates is the permeability of the membrane 7.7.1.

$$Permeability = \frac{\dot{n}_{p,av}}{\dot{n}_{f,av}} \quad (8.3)$$

The permeability of the membrane is only 0.154, this means that only 15% of the inlet N₂ permeates through the membrane the other part is not permeated. This means that the membrane is really inefficient for the permeation of N₂.

Feed (l/h)	flowrate	Permeate flowrate (l/h)
50		7.66

Table 8.3: Average feed and permeate flowrate of N2 gas.

8.3.2 Test 1

In this subsection we are sharing the lab results of the test held with SF₆ at constant flowrate of 50 l/h, here below the table is reported. As noted from the experimental

Inlet flowrate (l/h)	Non Per- meate flowrate (l/h)	Permeate flowrate (l/h)	Inlet pres- sure (bar)	Outlet Pes- sure (bar)	Permeate Pressure (bar)
50	34.23	7.54	0.35	0.29	-0.9
50	35.17	36.13	0.3	0.295	-0.7
50	36.13	6.7	0.3	0.29	-0.5
50	36.83	7.09	0.3	0.29	-0.3

Table 8.4: SF₆ gas in UBE membrane. Test 1 at Constant inlet flowrate : 50 l/h

results, the mass balance (7.9) is not exactly respected. This discrepancy is attributed to calibration errors in the mass flow meter, which are more pronounced at lower flow rates. Consequently, we can quickly estimate the membrane's permeability by calculating the average flow rate at the feed side (7.11) and the permeate side (8.3) measured by the OMRON flowmeters.

Feed (l/h)	flowrate	Permeate flowrate (l/h)
50		7.34

Table 8.5: Average feed and permeate flowrate of N2 gas.

After that, the ratio of the calculated flowrates gives us the permeability of the membrane 8.3. The value of the calculated average flowrate is even lower than the previous one, and it is equal to 0.147. This means that due to our initial configuration the membrane is not able to separate the two gases.

For confirmation of the obtained results, test at 100 l/h will be performed. In the next subsection, this test will be described.

8.3.3 Test 2

In the following table 8.6, the experimental test conducted with the UBE membrane for N₂ gas at 100 l/h is presented.

As observed from the experimental results, the mass balance (7.9) is not precisely maintained, and to estimate the permeability of the membrane, we can calculate the average flow rates on the feed side (7.11) and the permeate side (8.3).

In the following table, the average flow rates for the feed and permeate sides are summarized 8.7.

Afterward, the ratio of these calculated flow rates gives the permeability of the membrane as it is calculated through equation (8.3).

Inlet flowrate (l/h)	Non-Permeate flowrate (l/h)	Permeate flowrate (l/h)	Inlet pressure (bar)	Outlet pressure (bar)	Permeate pressure (bar)
100	80	20	0.55	0.52	-0.9
100	92.2	18.86	0.49	0.47	-0.7
100	87.8	13.4	0.47	0.432	-0.5
100	88.4	9.0	0.51	0.498	-0.3

Table 8.6: N₂ gas in UBE membrane. Test 1 at constant inlet flowrate: 100 l/h

Feed flowrate (l/h)	Permeate flowrate (l/h)
100	15.9

Table 8.7: Average feed and permeate flow rates of N₂ gas.

The permeability of the membrane is 0.159, indicating that only 15.9% of the inlet N₂ permeates through the membrane, while the remaining part is not permeated. This suggests that the membrane is quite inefficient for the permeation of N₂.

8.3.4 Test 3

This subsection presents the lab results for the test conducted with SF₆ at a constant flow rate of 100 l/h, but at variable retanate pressure as shown in the table below 8.8.

Inlet flowrate (l/h)	Non-Permeate flowrate (l/h)	Permeate flowrate (l/h)	Inlet pressure (bar)	Outlet pressure (bar)	Permeate pressure (bar)
100	68.46	15.08	0.35	0.29	-0.9
100	70.34	14.17	0.3	0.295	-0.7
100	72.26	13.4	0.3	0.29	-0.5
100	73.66	14.18	0.3	0.29	-0.3

Table 8.8: SF₆ gas in UBE membrane. Test 1 at constant inlet flow rate: 100 l/h

As noted from the experimental results, the mass balance (7.9) is not precisely maintained due to calibration errors in the mass flow meter, which are more significant at lower flow rates. To estimate the membrane's permeability, we calculate the average flow rate at the feed side (7.11) and the permeate side (8.3). In table 8.9, they are reported.

Feed flowrate (l/h)	Permeate flowrate (l/h)
100	14.68

Table 8.9: Average feed and permeate flow rates of SF₆ gas.

Subsequently, the ratio of these average flow rates provides the permeability of the membrane 8.3. The average value of the calculated average flow rate is 0.147, which is lower than the previous result. This indicates that under the initial configuration, the membrane is not effective in separating the two gases. So at the end with this second

result we have confirmed that the membrane is not able to separate this two gases. In conclusion, the membrane is not suitable for our application, so, the test held was unsuccessful.

8.4 Conclusion of the R&D Activity Performed with Membrane

As Yang Chuah and Lee noted in their review [30], the permeation of N_2 is faster than that of SF_6 in polymeric membranes, making the performance of membranes typically evaluated based on N_2/SF_6 separation [26].

We must also consider that the permeability of N_2 in a membrane is typically low, and SF_6 has a high kinetic diameter, resulting in low diffusivity. Permeability can also be defined as the product of solubility (S) and diffusivity (D) of a given component, as shown in Equation 8.4 [30].

$$P = SD \quad (8.4)$$

N_2 has low solubility, while SF_6 has low diffusivity, meaning that the permeability of these two components in the membrane should be comparable. This was verified in our experimental tests, where the permeability of the two components was nearly the same (0.157 for N_2 and 0.148 for SF_6). Therefore, for a 50/50 mixture of N_2 and SF_6 , determining the permeability as the ratio of the two permeabilities yields a value close to 1. This value is consistent with literature findings, as shown in Figure 8.5.

Membrane			Separation performance				Ref.	
Category	Configuration	Materials	Testing condition N_2/SF_6 feed composition	Pressure (bar)	Temperature (°C)	N_2 permeance (GPU)	N_2/SF_6 selectivity	
Polymeric (Organic) membrane	Flat sheet	3-aminopropyl trimethoxysilane (APrTMOS)	Pure	–	–	29.8	11.0	[126]
		Poly(1-trimethylsilyl-1- propyne) (PTMSP)	Pure	10	0	7700	3.3	[127]
		Poly(1-trimethylsilyl-1- propyne) (PTMSP)	30/70	10	0	838	0.4	[127]
		Poly(4-methyl-1-pentene)	Pure	6	40	10.2 ^[a]	194	[30]
		Poly(4-methyl-1-pentene)	50/50	6	40	10.3 ^[a]	242	[30]
		Polydimethylsiloxane (PDMS)	Pure	3	25	320 ^[a]	1.3	[128]
		Polyimide (Matrimid)	Pure	–	–	0.3 ^[a]	45.8	[129]
		Polyether block amide (PEBAX)	Pure	3	25	9.2 ^[a]	3.3	[128]
		<i>n</i> -butyl-trimethoxysilane (BTMOS)	Pure	–	–	3.0	4.0	[126]
	Hollow fiber	Polycarbonate (Standard-PC)	Pure	3	25	5.7	2.4	[130]
		Polyethersulfone	10/90	3	35	15.1	5.6	[131]
		Polyimide (Matrimid)	Pure	1	50	4.0	66.0	[132]
		Polyimide (PA4050-P3)	7/93	3	25	1.0	43.9	[133]
		Polyimide	–	–	40	108	100.0	[134]
		Polyimide	Pure	11	25	1.1	38.9	[135]

Figure 8.5: Polymeric membranes, Permeability and Selectivity

When comparing the MATLAB modeling performed in the previous chapter with the experimental tests, we found that the results did not match. In the membrane modeling (Figure 7.25), it was shown that after a modeled specific area of 8 m^2 , the efficiency of SF_6 recovery in the permeate side was 65%. However, this was not verified experimentally, where we observed a recovery of only 17% of SF_6 .

This discrepancy is explained by the simplicity of our MATLAB model, which only considered the pressure gradient (ΔP) as a driving force, neglecting the significant diffusive contribution. This means that the equation used for the modelling, where not properly correct instead, we should have taken into account the diffusivity term. Here below, as a reference the membrane differential equation 8.5, that should had been used for a proper modelling [18].

$$d((n)_r y_r) = -J_y p ds \quad (8.5)$$

In conclusion, the R&D tests performed with the UBE membrane were unsuccessful for the separation of SF_6/N_2 . The next step for our R&D purposes will be to test zeolite adsorbers, specifically molecular sieves 5A and 13X, to explore the possibility of achieving the desired separation.

Chapter 9

Reasons behind the SF₆ recovery plant

In this chapter, we will delve into the main reasons for constructing this plant and demonstrate why recovery systems are preferred over the installation of abatement systems. An extensive economic analysis will be conducted to justify these decisions, ultimately confirming the rationale behind building recovery systems.

9.1 SF₆ recovery system, and cost of fresh

As mentioned in the previous, section the new SF₆ plant is planned to be built in CMS, at the exhaust of the detector loop. More specifically it will be placed in series of the R134a recovery system in CMS. In the following picture 9.1, it is shown it's exact location in the exhaust module.

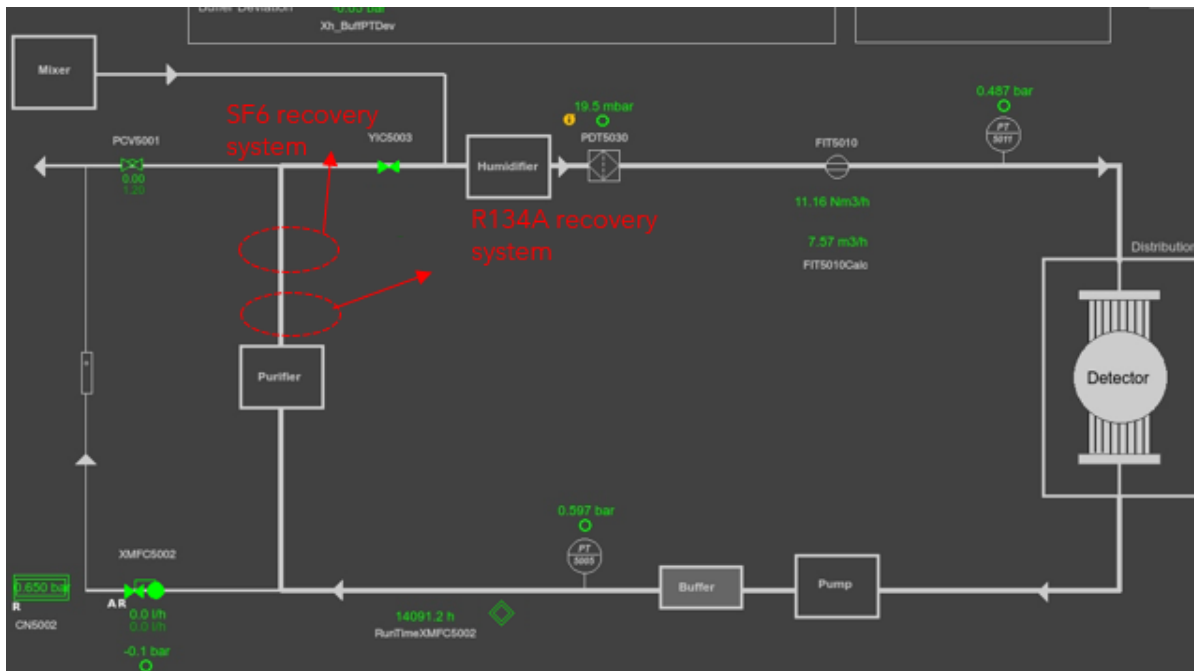


Figure 9.1: Exhaust module of the RPC detectors

At our CMS facility the recovery system of R134a intake the gas mixture in two different flow rate configurations, in high flow (600-500)l/h for 26 weeks/ year and in

low flow 24 weeks/ year between (100-200)l/h. Considering that the mixture sent in the recovery it is the one mentioned in table 2.1, and considering that almost all the SF₆ is not going to condensate in the R134a recovery, this will come out and will be sent to from the exhaust to air. This means that this exhausted fraction have to be reinjected from the mixer.

Here, below there is a table that synthethises, all the fresh injected SF₆ at the mixer in the two different configurations.

Run configuration	SF ₆ injected in (l/h)	SF ₆ injected in (l/year)
High Flow (6 months)	2,4	10368
Ion Run (1 month)	1,2	864
Low Flow (4months)	0,9	2592

Table 9.1: Flowrate of SF₆ injected at the mixer .

Here, we present a table summarizing the fresh SF₆ injected at the mixer in the two different configurations.

SF ₆ injected (l/h)	SF ₆ injected (l/year)
4,5	13824

Table 9.2: Flowrate of SF₆ injected at the mixer.

From Table 9.2, we can clearly see that the total amount of injected SF₆ per year is almost 14 m³/year. Considering that the cost of fresh SF₆ is 617 CHF/kg [27], we can easily calculate the yearly expenditure on fresh SF₆.

Total SF ₆ flow rate injected in the mixer (m ³ /year)	Total weight of SF ₆ (kg/year)	converted of SF ₆ (CHF/kg)	Price of SF ₆ (CHF/kg)	Price of fresh SF ₆ spent per year (CHF/year)
14	84		617	51572

Table 9.3: Yearly expenditure on fresh SF₆.

From Table 9.3, we see that the annual cost of SF₆ is approximately 52 kCHF. According to Table 7.17, the recovery rate of SF₆ is about 60%, so from the injected 14 m³ at the mixer, the recovered SF₆ will be 8.4 m³/year. Assuming that we recover almost 90% of the N₂/SF₆ mixture after membrane recovery, we have 8 m³/year of fresh SF₆.

In this way, we save almost 31 kCHF/year solely on fresh SF₆ (refer to Table 9.4).

Fresh SF ₆ needed (kg/year)	Fresh SF ₆ needed with recovery (kg/year)	Total cost of fresh SF ₆ with-out recovery (kCHF/year)	Total cost of fresh SF ₆ with recovery (kCHF/year)	Net savings (kCHF/year)
84	33	52	21	31

Table 9.4: Cost savings from SF₆ recovery per year.

In the next section, we will extend this economic analysis to all the recovery systems present in CMS and compare them to the maintenance costs of the abatement systems.

9.2 Economic Analysis

As previously mentioned, this section will summarize the economic analysis of the gas recovery systems at CMS and compare the results with the abatement system Ebara 5G, which effectively abates all fluorinated gases. We will determine whether it is more economically feasible, presenting the results in terms of kCHF/year and tCO₂eq/year.

9.2.1 Gas Consumption at CMS

The main fluorinated gases used in CMS are R134a, SF₆, and CF₄. An extensive explanation of their usage in the RPC and CSC chambers was provided in the introduction (refer to Section 1.4). In this subsection, we will estimate gas consumption for each period of RUN and LS (long shutdown). Data from 2012 to 2018 were taken from the article [22]. Data from 2019 to 2024 were obtained directly from trends in the WinCC-OA software. For 2025 to 2035, the reported data come from [22], which states that from RUN 4, the injected gas flow rate will increase from 9 m³/hr to 15 m³/hr, and during each shutdown, the flow rate will decrease by 30%, though the composition will remain the same: 95.2% R134a, 0.3% SF₆, 4.5% iC₄H₁₀ for RPCs, and 40% Ar, 50% CO₂, and 10% CF₄ for CSCs.

In Figure 9.2, the referenced consumption of fluorinated gases from 2012 to 2035 is reported for each gas.

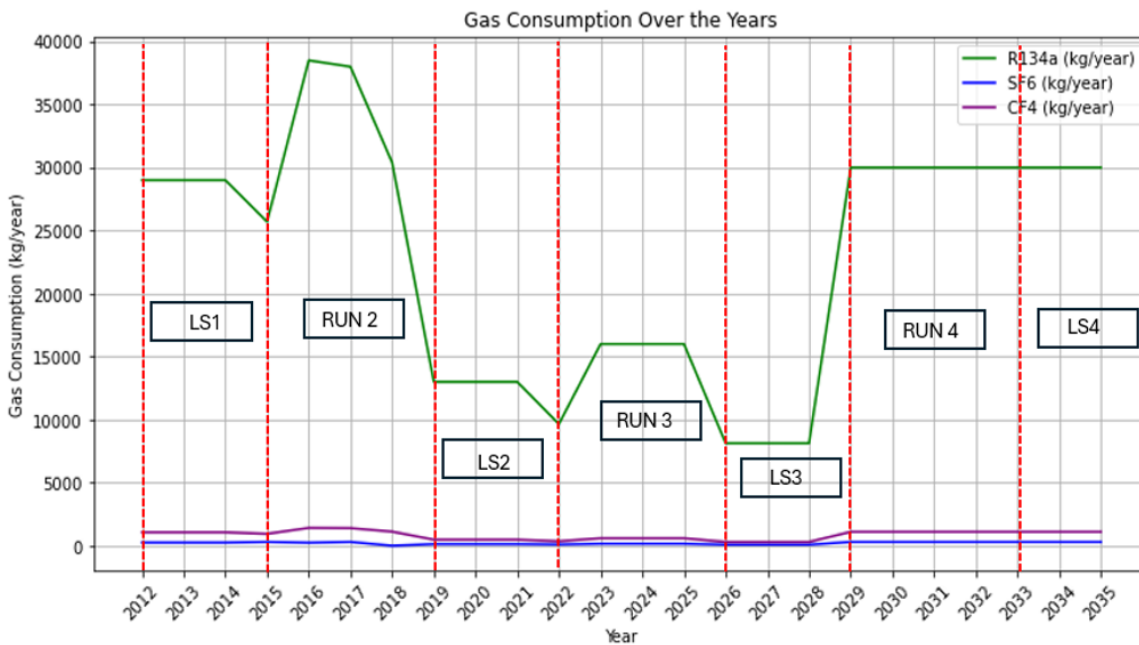


Figure 9.2: Gas consumption for each period divided in LS (Lung Shutdown) RUN (Run of the beam)

From the graph it is clearly seen that in LS2 (lung shut down 2) the gas consumption decreases, this is because between the flowrate sent in the loop of the detector is decreased and some of the RPC chambers were deactivated. Consequence of this, is that the flowrate was decreased from 15 m³/hr to 9 m³/hr. Then in Run 4 is planned to increase again the flowrate of gas in the detector to 15 m³/hr. For reference we report here a table 9.5, summarizing the gas consumption per each period. Each year, we incur varying amounts of expenses for different gases. The following graph 9.3 summarizes the annual expenditures for each gas. It is important to note that the figures from 2012 to 2024

Year	mass flowrate of R134a (kg/year)	mass flow rate of SF ₆ (kg/year)	Mass flowrate of CF ₄ (kg/year)
2012-2014	29000	250	1063
2015-2017	34000	270	1240
2018-2020	19000	143	689
2021-2023	13000	130	473
2024-2026	13400	134	490
2027-2029	15400	154	565
2030-2032	30000	300	1100

Table 9.5: Average Mass flowrate consumption of gas per year kg/year

are actual amounts sourced from the CERN gas store. For the years 2025 to 2035, the expenditures were estimated based on an assumed annual increase of 3% for R134a, 3.5% for CF₄, and 4% for SF₆.

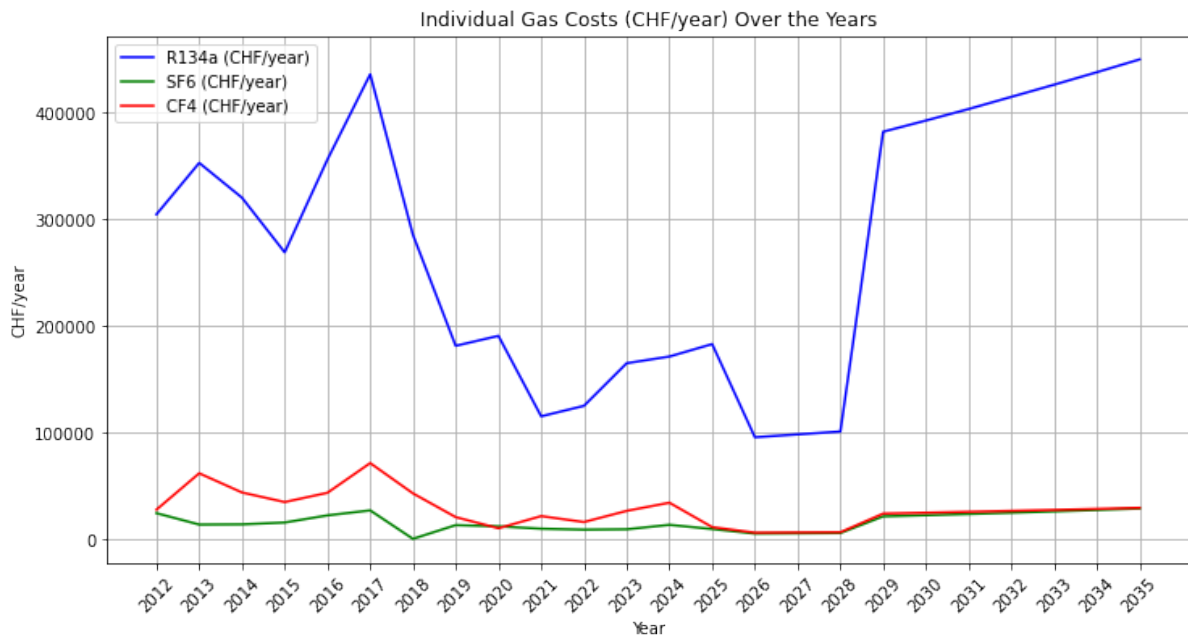


Figure 9.3: Amount of money spent per each gas in the period (2012 to 2035)

9.2.2 Recovery system cost estimation

After analyzing gas consumption, it is now crucial to focus on the economic analysis of recovery systems at CMS. In 2012, the recovery system for CF₄ was constructed, achieving an annual recovery efficiency of 50% until 2021, when the efficiency increased to 70%. The instrumentation required for the recovery system cost approximately 125 kCHF in 2012.

In 2022, the commissioning of the R134a recovery system was completed. After several improvements made in 2023, this system now operates with an efficiency of 80% and its construction cost was 200 kCHF. From August to December 2023 this system was able to recover 1200 kg of freon. From 2024 onwards, this recovery system can inject the recovered mixture into the RPC mixer, covering 50% of the R134a required at the mixer.

Looking ahead to 2025, the construction and operation of an SF₆ recovery system is planned. The SF₆ recovery system is expected to achieve an average recovery efficiency

of 60%. The initial cost estimate for the necessary equipment for this plant is around 200 kCHF.

In the following table, the voices of costs associated with the recovery plants are provided 9.6. The graph 9.5 , depicts the amount of money spent over the years per each

Voices of costs	R134a recovery	SF ₆ recovery	CF ₄ recovery
CAPEX (kCHF)	200	200	125
Technician + Phd student for analysis	20	20	20
M&O (kCHF)	15	15	10
Total (kCHF)	235	235	155

Table 9.6: CAPEX + M&O for each recovery system at CMS

recovery system from 2012 to 2035. The red dashes line indicates the cumulative amount per money spent over the years.

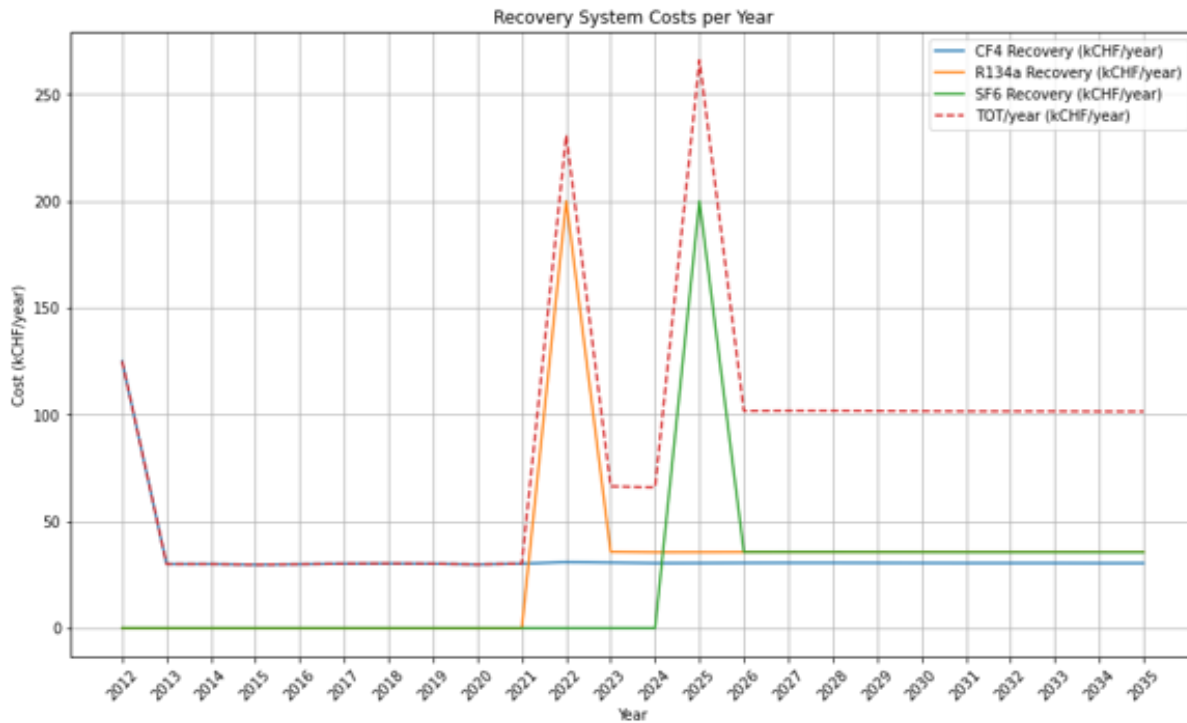


Figure 9.4: Amount of money spent per recovery systems in the period (2012 to 2035)

By knowing the efficiencies of the recovery systems and the price of fresh gas, we can easily calculate the amount of money saved through gas recovery. We can then compare the cumulative expenditure on recovery systems (including maintenance and operation costs) with the cumulative savings from recovered gas, measured in kCHF. This comparison will allow us to determine the break-even point, which is the time at which the total savings equal the total costs. The break-even analysis is illustrated in Figure 9.5.

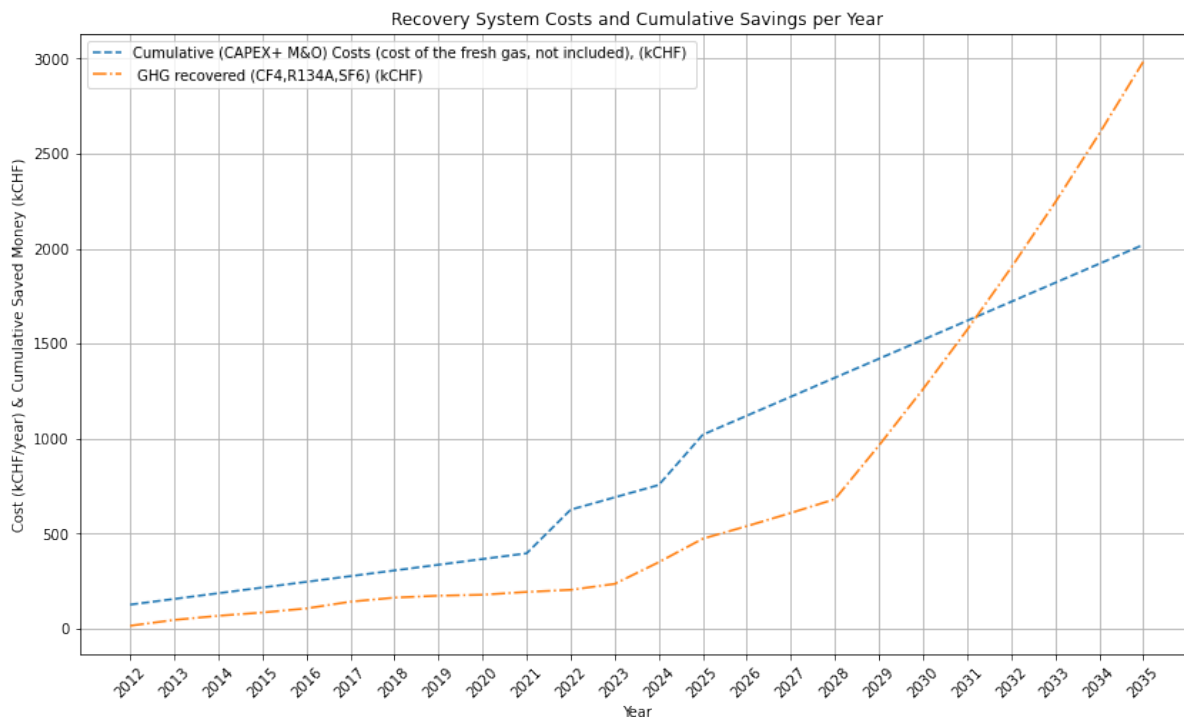


Figure 9.5: Cumulative curve of all the recovery system at CMS (blue curve). Cumulative cost saving from the gas recovered (yellow curve) in the period (2012 to 2035)

In the provided graph, two curves are displayed:

- The Blue Curve: This represents the cumulative costs associated with all recovery systems at CMS. These costs encompass construction, Front-Side Unit (FSU), maintenance, and operation of the recovery plants. Importantly, the cost of fresh gas injected into the mixer is not included in this curve.
- The Yellow Curve: This illustrates the cumulative cost savings from the gas recovered over the years.

The break-even point is projected to be reached in 2031.

The payback period, starting from the construction of the first system, is estimated to be 19 years. However, it is important to note that the financial benefits will start to increase notably when the R134a system begins recovery and reinjection into the mixer at the end of 2023. From this point, it will take six years to reach the break-even point. Additionally, from 2028 onwards, gas prices are expected to rise steadily. This increase in gas prices will result in higher financial gains from the fraction of gas recovered, further improving the economic efficiency of the recovery systems

The cumulative curve presented in Figure 9.5 does not account for the fresh gas required for reinjection into the mixer. Therefore, for a more comprehensive analysis,

it is essential to also consider the cost of fresh gas. The relevant cumulative curves are shown in Figure 9.6. From this figure, it is evident that reaching the break-even point is challenging. This difficulty arises because the amount of recovered gas is less than the amount injected into the mixer directly from cylinders. If the recovery efficiency were higher, the slope of the blue curve would change, and the break-even point would be reached sooner. Thus, improving recovery efficiency is of paramount importance.

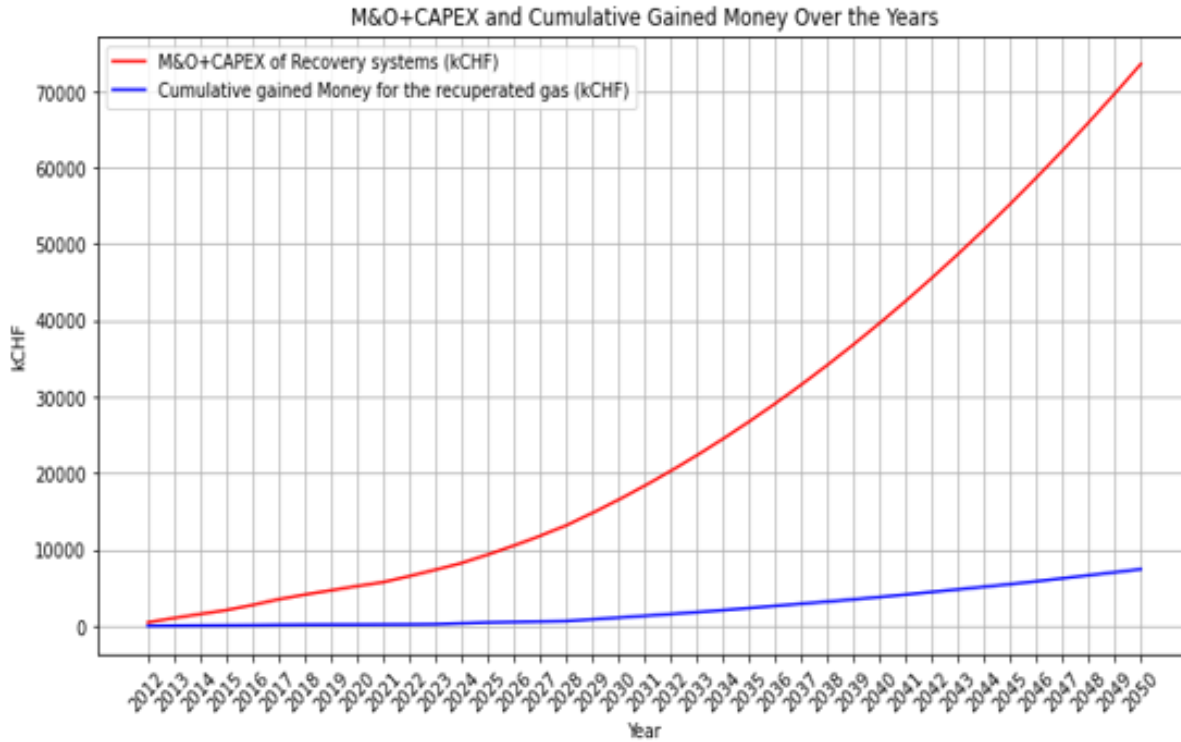


Figure 9.6: Cumulative curve of all the recovery system at CMS, cost of fresh gas at the mixer included (red curve). Cumulative cost saving from the gas recovered (blue curve) in the period (2012 to 2035)

Obviously, the gain with the recovery system ,it is the recovered gas itself. We than summarize the amount of F-gases recovered with the recovery systems in each period in table 9.7 and we provide the results in terms of kCHF per year, and tCO₂ emitted per year.

Year	R134a recovered (kg recovered in each period)	SF ₆ recovery (kg recovered in each period)	CF ₄ recovered (kg recovered in each period)	TCO ₂ eq Emitted in each period	Money saved in each period (kCHF)
LS1 (2012-2015)	0	0	1596	141393	124
Run 2 (2015-2019)	0	0	1874	208258	491
LS2 (2019-2022)	0	0	1034	64049	541
Run 3 (2022-2026)	17200	0	1430	66961	1240
LS3 (2026-2029)	12200	150	759	19045	1703
Run 4 (2029-2033)	45000	540	3740	93762	4806
LS4 (2033-2035)	31500	378	1965	43225	5759

Table 9.7: Recovery and Emissions Data

9.2.3 Abatement system- economic Analysis

After giving a quick summary on recovery systems, we will now estimate the cost needed for the abatement system for F-GHG. The two system that will be evaluated in this thesis are the Ebara 5g system and the Edwards ATLAS Etch System, see figure (9.7).



Fig. 5.2 The EBARA G5 [8] and EDWARDS ATLAS [9] waste gas abatement units.

Figure 9.7: The EBARA G5 and EDWARDS ATLAS waste gas abatement units

The system uses a two-stage "burn-and-wash" method, commonly used in the semiconductor industry. In this process, fluorinated greenhouse gases (F-GHG) are burned in a combustion chamber at high temperatures (800-1800°C) and then cooled and cleaned. The cooling unit acts as a dust collector, and a reservoir collects water containing byproduct powders and soluble gases from the wash process. The treated gas stream, mainly CO₂, water vapor, and traces of HF, is vented, while a scraper removes combustion by-products like SiO₂ powders from the reactor, see figure (9.8) The abatement system is

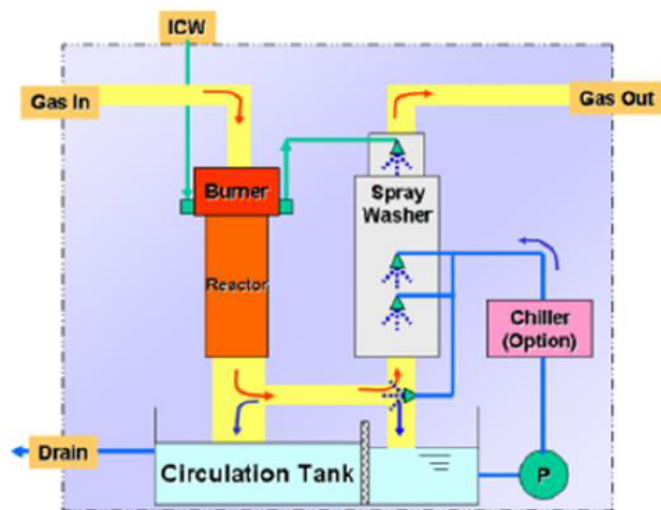


Figure 9.8: Flow diagram of the abatement process

able to abate F-GHG with high efficiency more than 90% the table 9.8 summarize the abatement efficiency, the characteristics and the costs for the two models.

	EBARA G5 model	EDWARDS ATLAS Etch System
R134a and SF₆ abatment efficiencies (ϵ_{eff})	≥ 95	≥ 95
CF₄ abatment efficiency (ϵ_{eff})	≥ 90	99
Burner (material/T)	Inox/1600°C	Ceramic/800°C
CAPEX (kCHF)	116	119
Maintenance & Operation (kCHF/year)	10	16

Table 9.8: Carachteristics, Efficiencies, and costs of the two abatment systems

The abatment system produces more than 15 m^3 of wastewater per day in the combustion and washing phase. From the combustion of CF₄ and R134a, big amounts of HF and F₂ are produced, while from the combustion of SF₆, H₂SO₃ and H₂SO₄ were produced but in lower quantities. All this products, makes the waste water acidic (pH = 2). In figure 9.9 all the reaction occuring in the two phases are reported.

abatment phase	Chemical reaction
Burning phase	$\text{CF}_4 + \text{O}_2 \rightarrow \text{CO}_2 + 2 \text{F}_2$
	$\text{SF}_6 + \text{O}_2 \rightarrow \text{SO}_2 + 3 \text{F}_2$
	$2 \text{C}_2\text{H}_2\text{F}_4 + 5 \text{O}_2 \rightarrow 4 \text{CO}_2 + 2 \text{H}_2\text{O} + 4 \text{F}_2$
Washer phase	$2 \text{F}_2 + 2 \text{H}_2\text{O} \rightarrow 4 \text{HF} + \text{O}_2$
	$\text{SO}_2 + \text{H}_2\text{O} \rightarrow \text{H}_2\text{SO}_3$
	$\text{SO}_3 + \text{H}_2\text{O} \rightarrow \text{H}_2\text{SO}_4$

Figure 9.9: Chemical reactions occurring during the waste-gas abatment process

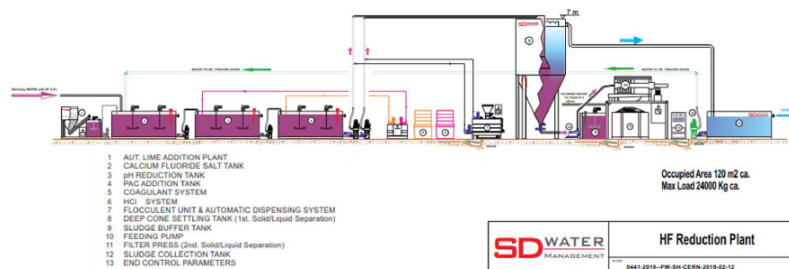
This wastewater, being highly acidic and toxic, cannot be disposed of directly into local watercourses or sewage systems. The two alternative options are:

- Transfer off-site for treatment and disposal
- On-site treatment and disposal

The first option involves storing approximately 15 tons of wastewater per day. Storage tanks must be capable of holding the large volumes accumulated over several days before periodic transportation to a disposal plant. A preliminary cost evaluation for the transport of 500 kg of RPC waste gas, equivalent to 1 week of operation, is 17 kCHF.

The second option is to construct an on-site treatment plant to neutralize the acidic and toxic components of the wastewater (figure 9.10). After treatment, the cleaned water can be safely discharged into the sewage systems or local watercourses. For the waste water treatment plant a price quotation for the entire construction was asked and Envirochemie for the entire plant asked for 500 kCHF, the M&O costs are provide in table 9.9

It is important to highlight that the data presented in Tables 9.8 and 9.9, which pertain to the abatment system during the Maintenance and Operation (M&O) phases, do not account for the cost of fresh gas. In Table 9.10, we summarize the quantities of fresh gas used in each LS and RUN period. The results are expressed in terms of the

Figure 9.10: Waste water plant scheme *Envirochemie*

Voices of costs	Envirochemie
CAPEX (kCHF)	500
FSU (kCHF/year)	84
Maintenance & Operation (kCHF/year)	12

Table 9.9: CAPEX, M&O, FSU costs for *Envirochemie* waste water treatment plant

mass of gas used per year (kg/year), costs (kCHF/year), and emissions (tCO₂eq). This deliberate separation of fresh gas costs aims to underscore the significant impact this factor has on overall expenses.

Year	R134a (kg/year)	SF ₆ (kg/year)	CF ₄ (kg/year)	R134a (kCHF/year)	SF ₆ (kCHF/year)	CF ₄ (kCHF/year)	Total costs (kCHF/year)	Total tCO ₂ eq (tCO ₂ eq/year)	tCO ₂ eq emitted with abatement system (tCO ₂ eq/year)
LS1 2012- 2014	29000	250	1063	325454	17016	44091	386561	50587	3035
RUN2 2015- 2018	34000	270	1240	336152	15991	47825	399968	56248	3465
LS2 2019- 2021	19000	143	689	162018	11352	17191	190561	23105	1386
RUN3 2022- 2025	13000	129	473	160680	9963	21706	192350	24520	1426
LS3 2026- 2028	13400	134	490	97906	5165	5982	109053	14440	866
RUN4 2029- 2032	15400	154	565	397725	22734	24918	445377	53321	3199
LS4 2033- 2035	30000	300	1100	306250	18943	19658	344852	37324	2239

Table 9.10: Fresh Gas consumption, costs, and emissions if no recovery system is present

9.2.4 Comparison of abatement system and recovery system- economic and enviromental analysis

After defining all the cost components associated with the recovery system and the abatement system, we aim to compare the configurations to determine the more cost-effective option. Specifically, we will compare:

1. The costs of the recovery system.
2. The costs of the abatement system, considering two scenarios:

- **Scenario 1:** Transportation of waste acid water from the abatement system to an external site for disposal.
- **Scenario 2:** Sending the waste acid water from the abatement system to an on-site wastewater treatment plant located at CMS.

This analysis will help us identify which option is more economical. For doing this cumulative curves of the recovery system and for the abatement system including the two cases are presented in the referenced figure 9.11b and 9.11a

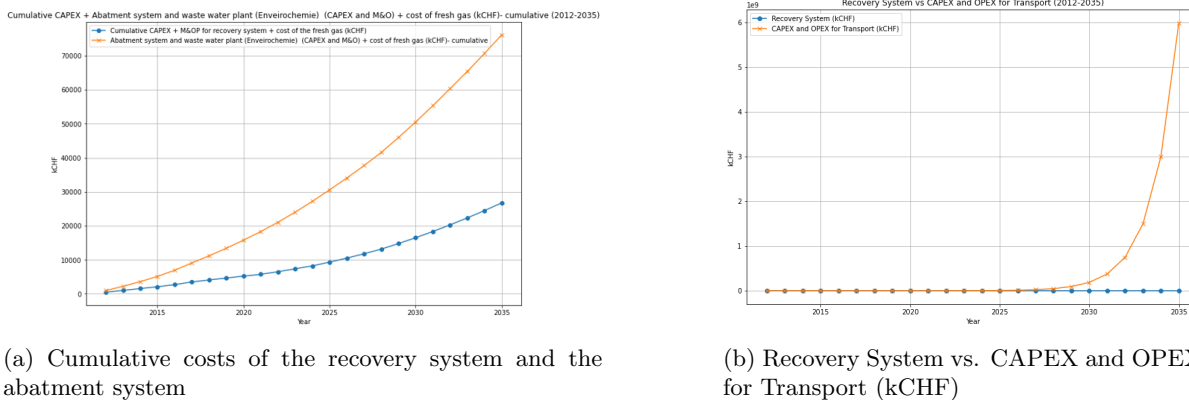


Figure 9.11: Comparison of Costs between Recovery and Abatement Systems

The graph at the right presents, the cumulative costs for the abatement system and recovery systems

- **Yellow Curve:** Represents the cumulative cost of the abatement system, including the transport and maintenance and operation (M&O) costs for fresh gas over the years.
- **Blue Curve:** Represents the cumulative costs spent on the construction of the recovery systems, including maintenance and operation, as well as the cost of the fresh gas needed per year.

In 2025, the cumulative cost of plant maintenance has reached approximately 58 million CHF. A significant portion of this expense, (17,000 CHF per week), is attributed to the transport of untreated wastewater. Clearly, foregoing the it is not convenient to transport the waste water to another site. Therefore, we will eliminate this option and instead focus on analyzing the comparative benefits between implementing a recovery system versus employing an abatement system alongside the wastewater treatment plant. On contrary the graph on the left presents the cumulative costs for the abatement system and the waste water treatment plant and recovery systems .

- **Yellow Curve:** Represents the cumulative cost of the abatement system, including the waste water treatment plant and maintenance and operation (M&O) costs for fresh gas over the years.
- **Blue Curve:** Represents the cumulative costs spent on the construction of the recovery systems, including maintenance and operation, as well as the cost of the fresh gas needed per year.

It is evident that maintaining the abatement system is economically disadvantageous compared to the recovery systems. If the abatement system and waste water plant had

been installed since 2012, an additional 2 million CHF would have been spent by 2024 compared to the current situation. Furthermore, if the cost of fresh gas increases over the years, this difference will widen. The gap will become even more pronounced with the installation of the R134a recovery system in 2024 and the SF₆ recovery system in 2026, as less fresh gas will be required to be sent to the mixer at CMS.

We will now delve into the environmental analysis comparing the two systems. This analysis will focus on providing emissions data in terms of CO₂ equivalents (eqCO₂), and then comparing the two systems. Naturally, we expect the emissions with the abatement system to be slightly lower.

In Figure 9.12, the results show the equivalent amount of CO₂ emitted per year for both the recovery system and the abatement system.

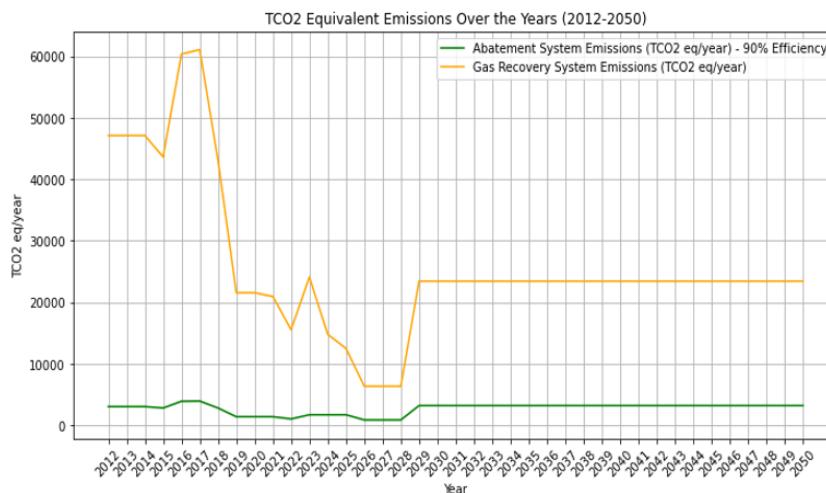


Figure 9.12: Equivalent amount per year of tCO₂ emitted in the period (2012-2050). The yellow curve represent the emission per each ear having the recovery systems while the green curve represent the emission from the abatement system

9.2.5 Discussion of the results of the analysis

In this subsection, we will summarize the results of the economic analysis. The following table 9.13 presents a summary of the results for both the recovery and abatement system (including the costs for the waste water treatment plant) .

When comparing the recovery system to the abatement system, it becomes evident that the recovery system offers significant cost savings. Between 2012 and 2025, the recovery system is projected to reclaim 17,200 kg of R134a, 96 kg of SF₆, and 6,505 kg of CF₄, resulting in approximately 500 kCHF in savings from the recovered gases. Additionally, the construction and maintenance costs for the recovery system are lower compared to the abatement system.

However, it is important to note that the recovery system has a substantial drawback: its air emissions are 15 times higher than those of the abatement system. This significant difference in emissions must be carefully considered when evaluating the overall environmental impact of each system.

In summary, while the recovery system is economically advantageous, it cannot be considered more environmentally friendly compared to the abatement system.

gas recovered (from 2012 -2025)	Recovery systems			Abatement systems		
	R134a (kg)	SF6 (kg)	CF4 (kg)	R134a (kg)	SF6 (kg)	CF4 (kg)
	17200	96	6505	0	0	0
Money saved for fresh gas recovered (kCHF) (from 2012 - 2025)	455			0		
Money spent for construction -CAPEX (kCHF)	525			617		
M&O (kCHF/year)	15			16		
FSU (kCHF/year)	60			84		
Emissions (tco2 eq/year)	39114			2347(CFC emissions+260 (propane consumption))		

Figure 9.13: Summary of recovery systems and abatement system in the years 2012 to 2025

Chapter 10

Conclusions

The primary objective of this thesis is to simulate and design a recovery system for SF₆ in the exhaust line at CMS, aiming to minimize atmospheric emissions. The project specifications require an SF₆ recovery efficiency above 60% and a purity between 90% and 99%. The input gas mixture consists of R134a (79%), iC₄H₁₀ (19%), SF₆ (1.3%), and N₂ (0.36%). The gas flow is intermittent, with an inlet temperature and pressure of 20°C and 1.2 bara, respectively.

Cryogenic distillation was selected as the separation method, given its efficiency in liquefying large gas volumes. The entire process was simulated using ASPEN PLUS. The fixed gas flow rate for the described mixture was set to 95 l/h. Two distillation columns were simulated in series, with sensitivity analyses performed to achieve optimal separation performance. High reflux ratios of 20 and 13 were chosen for the columns, balancing thermal costs at the condenser and reboiler. Both columns were set to 10 stages, with the feeding stage set respectively at 5 and 9. A boilup ratio of 0.8, representing an optimal trade-off between purity and recovery.

The second column's distillate output is 1 l/h, comprising 70% SF₆ and 30% N₂. Based on these results, the column dimensions were set to a diameter of 3 cm, an HETP of 0.5 m, the total height of the column was set to 1.5 m. The process design, including necessary equipment and control logic, was completed based on simulation results.

The process consists of three main sections: accumulation and emptying, distillation, and storage. In the first section, the gas is collected in a 1 m³ tank filled to 500 liters before being emptied. Subsequently, the gas is sent to a compressor where the pressure is increased to 3 bar. Then, the mixture is regulated by a flowmeter upstream the first distillation column. A consistent flow of 95 l/h is fed into the column, initiating the first separation. An 8 l/h flow from the distillate of the first column is directed to the second column for further separation, resulting in a 1 l/h distillate of 70/30 SF₆/N₂, which is stored in a cylinder at 30 bar. This mixture is then processed in a membrane module to concentrate SF₆ to 90-95% purity.

For the final purification phase, two "hollow fiber membrane" types in polyamide, initially optimized for CO₂ separation, were tested. Contrary to literature claims, experimental results showed low SF₆ permeability. Despite these challenges, ongoing R&D activities aim to better understand the mixture's properties and refine the separation process. Research includes single-stage cryogenic distillation, adsorption testing with molecular sieves z5 and z10, and testing selective membranes in polycarbonate and zeolite, acquired

from the Frankfurt Ceramic Institute.

Building an entire system requires the collaboration of many individuals and a concerted effort from various teams. Each part plays a fundamental role, and the work is divided into several key steps. Here, we outline the steps necessary for building the system: (1) define the objective and analyze the problem, (2) identify potential solutions, (3) design and simulate solutions, (4) conduct experimental campaigns, (5) commission components and build the system, (6) clean and insulate the system, (7) define control logic and implement sensors, control software, and electrical components, (8) conduct safety inspections and leak tests, and (9) characterize system performance. The project is currently in phase 4, with research and experimental campaigns planned throughout 2024. Successful results will lead to commissioning in 2025.

An economic analysis highlights the benefits of SF₆ recovery over gas abatement. With a 60% efficiency rate, approximately 9 m³ of SF₆ can be recovered annually, resulting in savings of around 31 kCHF. As European suppliers plan to halt SF₆ distribution by 2050, the prices of fluorinated gases will rise steadily, making recovery essential to minimize fresh gas costs. The construction cost of the recovery system is estimated at 200 kCHF, with annual maintenance at 15 kCHF. In contrast, a CFC abatement system would cost 625 kCHF to build and 22 kCHF annually to maintain, without any gas recovery benefits. Recovery systems collectively cost 525 kCHF to build and 35 kCHF annually to maintain. Since 2012, these systems have recovered approximately 17,200 kg of R134a and 6,505 kg of CF₄, equivalent to 494 kCHF, with estimated emissions of 39 ktCO₂ eq. These results clearly demonstrate that while abatement systems are highly effective in significantly reducing emissions by 2.6 ktCO₂ eq, they are more costly to manage when gas recovery benefits are not factored in.

In conclusion, implementing the SF₆ recovery system is both economically and environmentally advantageous, aligning with long-term goals to reduce dependency on fresh gas supplies and mitigate atmospheric emissions.

Additionally, my experience at CERN has been immensely rewarding for my personal and professional growth. Collaborating in a dynamic environment with diverse profiles has greatly contributed to my development. Building this plant will undoubtedly enhance my skills and help fulfill my aspirations as a chemical engineer.

Appendix A

R134a system P&ID

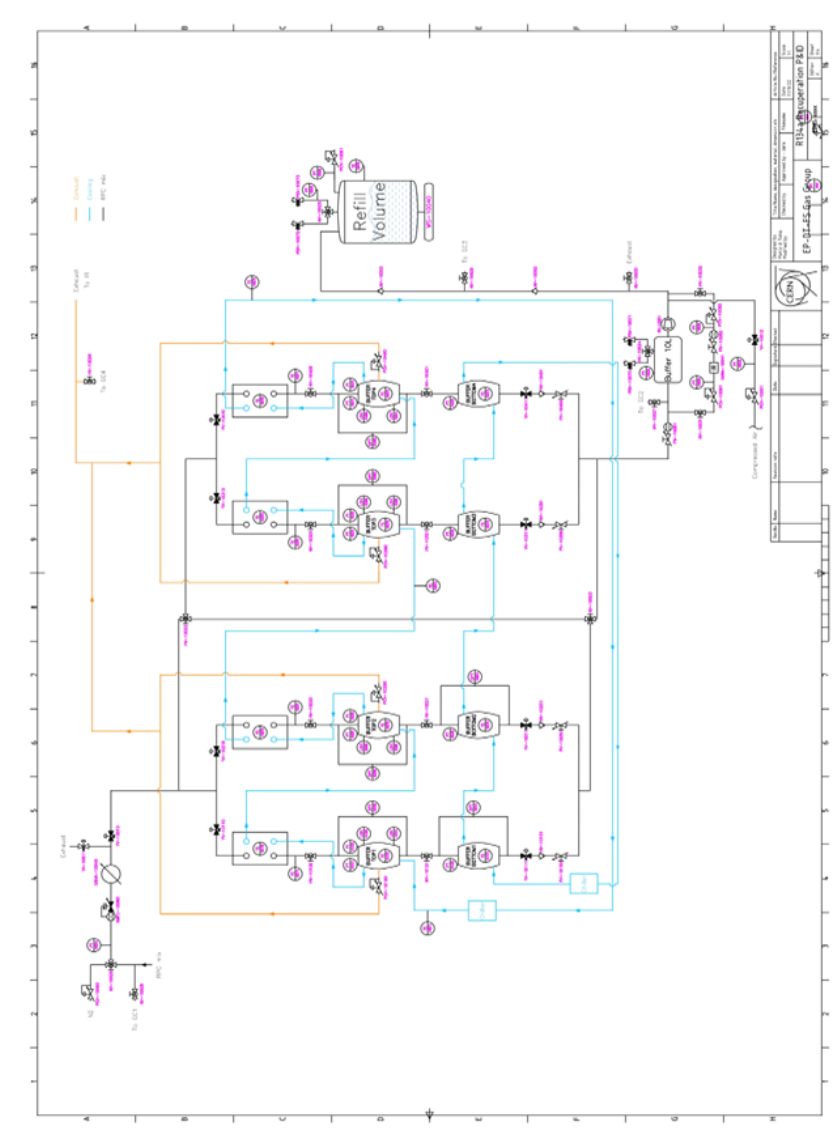


Figure A.1: R134a recuperation system P&ID

Appendix B

WinCC OA software interface

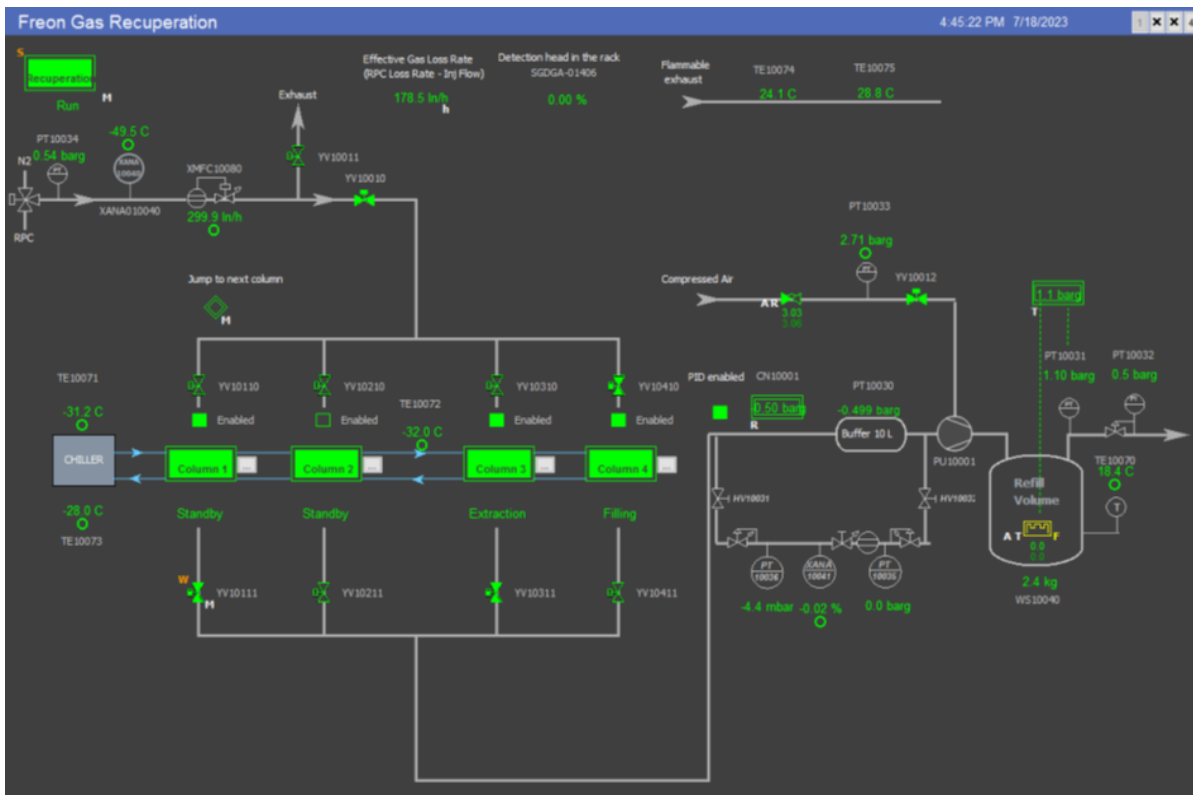


Figure B.1: WinCC OA software interface.

Appendix C

First and Second Buffer P&ID of R134a recovery system

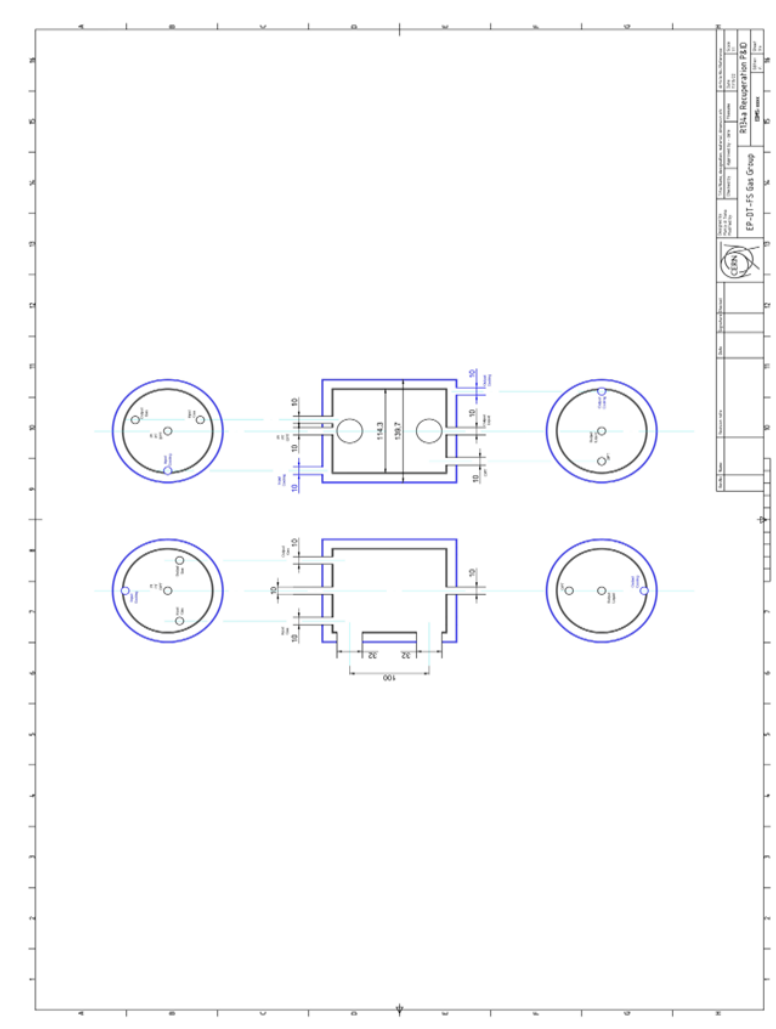


Figure C.1: Buffer with a 10 cm height, used as bottom buffers for columns 1 and 2.

Appendix D

Third Buffer P&ID of R134a recovery system

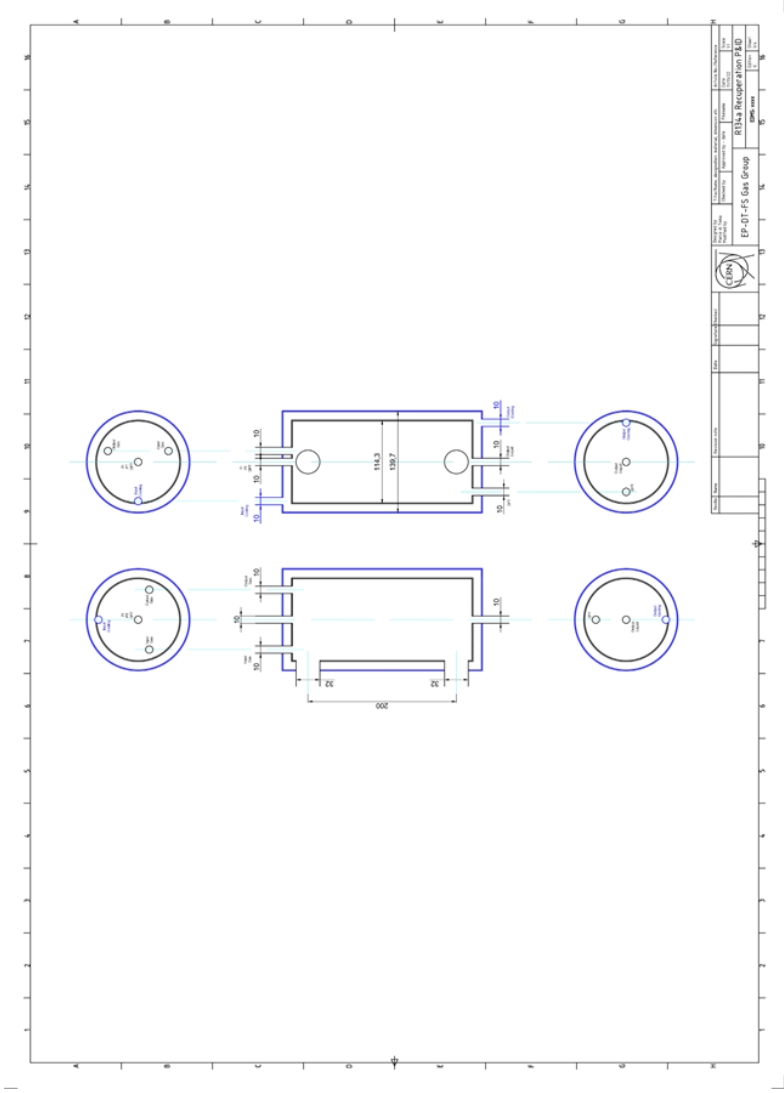


Figure D.1: Buffer with a 20 cm height, used as bottom buffers for columns 3 and 4.

Appendix E

Fourth Buffer P&ID of R134a recovery system

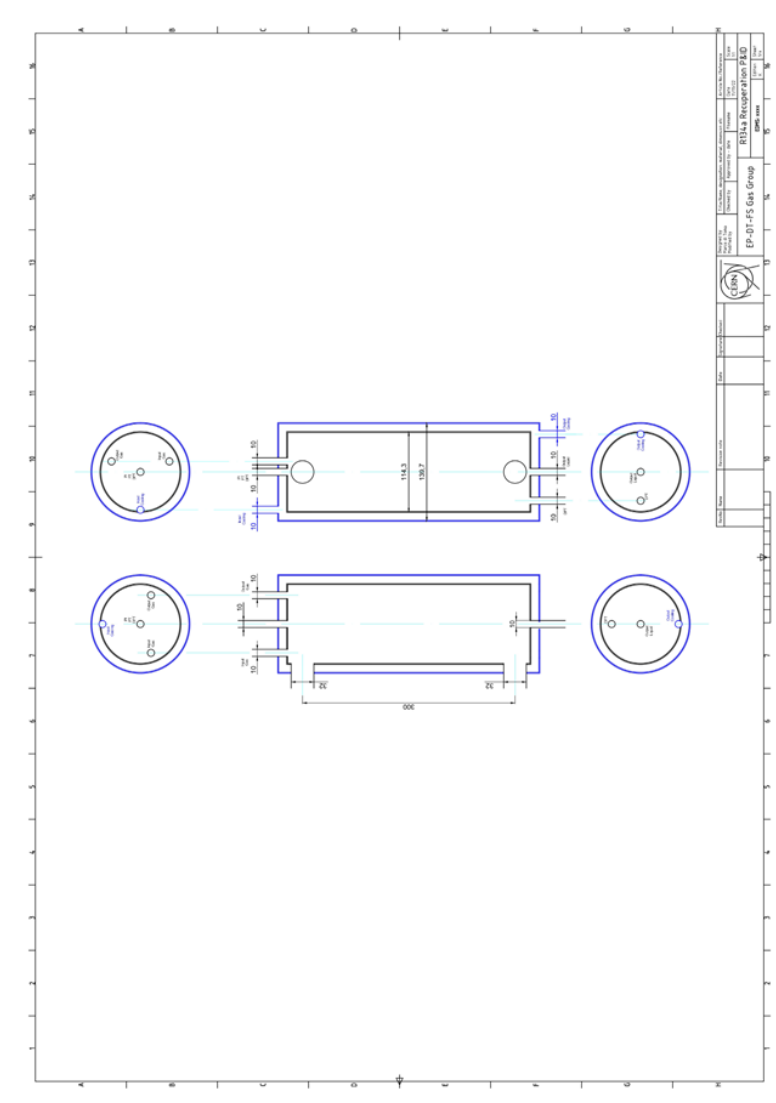


Figure E.1: Buffer with a 30 cm height, used as bottom buffers for columns 1 and 2.

Appendix F

Huber Unistat 915w, Technical data sheet

Technical data according to DIN 12876	
Operating temperature range	-90...250 °C
Temperature stability at -10°C	0,01 K
temperature set point / display	5,7" colour Touchscreen
Resolution of display	0,01 K
Internal temperature sensor	Pt100
Sensor external connection	Pt100
Interface digital	Ethernet, USB (Host u. Device), RS232
digital input	ECS ONE
digital output	POKO ONE
Alarm message	optic, acoustic, relay
Safety classification	Class III / FL
Heating power	6 kW
Cooling power with	Thermooil
at 250°C	6,5 kW
at 200°C	7,5 kW
at 150°C	9 kW
at 100°C	11 kW
Cooling power with	Ethanol
at 0°C	11 kW
at -20°C	11 kW
at -40°C	8,2 kW
at -60°C	4,2 kW
at -80°C	1,3 kW
at -90°C	0,6 kW
Refrigeration machine	water-cooled, CFC- and HCFC-free
Refrigerant (ASHRAE, GHS)	R507 (A1, H280)
Refrigerant quantity	2,9 kg
Refrigerant 2nd stage (ASHRAE, GHS)	R23 (A1, H280)
Refrigerant quantity 2nd stage	1,23 kg
Circulation pump:	MK pump
max. delivery	110 l/min
max. delivery pressure	1,5 bar
Förderleistung bei 0,65 bar	90 l/min
Delivery at 1,0 bar	74 l/min



Order-No.: 1080.0001.01

Peter Huber Kältemaschinenbau AG Werner-von-Siemens-Str. 1 D-77656 Offenburg Tel 0781/9603-0 Fax 0781/57211 www.huber-online.com

Technical data according to DIN 12876	
Delivery at 1,2 bar	59 l/min
Delivery at 1,4 bar	31 l/min
Pump connection	M30x1,5 male
max. permissible kin. viscosity	50 mm ² /s
Cooling water connection	G3/4 male
Consumption at water 15°C, flow 0°C	720 l/h
min. cooling water differential pressure	1 bar
max. cooling water pressure	6 bar
min. filling capacity	3,9 l
Filling capacity expansion tank	6,5 l
Overall dimensions WxDxH **	630x704x1565 mm
Net weight	382 kg
sound pressure level +/- 4 dB(A)	64 dB(A)
Power supply factory configured (3 Phase)	400V 3~ 50Hz
max. current (3 Phase)	28,5 A
Fuse (3 phase)	3x32 A
Degree of Protection	IP20
min. ambient temperature	5 °C
max. ambient temperature	40 °C
from Serial-No.:	402151
	1.0/21

Figure F.1: Technical data of Huber Unistat 915w

Appendix G

P&ID for SF6 recovery system, Prototype 0

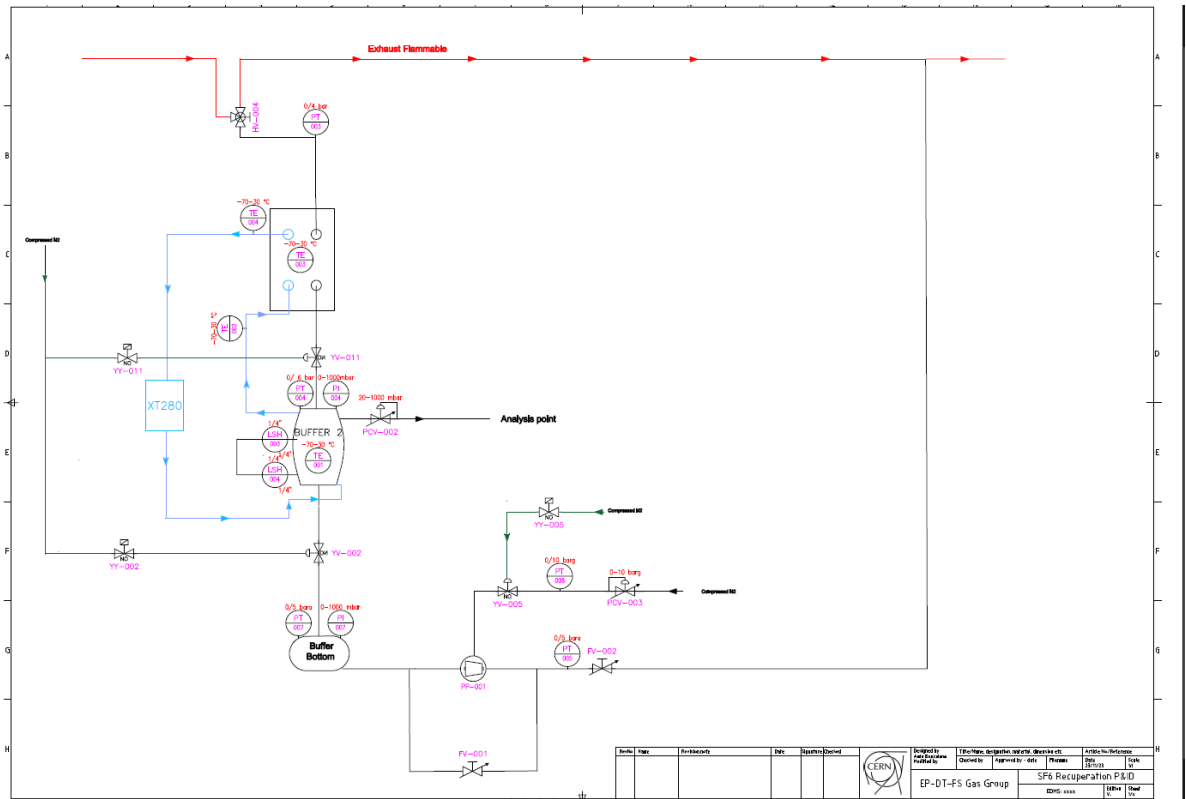


Figure G.1: P&ID for SF6 recovery system, Prototype 0

Appendix H

Matlab code : McCabe-Thiele method for the design of a distillation column Ideal mixture

```
%distillation (McCabe Thiele Method)
clear
clc
close all

% Givens
xf=0.016;
xD=0.99;
xW=0.01;
options=optimset('display','off');
q=0;
alpha=5.1;
Effeciency=0.5;

% 45 line\
plot([0 1],[0 1],'-k','linewidth',0.2)
xlabel('x'),ylabel('y')
set(gca,'Xlim',[0 1])
set(gca,'Ylim',[0 1])
hold on
grid on
grid minor
xticks(0:0.05:1);
yticks(0:0.05:1);
title('MChabe-Thiele method for SF_6/R134a')
%Equilibrium curve
y_eq=@(x) alpha*x/(1-(1-alpha)*x);
x_eq=@(y) y/(alpha+(1-alpha)*y);
fplot(y_eq,[0 1],'b',LineWidth=2)

%q-line
```

```

q_slope=q/(q-1);
q_intercept=xf/(q-1);

if q>1
    xq2=1;
    yq2=q_slope*xq2-q_intercept;
elseif q==1
    xq2=xf;
    yq2=1;
elseif q<1 && q>0
    xq2=0;
    yq2=q_slope*xq2-q_intercept;
elseif q==0
    xq2=0;
    yq2=xf;
else
    xq2=0;
    yq2=q_slope*xq2-q_intercept;
end

plot([xf xq2],[xf yq2],'--k','linewidth',0.1)

% Reflux ratio
if q==1
    x_Rmin=xf;
    y_Rmin=y_eq(x_Rmin);
elseif q==0
    y_Rmin=xf;
    x_Rmin=fsolve(@(x) y_Rmin-alpha*x/(1-(1-alpha)*x),xf,options);
else
    x_Rmin=fsolve(@(x) alpha*x/(1-(1-alpha)*x)-...
        ... (q_slope*x-q_intercept),0.5,options);
    y_Rmin=y_eq(x_Rmin);
end
R_min=(xD-y_Rmin)/(y_Rmin-x_Rmin);
R=2*R_min;

% Intersection of top section line and q line
if q==1
    x_intersect=xf;
else
    x_intersect=fsolve(@(x) R/(R+1)*x+xD/(R+1)-...
        ... (q_slope*x-q_intercept),xf,options);
end
y_intersect=R/(R+1)*x_intersect+xD/(R+1);

% Top section line
plot([x_intersect xD],[y_intersect xD]','-k','linewidth',0.5)

```



```

% Bottom section line
plot([x_intersect xW],[y_intersect xW],'-k','linewidth',0.5)

%Drawing top section stages
x_top_a=xD;
y_top_a=xD;
x_top_b=xD;
y_top_b=xD;
x_top_c=xD;
y_top_c=xD;
Top_sec_line=@(x) R/(R+1)*x+xD/(R+1);
i=0;

while x_top_a>x_intersect

    y_top_b=y_top_a;
    x_top_b=x_eq(y_top_b);
    plot([x_top_a x_top_b],[y_top_a y_top_b],'-r')
    x_top_c=x_top_b;
    y_top_c=Top_sec_line(x_top_c);
    plot([x_top_b x_top_c],[y_top_b y_top_c],'-r')
    x_top_stage_calc=x_top_a;
    x_top_a=x_top_c;
    y_top_a=y_top_c;
    i=i+1;
end
NTS_TOP=i-(x_top_c-x_intersect)/(x_top_c-x_top_stage_calc);

%Drawing Bottom section stages
x_bot_a=xW;
y_bot_a=xW;
x_bot_b=xW;
y_bot_b=xW;
x_bot_c=xW;
y_bot_c=xW;
Bot_sec_slope=(y_intersect-xW)/(x_intersect-xW);
Bot_sec_intercept=y_intersect-Bot_sec_slope*x_intersect;
Bot_Sec_line=@(y) (y-Bot_sec_intercept)/Bot_sec_slope;
j=0;

while x_bot_c<x_intersect
    x_bot_b=x_bot_a;
    y_bot_b=y_eq(x_bot_b);
    plot([x_bot_a x_bot_b],[y_bot_a y_bot_b],'-b')
    y_bot_c=y_bot_b;
    x_bot_c=Bot_Sec_line(y_bot_b);
    plot([x_bot_b x_bot_c],[y_bot_b y_bot_c],'-b')
    y_bot_stage_calc=y_bot_a;
    x_bot_a=x_bot_c;

```

```
        y_bot_a=y_bot_c;
        j=j+1;
    end

    NTS_BOT=j-(y_bot_c-y_intersect)/(y_bot_c-y_bot_stage_calc);
    fprintf('\n\nThe number of top section theoretical stages is %2.2f',NTS_TOP)
    fprintf('\n\nThe number of bottom section theoretical stages is %2.2f',NTS_BOT)
    fprintf('\n\nThe number of top section actual stages ...
    ...is %2.0f',ceil(NTS_TOP/Effeciency))
    fprintf('\n\nThe number of bottom section actual stages ...
    ...is %2.0f\n',ceil(NTS_BOT/Effeciency))
```

Appendix I

P&ID of new SF₆ recovery system

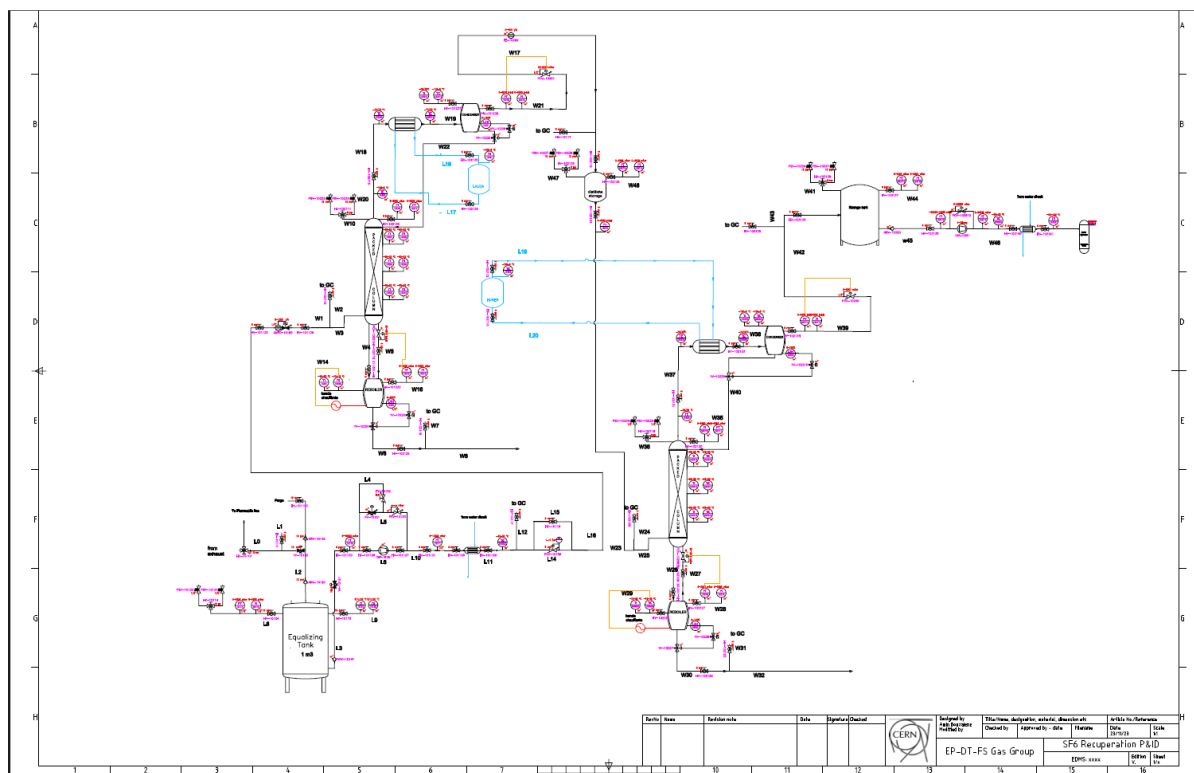


Figure I.1: Full P&ID of the new SF₆ recovery system

Appendix J

Calibration lines for SF₆/N₂ with Omron Flowmeter

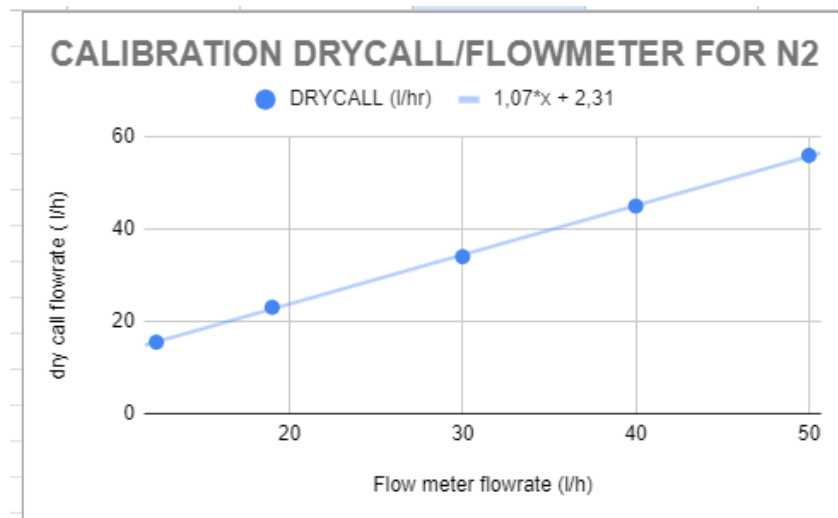


Figure J.1: Calibration line for N₂

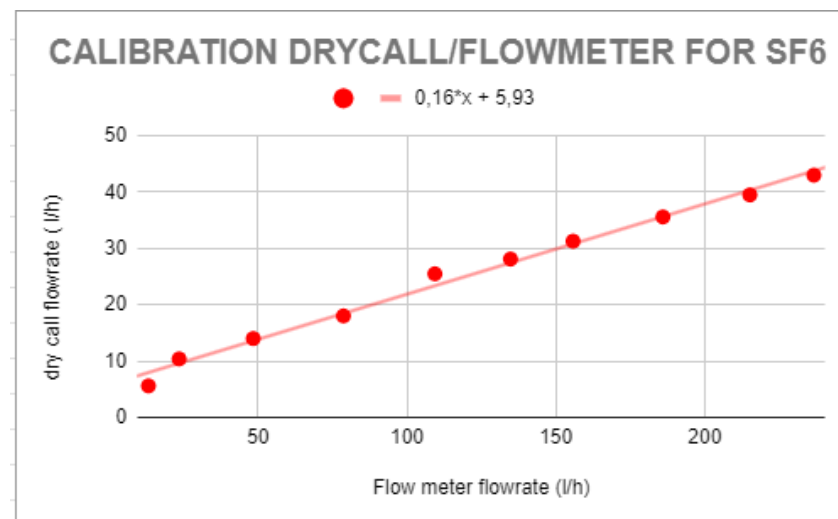


Figure J.2: Calibration line for SF₆

Appendix K

OMRON D6F-10A6-000

D6F-A6


MEMS Flow Sensor

High-accuracy Sensing with a Compact Body for Flow Rates up to 50 L/min.

- Accurately measures an air mass flow rate of 10 to 50 L/min.
- A compact size of 30 × 78 × 30 mm (H × W × D).

RoHS Compliant

Refer to the Common Precautions for the D6F Series on page 40.



Ordering Information

Flow Port Type	Applicable fluid	Flow rate range	Model
Rø 1/4 thread	Air	0 to 10 L/min	D6F-10A6-000
		0 to 20 L/min	D6F-20A6-000
NPT 1/8 thread	Air	0 to 10 L/min	D6F-10A61-000
		0 to 20 L/min	D6F-20A61-000
		0 to 50 L/min	D6F-50A61-000

Accessory (Sold separately)

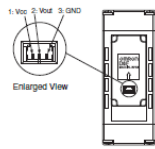
Type	Model
Cable	D6F-CABLE1

Note: Refer to Accessories for the D6F Series on page 39.

Connections

D6F-10A6-000	D6F-10A61-000
D6F-20A6-000	D6F-20A61-000
D6F-50A6-000	D6F-50A61-000

Pin No. 1: Vcc, 2: Vout, 3: GND
 Connector: S3398-03** (Made by Molex Japan)
 Use the following connectors for connections to the D6F:
 Housing: 51021-0200 (Made by Molex Japan)
 Terminals: 50079 (Made by Molex Japan)
 Wires: AWG26 to AWG28



D6F-A6 MEMS Flow Sensor

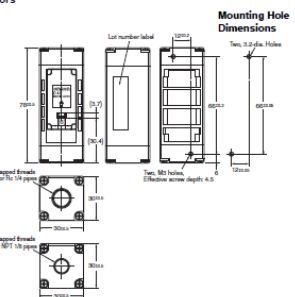
Characteristics/Performance

Model	D6F-10A6-000	D6F-20A6-000	D6F-50A6-000	D6F-10A61-000	D6F-20A61-000	D6F-50A61-000
Flow Range (See note 1.)	0 to 10 L/min	0 to 20 L/min	0 to 50 L/min	0 to 10 L/min	0 to 20 L/min	0 to 50 L/min
Calibration Gas (See note 2.)	Air					
Flow Port Type	Rø 1/4 thread			NPT 1/8 thread		
Electrical Connection	Three-pin connector					
Power Supply	10.8 to 28.4 VDC					
Current Consumption	15 mA max. with no load, with a Vcc of 12 to 24 VDC, and at 25°C					
Output Voltage	1 to 5 VDC (non-linear output, load resistance of 10kΩ min.)					
Accuracy	±5% F.S. (25°C characteristic)					
Repeatability (See note 3.)	±0.3% F.S.					
Output Voltage (Max.)	5.7 VDC (Load resistance: 10 kΩ)					
Output Voltage (Min.)	0 VDC (Load resistance: 10 kΩ)					
Rated Power Supply Voltage	28.4 VDC					
Rated Output Voltage	5 VDC					
Case	PPG/aluminum alloy					
Degree of Protection	IEC IP40 (Excluding tubing sections.)					
Withstand Pressure	500 kPa					
Pressure Drop (See note 3.)	0.10 kPa	0.28 kPa	1.44 kPa	0.15 kPa	0.52 kPa	2.31 kPa
Operating Temperature (See note 4.)	-10 to 80°C					
Operating Humidity (See note 4.)	35% to 85%					
Storage Temperature (See note 4.)	-30 to 80°C					
Storage Humidity (See note 4.)	35% to 85%					
Temperature Characteristics	±5% F.S. for 25°C characteristic at an ambient temperature of -10 to 80°C					
Insulation Resistance	Between sensor outer cover and lead terminals: 20 MΩ min. (at 500 VDC)					
Dielectric Strength	Between sensor outer cover and lead terminals: 500 VAC, 50/60 Hz min. for 1 min (leakage current: 1 mA max.)					
Weight	103 g					

Note 1: Volumetric flow rate at 0°C, 101.3 kPa.
 Note 2: Dry gas. (must not contain large particles, e.g., dust, oil, or mist.)
 Note 3: Reference (typical)
 Note 4: With no condensation or icing.

Dimensions (Unit: mm)

MEMS Flow Sensors



D6F-10A6-000
 D6F-20A6-000
 D6F-50A6-000

D6F-10A61-000
 D6F-20A61-000
 D6F-50A61-000

Figure K.1: Flowmeter datasheet: Omron D6F-10A6-000

Bibliography

- [1] Michele Bruno. R134a recuperation system for the resistive plate chambers at cms experiment, 2023.
- [2] CERN. Cern's accelerator complex, 2003.
- [3] CERN. The third run of the large hadron collider has successfully started, 2003.
- [4] CERN. Resistive plate chambers overview, 2004.
- [5] CERN. Vol. 2 (2021): Cern environment report, 2021, 2021.
- [6] The CMS Collaboration, S.Chatrchyan, G.Hmayakyan, V.Khachatryan, A.M.Sirunyan, W.Adam, T.Bauer, T.Bergauer, H.Bergauer, and M. Dragicevic. The cms experiment at the cern lhc., 2008.
- [7] Hydraulic International Inc. Pumps Division. Air driven gas boosters - low pressure, high flow, oil-free.
- [8] Marylee Z. Southard Don W. Green. *Perry's Chemical Engineer Handbook, Ninth Edition*. Mc Graw Hill, 2021.
- [9] Environmental Protection Agency. Overview of greenhouse gases, 2023.
- [10] Damiano Galassi. Design of a separation system to recover n-decafluorobutane from a gas mixture engineering of a small chemical plant, 2023.
- [11] F. Gianotti and the Directorate. New year presentation. 2018.
- [12] R. Guida, M. Capeans, F. Hahn, S. Haider, and B. Mandelli. The gas systems for the lhc experiments., 2013.
- [13] R. Guida and B. Mandelli. A portable gas recirculation unit for gaseous detectors, 2017.
- [14] J.F. Richardson J.M. Coulson. *Coulson and Richardson's Chemical Engineering (3rd Edition)*. BH, 1999.
- [15] Kirk-Othmer. Encyclopedia of chemical technology, 5th ed ., vol . 8, 2004.
- [16] Henry Z. Kister. *Distillation Design*. Mc Graw Hill, 1992.
- [17] Luigi Manna. Metodo di mccabe e thiele, corso di processi di separazione, 2021.
- [18] Matteo Gazzani Marco Mazzotti. Membrane separations: Rate controlled separation processes. 2016.
- [19] US Department of Labor. Occupational safety and health administration., 2018.

- [20] National Institute of Standards and Technology. Nist chemistry web- book, standard reference database number 69., 2023.
- [21] Aspen Plus. Aspen plus user guide, version 10.2, 2020.
- [22] B.Mandelli R.Guida. Reduction of greenhouse gas emissions and consumption at the cms experiment. 2018.
- [23] B. Kim S.E. Nam, A. S. Park. Separation and concentratio of sf6 from n2/sf6 gas mixtures. 2012.
- [24] S. T. Sehgal, R. Sehgal, and Lalit Mohan Pant. Humidifier for rpc gas mixture for bakelite rpcs, 2011.
- [25] SIEMENS. Simatic wincc oa - basic software.
- [26] Yuanhui Shen Sirui Chen. Adsorption properties of sf6 on zeolite nay, 13x, activated carbon, and silica gel. 2020.
- [27] CERN Stores. <https://edh.cern.ch/edhcat/browser?command=showpage&argument=299018&top=299018>
- [28] R.E. Treyball. *Mass Transfer Operations (3rd Edition)*. Mc Graw Hill, 1981.
- [29] Wikipedia. Global warming potential, 2023.
- [30] Y. Lee Yang ChuahC. Potential of adsorbents and membranes for sf6 capture and recovery: a review. 2020.